RHEOLOGICAL PROPERTIES OF HIGH AND LOW CONCENTRATED ORANGE PULP

By

ELYSE MEREDITH PAYNE

A THESIS PRESENTED TO THE GRADUATE SCHOOL
OF THE UNIVERSITY OF FLORIDA IN PARTIAL FULFILLMENT
OF THE REQUIREMENTS FOR THE DEGREE OF
MASTER OF SCIENCE

UNIVERSITY OF FLORIDA

2011

To my parents, brother, and all my family and friends who helped, encouraged, and guided me through my pursuit of higher education.

ACKNOWLEDGMENTS

I would like thank all who helped me through my academic career, including: my parents, brother, grandparents, family and friends for their relentless support. I would also like to thank my academic advisor Dr. Reyes for his suggestions, encouragement and supervision. I would also like to thank my remaining graduate committee members, Dr. Yang and Dr. Ehsani for their valuable suggestions. Also a special thanks to my lab group John Henderson, Shelley Jones, Brittany Tomlin, Juan Fernando Munoz, Sabrina Terada, Dr. Giovanna Iafelice, and Dr. Faraj Hijaz for all your help. I would also like to extend thanks to Dr. Paul Winniczuk of Sun Orchard for providing a pump, Dr. Wilbur Widmer of the USDA for providing a flowmeter, Mr. Thomas Fedderly of Coca-Cola and Mr. Marcelo Bellarde of Citrosuco for providing orange pulp. Additionally I would like to extend my gratitude to Debra Abbott for instilling the love of science in me. Lastly, I would like to thank all the assistance provided to me from the University of Florida who without any of this could not have been possible.

TABLE OF CONTENTS

page

LIST OF TABLES

LIST OF FIGURES

LIST OF ABBREVIATIONS

A	Constant (s^{-1})
B	Constant
c_p	Specific heat of the fluid ($J \cdot kg^{-1}\ K^{-1}$)
D	Pipe diameter (m)
DS	Dynamic stress/strain sweep
E_a	Activation energy ($kJ \cdot mol^{-1}$)
f	Friction factor
FCOJ	Frozen concentrated orange juice
g	Gravity (9.81 m/s^2)
g_c	Newton's law proportionality factor for gravitational force (1 kg m/(s^2 N)
k	Rate Constant (s^{-1}) for first order reactions
K	Consistency coefficient (Pa·s)
K_{fc}	Sudden contraction friction loss
K_{fe}	Sudden expansion friction loss
K_{ff}	Friction loss from fittings
L	Length of pipe (m)
n	Flow behavior index (unit less)
ND	No Data
p_m	Pressure (Pa)
PME	Pectin methyl esterase
Q	Volumetric flow rate ($m^3 \cdot s^{-1}$)
Q_m	Measured volumetric flow rate ($m^3 \cdot s^{-1}$)

Q_{ws}	Flow rate without slip ($m^3 \cdot s^{-1}$)
r	Pipe radius (cm)
R	Universal gas constant ($J \cdot mol^{-1}\ K^{-1}$)
Re	Reynolds number for Newtonian fluid
Re_n	Reynolds number for power law fluids in laminar flow
SR	Steady rate sweep
SS	Steady stress sweep
T	Temperature in Kelvin
u_s	Slip velocity ($m \cdot s^{-1}$)
V	Volume (m^3)
v	Velocity ($m \cdot s^{-1}$)
$\bar{v}_a$	Velocity upstream from a sudden expansion ($m \cdot s^{-1}$)
$\bar{v}_b$	Velocity downstream from a sudden contraction ($m \cdot s^{-1}$)
$\dot{W}$	Mass flow rate ($kg \cdot s^{-1}$)
X	Concentration (%w/w)
z	Elevation (m)
β	Slip coefficient ($\beta = u_s / \sigma_w$) (m/Pa·s)
β_c	Corrected Slip coefficient (m^2/Pa·s)
$\beta_0, \beta_1, \beta_2$	Model parameters
γ	Shear rate (s^{-1})
Δp_e	Entrance losses (psi)
Δp_t	Total pressure drop across capillary (psi)

Δp_v	Viscous pressure drop across capillary (psi)
μ	Viscosity (Pa·s)
μ_{app}	Apparent viscosity (Pa·s)
π	Pi
ρ	Density (kg/m^3)
σ	Shear stress (Pa)
σ_a	Apparent shear stress at the wall ($dynes/cm^2$)
σ_0	Yield stress (Pa)
σ_w	Apparent shear stress a the wall (Pa)
Φ	Power (W)

Abstract of Thesis Presented to the Graduate School
of the University of Florida in Partial Fulfillment of the
Requirements for the Master of Science

RHEOLOGICAL PROPERTIES OF HIGH AND LOW CONCENTRATED ORANGE PULP

By

Elyse Meredith Payne

December 2011

Chair: José I. Reyes-De-Corcuera
Major: Food Science and Human Nutrition

The demand for “fresh like” beverages that use orange pulp is increasing. A complete rheological characterization of orange pulp is needed for the design and optimization of pulp handling and processing equipment. Orange pulp is a difficult fluid to characterize because it displays slippage over a range of temperatures (4 to 80 °C) and concentrations (~500 to ~850 $g \cdot L^{-1}$). Orange pulp is a non-Newtonian pseudoplastic fluid that can be modeled by the power law at very low shear rates. Rheological determination showed that slippage takes place at shear rates between 2 and 4 s^{-1}. Slippage was more pronounced at low temperatures and high concentrations and is a consequence of particle arrangement and resistance to flow. Slippage can be characterized by rotational rheology using a vane geometry. Both temperature and concentration did not have much effect on the flow behavior index (n) which ranged from 0.18 to 0.42. The consistency coefficient K was greatly affected by temperature and concentration. As the temperature increased K decreased, while as the concentration increased K increased from 47.9 to 233.6 $Pa \cdot s^{n}$. Along with the power law parameters, the activation energy of the consistency coefficient was determined. It ranged from 7.1 to 10.2 $kJ \cdot mol^{-1}$ and as the concentration increased the activation

energy increased. Although similar in trend, the rheological behavior of orange pulp varied depending on source.

The second part of this study determined the effect of slippage on pressure drop and flow rate in capillary flow. The experimental pressure readings were consistently less than the calculated assuming no slippage for all studied temperatures and concentrations. As the measured flow rate increased the measured pressure drop increased and was a consequence of friction. Also as the concentration decreased the measured flow rate increased at every temperature because there was less resistance to flow. As the temperature increased the measured flow rate also increased because at higher temperatures more molecular movement causes increased flow. The difference between the measured flow rate and the flow rate without slippage at the same pressure drop was related through a slippage coefficient. Generally as the measured flow rate increased the slippage coefficient increased.

CHAPTER 1
LITERATUERE REVIEW

Introduction

Citrus fruits are grown or imported and enjoyed in most countries of the world. During the 2004/05 growing season, Brazil and the United States were the leading orange producers (39%); China (7%) and the European (17%) region accounted for a smaller portion. Over 36% of oranges produced in the world were processed into juice. A significant 64% increase in world citrus production was seen from the 80's to the 2004/05 season and Brazil gained dominance in citrus production and other regions began to expand after Florida's crop was destroyed by frost and hurricanes (FAO, 2006). The United States 2009/10 season produced 134 million boxes valued at $2.88 billion with Florida producing 65% of citrus crop (NASS, 2010). Since the improvements of transportation and packaging, larger production levels have been reached which have in turn lowered the cost of citrus fruits. Sao Paulo, Brazil and Florida have retained their title as the flagship citrus capitals of the world; while new regional citrus markets like China, Spain, and Africa are expected to expand (Spreen, 2001). The world citrus belt falls between 20 °N – 40 N° and 20 °S – 40 S° latitudes. In this main growing region, the, seasons are defined with a combination of rainfall/droughts and where a relative humidity around 40-60% is the standard climate (FAO, 2001). In the 2007/08 season, Florida's citrus was processed into juice/juice products totaling 3,303.6 million dollars while the by-products—citrus pulp, molasses, and essential oils were sold for 136 million dollars (Rahmani & Hodges, 2009). Citrus pulp is an important by-product that consists of ruptured juice sacs obtained by finishing (separating through a fine mesh) pulpy juice. Citrus pulp market is increasing because the market for beverages

with pulpy mouth feel has increased in particular in Asia. Therefore, larger amounts of pulp are handled and processed every season. However, the rheological properties of citrus pulp at different concentrations and temperature have not been reported, making it impossible to optimize pulp handling and pasteurization conditions. With this high economic value crop, complete rheological characterizations of citrus and citrus by-products are imperative. The overall objective of this research is to characterize the rheological properties of citrus pulp at selected temperatures and pulp concentrations. The reported properties are expected to be used by citrus pulp manufacturers, equipment manufacturers, process design engineers and by-product end users to design and optimize flow systems. In this chapter fundamental theoretical background on flow of viscous liquids, rheology, and methods of rheological characterization; a literature review (1952-2010) of the citrus pulp processing and the most recent rheological properties of food pastes; as well as the specific objectives of this research are presented.

Theoretical Background

Flow of Liquids

Bernoulli's equation

Bernoulli's equation is known as the conservation of energy for fluid flow (Smith, 2003). In an ideal system in the absence of friction it can be written as:

$$\frac{p_1}{\rho} + \frac{gz_1}{g_c} + \frac{v_1^2}{2g_c} = \frac{p_2}{\rho} + \frac{gz_2}{g_c} + \frac{v_2^2}{2g_c} \quad (1\text{-}1)$$

where p is pressure, ρ is density, g is the acceleration of gravity, z is elevation, g_c is Newton's law proportionality factor for gravitational force, and v is the mean velocity. In a real flowing system, frictional energy losses impact the energy balance. Major losses

are due to the friction of the liquid against the pipe (skin friction) while minor friction losses are due to fittings and sudden contractions and expansions in the system. The energy balance for a liquid flowing system can be expressed as (Equation 1-2):

$$E_p = \frac{p_2 - p_1}{\rho} + \frac{g(z_2 - z_1)}{g_c} + \frac{(v_2^{\,2} - v_1^{\,2})}{2g_c} + \frac{2f\bar{v}^{\,2}L}{g_c D} + K_{fe}(\frac{\bar{v}_a^{\,2}}{2g_c}) + K_{fc}(\frac{\bar{v}_b^{\,2}}{2g_c}) + K_{ff}(\frac{\bar{v}_a^{\,2}}{2g_c}) \quad (1\text{-}2)$$

Where *f* is the friction factor, L the pipe length, D the pipe diameter, K_{fe} is the coefficient for expansion, $\bar{v}_a$ is the velocity after expansion, K_{fc} is the coefficient for contraction, $\bar{v}_b$ is the velocity before contraction and K_{ff} is the coefficient for valves and fittings.

To determine the power requirements (Equation 1-3) of a pump the work must be determined and then multiplied by the mass flow rate ($\dot{W}$) (Singh & Heldman, 2001). Bernoulli's equation is widely used in fluid dynamics. Several parameters for standard pipes are readily available such as dimensions and relative roughness. Other design terms like the velocity, friction factor and Reynolds number can be readily calculated.

$$\Phi = E_p * \dot{W} \quad (1\text{-}3)$$

Flow regimes and velocity profiles

In order for fluids to flow in pipes, a pressure difference must be present (Wilhelm, Suter & Brusewitz, 2004). For incompressible fluids, such as in piping systems, the average fluid velocity for a particular point across the cross section of a pipe is a function of location. The fastest velocities are in the center of the stream while the slowest velocities are against the boundary layer near the pipe wall where, due to friction, velocity is practically null. There are two types of flow through pipes—laminar and turbulent.

Laminar Flow. Laminar flow occurs when the particles in the fluid move in parallel paths. The fluid can be both very viscous and/or have a low velocity. The laminar flow velocity profile takes on a parabolic shape and has a mean velocity about 50% of the maximum velocity and flow is stratified so that at constant flow rate the velocity at any particular point is constant. In laminar flow, for a given length of pipe the pressure drop is proportional to the flow rate of the fluid (Smith, 2003).

Turbulent Flow. Turbulent flow can be described as flow with particles bouncing in all directions causing mixing and heat transfer (Smith, 2003; Wilhelm, Suter & Brusewitz, 2004). The turbulent flow takes on a plug shape and has a mean velocity approximately 82% of the maximum velocity (Smith, 2003). When turbulent flow occurs eddies form and velocity at any particular flow rate fluctuates. In turbulent flow, the pressure drop increases with an increase in flow rate and follows an approximate squared relationship (Smith, 2003).

Friction Factor. The friction during flow varies with flow rates and surface roughness. The effect of skin friction forces is in part accounted for by a friction factor (Equation 1-4). Depending on fluid classification, different friction factor equations are needed and because citrus pulp is a non-Newtonian fluid flowing in laminar flow only this equation will be discussed (Singh & Heldman, 2001).

$$f = 16/\mathrm{Re} \tag{1-4}$$

The friction factor can also be determined using a modified friction factor chart for power law fluids (McCabe, Smith & Harriott, 1985).

Reynolds Number and Generalized Number. Laminar and turbulent flows are determined through the use of the Reynolds number. Reynolds number is a

dimensionless number that indicates the turbulence in fluid flow (Smith, 2003). Reynolds number is calculated from the fluid properties and the type/size and geometry of the pipe or reservoir where the fluid is flowing. For a pipe with circular cross section, Reynolds number can be expressed as:

$$\mathrm{Re} = \frac{D v \rho}{\mu} \tag{1-5}$$

Where D is the pipe diameter, v the fluid velocity, ρ the fluid density and μ the fluid viscosity. The transition between laminar and turbulent flow is not well defined. For Newtonian fluids laminar flow occurs at Reynolds number of less than 2,000-2,300; while higher Reynolds values (3,000 and beyond) correlate to turbulent flow (Smith, 2003; Wilhelm, Suter & Brusewitz, 2004).

For non-Newtonian fluids a generalized Reynolds number can be used:

$$\mathrm{Re}_n = 2^{3-n}\left(\frac{n}{3n+1}\right)^n\left(\frac{D^n \rho v^{2-n}}{K}\right) \tag{1-6}$$

Where Re_n is used to denote a generalized Reynolds number and is based on the flow behavior index (n), consistency coefficient (K), pipe diameter (D), fluid density (ρ), and fluid velocity (v) (Johnson 1999). The power law parameters n and K are calculated from the mathematical model discussed in the next section.

Principles of Rheology

Flow Behavior. Rheology can be defined as the science of deformation and flow of matter (Steffe, 1996). The flow behavior of a biological material can be broken down into categories. The two major subcategories are elastic and viscous. Elastic materials undergo irreversible deformation when stress is applied while viscous materials have reversible deformation when applied stress is removed. The viscous subcategory can

be further broken down into Newtonian and non-Newtonian. Newtonian fluids have a shear stress and shear force that is directly proportional to the rate of deformation (Kyereme, Hale & Farkas, 1999). Shear stress is defined as the stress component applied tangential to the plane on which the forces act. The unit of shear stress is the Pascal (Pa). Shear rate is defined as the velocity gradient established in a fluid as a result of an applied shear stress and has a unit of reciprocal seconds (s^{-1}) (Bourne, 2002). Newtonian foods can be represented by simple liquids like coffee, milk and tea (Barbosa-Canovas, 2005). The formula used to determine the viscosity of Newtonian fluids is

$$\mu = \sigma / \gamma \tag{1-7}$$

Where μ is viscosity, σ is shear stress, and γ is shear rate. The apparent viscosity of non-Newtonian fluids is not constant but depends on shear rate (Kyereme, Hale & Farkas, 1999).

The term apparent viscosity (μ_{app}) is commonly used to describe non-Newtonian behavior because viscosity depends on the shear rate at which it is measured (Kyereme, Hale & Farkas, 1999). Non-Newtonian foods include egg whites, tomato puree, mayonnaise, and concentrated fruit juices. Non-Newtonian fluids can be subdivided into two subcategories: time-independent and time-dependent. The two major types of time-independent fluids are—shear thinning and shear thickening. Shear thinning or pseudoplastics have an apparent viscosity that decreases when the shear rate increases and can be represented by condensed milk, fruit purees, or mayonnaise (Singh & Heldman, 2001). During the increasing shearing, a continuous breakdown and rearrangement of the fluid's structure causes the decrease in apparent viscosity

(Barbosa-Canovas, 2005). Shear thickening or dilatent fluids have the opposite effect with respect to apparent viscosity. As the shear rate increases, the apparent viscosity also increases. Time-dependent fluids are a function of shear rate and time. These types of fluids reach a constant apparent viscosity only after certain amount of time has elapsed after stress has been applied (Singh & Heldman, 2001). Time-dependent fluids are either thixotropic or rheopectic. Thixotropic fluids behave in the same fashion as the pseudoplastic fluid but the hallmark decrease in apparent viscosity becomes reversible when the stress is removed and the fluid is allowed to recover. Rheopectic fluids follow the behavior of shear thickening fluids and also have reversible affects of the apparent viscosity when recovery was allowed (Bourne, 2002).

Mathematical Models for Non Newtonian Fluids. Rheological properties of non-Newtonian fluids can be measured through multiple models. Four common models used are the power law (Equation 1-8), Herschel-Bulkley (Equation 1-9), Casson (Equation 1-10) and Modified Casson (Equation 1-11). In the absence of yield stress (σ_o), the power law is mainly used (Ozkanli, 2008). Yield stress is defined as the minimum shear stress required to initiate flow (Steffe, 1996). Determining the yield stress of structured fluids is necessary to predict product stability with reduced phase separation and sedimentation

$$\sigma = K(\gamma)^n \tag{1-8}$$

where shear stress is σ, K is the consistency coefficient, γ is the shear rate, and n is the flow behavior index. The last three rheology models are used for foods that have a defined yield stress (Ozkanli, 2008).

Herschel-Bulkley: $$\sigma = \sigma_o + K(\gamma)^n \quad (1\text{-}9)$$

Casson: $$\sigma^{0.5} = \sigma_0^{\,0.5} + K(\gamma)^{0.5} \quad (1\text{-}10)$$

Modified Casson: $$\sigma^{0.5} = \sigma_0^{\,0.5} + K(\gamma)^n \quad (1\text{-}11)$$

Predicting the apparent viscosity of non-Newtonian flow is complicated because it is affected by many parameters such as temperature, pressure, moisture content and solid concentration (Kyereme, Hale & Farkas, 1999; Ozkanli, 2008). The flow behavior index (n) varies slightly with an increase in temperature; while the consistency coefficient (K) is severely affected by temperature changes (Kyereme, Hale & Farkas, 1999). Depending on the type of fluid, the flow behavior index changes. For Newtonian fluids n is equal to one. For pseudoplastic fluids, n is less than one and for dilatent fluids the n is greater than one (Singh & Heldman, 2001).

Methods of Determination

Viscometers versus rheometers

Viscometers and rheometers are both instruments used to determine the viscosity of a material, while a rheometer can also determine the relationship between shear rate and shear stress.

Capillary Viscometers. The simplest viscometers are the capillary or tube viscometers. This type of viscometer works either through gravitational forces, hydrostatic forces or pressurized gas/piston movement. The main operating principle behind tube viscometers is to measure the resulting pressure drop from a flowing fluid through a known length of pipe over a period of time and relate this time to the fluid's viscosity. Glass capillary viscometers usually range from 0.1 mm to 4 mm in diameter while a typical pipe diameter is between 7 mm and a few feet (Rao & Steffe, 1997). The

glass capillary viscometers are used to determine viscosity through hydrostatic and gravitational forces and can be used for both Newtonian and Non-Newtonian fluids. Both glass and pipe capillary viscometers can determine time-independent fluid characteristics (Kress-Rogers & Brimelow, 2001; Steffe, 1996). The other type of capillary viscometer is the high pressure viscometer. High pressure viscometers differ from glass and pipe viscometers by relying on compressed gas or piston movement to induce fluid flow through pipes. The gas high pressure viscometer operates via constant pressure while the piston operates under a constant flow rate. High pressure gas viscometers are generally set up with capillary tubes ranging in size from 2.5 mm to 6 mm that are connected to an intake and receiving reservoir. When the gas supply passes through the pressure regulator into the intake reservoir the pressure force created causes the fluid in the reservoir to pass through the capillary tubing into the receiving reservoir. The intake reservoir is a cylindrical barrel with a fitted piston head that is used to force the liquid through the capillary tube to the receiving reservoir (Kress-Rogers & Brimelow, 2001).

Rotational Viscometers and Rheometers. Rotational viscometers are commonly found in the food industry because many Newtonian and Non-Newtonian fluids can be easily measured. The term viscosity only applies to Newtonian fluids while the apparent viscosity of non-Newtonian fluids can be determined with a viscometer. The principle of operation of rotational viscometers and rheometers is based on the viscous drag as a function of the speed of the rotating body in contact with the liquid. However, the rheological behavior of complex non-homogeneous foods and other biological materials cannot be characterized by viscosity alone. A more advanced

detection method is need for more complex materials. Rheometers can be used to determine other rheological characteristics like the relationship between shear rate and shear stress. Depending on the characteristics of the fluid, different surface geometries have been used:

Concentric Cylinder. The first geometry that can be used in a rotational viscometer is the concentric cylinder/Cuvette. A circular bob is placed concentrically inside a cup that holds the sample fluid and is allowed to rotate while the torque is measured. When the shear rate is changed the resulting change in shear stress is seen and then the viscosity can be calculated (Fung & Matthews, 1991).

Cone and Plate. The cone and plate viscometer can also be used to determine a materials viscosity. This type of viscometer is set-up with a flat bottom plate that has an inverted shallow angled (3-5º) cone that rests just above the tip of the plate and has the ability to rotate at multiple angular velocities. One advantage of the cone and plate viscometer is that a constant shear rate is observed at all points of the fluid when small conical angles are used which leads to a very useful measurement tool for non-Newtonian fluids. The shear stress is variable and dependent on cone diameter. If the diameter decreases, the shear stress will increase and the opposite will happen when the cone diameter increases. Another advantage of the cone and plate is that very small samples can be tested. In some cases, the viscosity of samples as small as 0.5 ml can be accurately measured. The one drawback of the cone and plate system is that the material being tested must have particles that are 10 times smaller than the size of the gap (Kress-Rogers & Brimelow, 2001).

Parallel Plate. The viscosity of a fluid can also be determined through the use of a parallel plate viscometer. The parallel plate viscometer has a similar design to the cone and plate geometry but instead of a cone a second flat plate is used and a variable gap can be accomplished. Due to the infinite gap size, a wide range of fluids and course materials can be tested. Even with the great flexibility of the parallel plates, multiple disadvantages occur. The first is the uneven shear rate distribution on the plates. The shear rate is zero at the center and reaches a maximum at the outer edge of plates. The second drawback is that slippage may occur (Kress-Rogers & Brimelow, 2001).

Vane Geometry. The vane geometry can also be used with a rotational viscometer. The vane geometry consists of a rotating spindle with numerous blades protruding into the sample. The vane geometry is used to reduce or prevent wall slip.

Rheometers have four modes of operation. The most common method is the ramp increase where either the shear rate or shear stress is steadily increased while the resultant stress or rate respectively is measured. The second method is the stepwise increase of shear rate or stress. The third mode is continuous operation at constant settings. In this mode, either the shear stress or shear rate is measured constantly over a period of time. The last method of operation is small-amplitude oscillatory. In small-amplitude oscillatory mode, small clockwise and counterclockwise angles are made measuring viscoelasticity with the geometry (Bourne, 2002). Rotational viscometers also have the ability to detect time-dependency attributes. With the great range of geometries available, the rotational viscometer is the most widely used type of viscometer (Van Wazer, Lyons, Kim & Colewell, 1963).

Controlled stress and strain rheometers have the ability to have rapid step changes in stress and strain which leads to a complete material characterization. In the controlled stress and strain modes, a complex range of rheological test can be performed. Such test can simulate spraying, mixing, leveling, extrusion, and sedimentation. A typical rheometer also includes a temperature control unit that holds a sample at a specified temperature or allows for different temperature ranges to be tested. Rheometers have a wide dynamic range and control which leads to a more versatile piece of equipment. Some rheometers also use a low-friction air bearing system as opposed to the mechanical bearing which allows for accurate measurement of low viscous materials. Rheometers also perform at wider shear rate ranges (10^{-6} to10^{5} s^{-1}) that allow characterizing a wide range of flow conditions. Rheometers can determine yield stress, perform sweeps (frequency, time, and temperature) and have oscillatory movement. Typical rheometers operate through rotation, capillary, oscillation or combination action (Carrington, 2005).

Yield Stress determination. Both power law parameters were determined after the linearization of the measured shear stress and shear rate. The slope of the resulting equation is the flow behavior index while the exponent of the y-intercept is the consistency coefficient. Determining the yield stress is important to structured fluids and helps give a better understand of product performance. The apparent yield stress is determined through the extrapolation of the equation of the relationship between shear stress and shear rate to zero.

There are multiple ways to determine the apparent yield stress depending on the materials viscosity (Chen, 2006). The most common methods to determine the apparent

yield stress are the Steady Stress Sweep (SS), Steady Rate Sweep from High to Low Shear Rates (SR), and Dynamic Stress/Strain Sweep (DS) (Chen, 2006) (Table 1-1).

The first method, steady stress sweep, is a very common method to measure the yield stress for medium viscosity materials Low viscosity materials do not respond well to extremely slow increases in stress which may lead to false yield stress measurements. High viscosity semi-solid materials like grease or pastes often produce wall slip which reduces accuracy and reproducibility. With the correct viscosity material, an accurate yield stress measurement can be taken by a step-wise increase of stress until the material starts to flow (Chen, 2006).

Steady rate sweep method is another method to determine the yield stress. The SR method is optimal for low viscosity materials that have a low yield stress and can be easily damaged upon loading into the test geometry. In this method, the shear rate is logarithmically decreased from high (10 s^{-1} to 100 s^{-1}) to low rates (10^{-5} s^{-1}). The yield stress is reached when the sample reaches a plateau and shear rate becomes independent. With this method, the yield stress can be measured to 4 x 10^{-4} Pa. An advantage of the SR method is that when the shearing takes place from high to low the sample history is eliminated (Chen, 2006).

Dynamic stress/strain sweep is the preferred method to determine yield stress for highly viscous materials but can work for all viscosities. In this type of test, small sinusoidal waves are applied and the stress/strain is measured in the linear region. In this method, new frequency dependent variables, G’ and G” are introduced. G’ is a measure of energy stored or released per cycle of deformation per unit volume; while G” is a measure of energy dissipated as heat per cycle of deformation per unit volume

(Gunasekaran & Ak, 2000). The yield stress is determined in a double log plot of G' as a function of oscillation stress (Chen, 2006). The benefits of DS include a more reliable and sensitive measurement while not destroying the sample matrix (Ahmed, Ayad, Ramaswamy, Am & Shao, 2007; Gunasekaran & Ak, 2000). Also, the incidence of wall slip is decreased (Chen, 2006).

Yield stress can also be referred to as the stress that must be exerted to just move one fluid layer past another (Missaire, Qiu & Rao, 1990). In food engineering, it is critical to know if a fluid will flow over given shear stresses and time courses (Rao & Steffe, 1997).

Temperature effects

One of the most important factors affecting the behavior of a fluid is the temperature. In the food industry, a wide range of temperatures are encountered from freezing to 135 ºC in ultra high temperature pasteurization. Viscosity and the consistency coefficient are greatly affected by temperature and the effect is most likely due to the interactions among molecules. For most liquids, viscosity of the consistency coefficient decrease with temperature. An Arrhenius-type equation (Equation 1-12) is commonly used to describe such effects:

$$\mu = Ae^{Ea/RT} \tag{1-12}$$

$$K = Ae^{Ea/RT} \tag{1-13}$$

where, A is a constant, E_a is activation energy of flow, R is the gas constant, and T is the absolute temperature in Kelvin. The viscosity of a sample was found to be most affected by temperature at the highest activation energy and concentration (Belibagli & Dalgic, 2007). Non-Newtonian fluids like fruit pulps can be affected by temperature. As

the temperature increases the viscosity generally decreases. The Arrhenius-like equation (Equation 1-12) can also describe the effect of temperature on non-Newtonian fluids at a constant shear rate. The apparent viscosity decreases exponentially with temperature (Haminiuk, Sierakowski, Maciel, Vidal, Branco & Masson, 2006; Haminiuk, Sierakowski, Vidal & Masson, 2006).

Concentration effects

In general as concentration (in particular of soluble solids) increases the apparent viscosity increases. Insoluble solids have the greatest effect on apparent viscosity and power law parameters and are usually most pronounced at low temperatures (Nindo, Tang, Powers & Takhar, 2007; Ozkanli, 2008). The effect of concentration on power law parameters n and K has been characterized empirically:

$$n = A_n \exp(b_n X) \tag{1-14}$$

$$K = A_k \exp(b_K X) \tag{1-15}$$

where coefficients A and b are empirical constants and X is concentration. As concentration increases n decreases while K increases.

Combined effect of concentration and temperature

The combined effects of temperature and concentration can be expressed as:

$$K = A\exp(E_a / RT)BX \tag{1-16}$$

$$\ln K = \beta_0 + \beta_1(\frac{1}{T}) + \beta_2 X \tag{1-17}$$

$\beta_0, \beta_1, \beta_2$ are empirical parameters (Velez-Ruiz & Barbosa-Canovas, 1998).

Wall slip

Slippage is a phenomenon that happens in multiphase liquids in which a thin layer of liquid of lower viscosity separate from the bulk is formed at the interface of the fluid and the solid geometry that causes a “slip” (Barnes, 1995). In suspensions, the general belief is that a thin layer of fluids exists next to the test geometry (the wall) with the particles either not interacting with the wall or interacting weakly causing a slip (Barnes, 1995; Walls, Caines, Sanchez & Khan, 2003). If there is sufficient shear rate, the fluid next to the wall has a higher velocity when compared to what would be expected of the bulk material in the absence of slippage (Walls, Caines, Sanchez & Khan, 2003). For extreme cases of shear rate, the particle-lean fluid near the wall flows, while the bulk material remains un-deformed (Walls, Caines et al. 2003). Liquids that are concentrated solutions of high molecular weight polymers or suspensions, exhibit the greatest slip effects (Barnes, 1995). According to Barnes (1995), four conditions usually lead to large and significant slip:

- large particles as the dispersed phase;
- a large dependence of viscosity on the concentration of the dispersed phase, smooth walls and small flow dimensions;
- usually low speeds or flow rates;
- walls and particles carrying like electrostatic charges and having the continuous phase electrically conductive.

One of the most accepted methods of compensating for wall slip is the use of vane-in-cup geometry (Figure 1-1) or the use of roughened surface (Figure 1-2). The effectiveness of the vane geometry to reduce wall slip greatly out weights the need to have a large sample volume. In the vane-in-cup method, a cylinder with multiple thin blades is placed in the sample and the shear stress is monitored versus the steady

rotation (Walls, Caines, Sanchez & Khan, 2003). An advantage with the vane geometry is that there is less sample disturbance which causes minimal structural damage to the sample prior to testing (Geraghty & Butler, 1999). The vane geometry also allows for the material to yield “within itself” meaning that the yielding takes place between the blades of the geometry (Leongpoi & Allen, 1992). Most often the use of vane geometry is used to determine the yield stress of food dispersions because the wall slip of suspension is greatly reduced. In addition to using the vane to reduce slippage, geometries can be fabricated that are material specific and can completely reduce slippage during measurement.

Determination of slip coefficient by tube viscometry

For most fluids that display slippage such as citrus pulp, it is impossible to determine rheological parameters that are useful for the design of flow systems by using only a rotational rheometer. An alternative method has been proposed based on the use of pressurized tube viscometers (Figure 1-3). In order to have accurate tube viscometer results, the data must be corrected for entrance losses, pressure drop, and the slip according to Jastrzebski (1967) and Steffe (1996). There are seven steps used to correct the data:

1. Determine entrance correction for each radius.

Entrance loss is the pressure drop required to cause the abrupt change in velocity and shear strain distribution from a large tank to a small tube. The total pressure is the pressure drop necessary to maintain a viscous flow in the tube plus the pressure drop associate with the entrance effects and a small amount of kinetic energy loss. Entrance losses can be calculated from (Jastrzebski, 1967):

$$\Delta p_t = \Delta p_v + \Delta p_e \tag{1-18}$$

Where Δp_t is the total pressure drop, Δp_v is the viscous pressure drop, and Δp_e is determined experimentally by plotting the flow rate (Q) versus Δp_t for at least three tubes of different lengths but the same diameter. Then the values of Δp_t are read for each tube length at a specific flow rate and plotted against Length/Radius for different tube lengths. This linear relationship can be extrapolated to the Length/Radius axis where Length/Radius =0 and Δp_e is the intercept. The kinetic energy losses are caused by the difference in kinetic energy from the acceleration of the fluid in high pressure capillaries. Kinetic energy losses are small and difficult to distinguish from entrance pressure losses and it is considered reasonable to assume kinetic energy losses are accounted for in the entrance effect correction. The entrance length can also be neglected if long tubes are used and the proper placement of pressure transducer is done to ensure the entrance region has no effect on data (Steffe, 1996).

2. Correct pressure drop data.

   Entrance effects should be evaluated for each tube radius before the measured pressure drop can be corrected.

3. Calculate shear stress at the wall.

   The apparent shear stress at the wall is a function of tube radius, tube length, and pressure difference. The shear stress is zero at center while the maximum is at the wall. The apparent shear stress at the wall is can be expressed as:

$$\sigma_a = (\Delta p) r / 2L \tag{1-19}$$

Where p is pressure, r is the radius, and L is the pipe length (Jastrzebski, 1967; Steffe, 1996).

4. Determine slip coefficient.

For a given pressure drop, slip manifests as the direct increase in flow rate through the tube when compared to the flow rate in the absence of slip (Jastrzebski, 1967). In theory, addition of an additional term to the flow rate term can be used to account for the difference:

$$Q_{ws} = \pi r^3 / (\sigma_w)^3 \int_0^{\sigma_w} (\sigma)^2 f(\sigma) d\sigma \tag{1-20}$$

Where Q_{ws} is the flow rate without slip. When the shear stress at the wall (σ_w) is constant the integral term is constant and a slip velocity can be added to account for the different values of flow rate measured (Q_m). The slip velocity is a function of shear stress at the wall and if no slippage occurs then the slip velocity (v_s=0) is zero:

$$Q_m = Q_{ws} + \pi r^2 u_s \tag{1-21}$$

Dividing equation 21 by σ_w: and the new equation becomes (Equation 1-22):

$$Q_m / \sigma_w = Q_{ws} / \sigma_w + (\pi r^2 u_s / \sigma_w) \tag{1-22}$$

Introducing a slip coefficient (β) and with further simplification equation 1-22 becomes

$$(Q_m / \pi r^3 \sigma_w) = (Q_{ws} / \pi r^3 \sigma_w) + (\beta / r) \tag{1-23}$$

The slip coefficient is a function of the wall shear stress and the inverse of the tube radius. With this relationship, the corrected slip coefficient β_c can be determined:

$$\beta = \frac{\beta_c}{r} \tag{1-24}$$

Substituting the corrected slip coefficient the flow rate becomes:

$$(Q_m / \pi r^3 \sigma_w) = (Q_{ws} / \pi r^3 \sigma_w) + (\beta_c / r^2) \quad (1\text{-}25)$$

β can be determined from capillary tube measurements using a minimum of three different radii. Data is plotted of $Q_m/(\pi r^3\sigma_w)$ versus σ_w. From this plot values of $Q_m/(\pi r^3\sigma_w)$ at different r values have a constant σ_w. β (slope) can be obtained from a plot of $Q_m/(\pi r^3\sigma_w)$ versus 1/r for each value of σ_w. The same procedure can be done for β_c with $1/r^2$.

The flow rate without slippage (Q_{ws}) is used in the Rabinowitsch-Mooney equation. With the slip coefficient or corrected slip coefficient the new volumetric flow rate becomes (Equation 1-26):

$$Q_{ws} = Q_m - \beta \sigma_w r^2 \pi \quad (1\text{-}26)$$

$$Q_{ws} = Q_m - \beta_c \sigma_w r^2 \pi \quad (1\text{-}27)$$

β_C (Equation 1-27) may only be useful for dense suspensions and purees but can be meaningless if negative β values are seen because of sliding friction. If this happens, a plug flow model should be used and not the traditional viscous flow model (Steffe, 1996).

5. Correct flow data with slip coefficient.
6. Calculate the shear rate (Equation 1-28) at the wall using the Rabinowitsch-Mooney equation for power law fluids. Since concentrated suspensions display considerable slippage, Equation 1-28 may produce inaccurate data.

The wall shear rate (γ) maximum can be estimated with

$$\gamma_w = (3n+1/4n)(4Q/\pi r^3) \quad (1\text{-}28)$$

7. Construct a rheogram of shear stress versus shear rate.

Literature Review

Citrus Pulp Recovery

Many concentrations of pulp can be produced from low (500 g/L), to high (800-900 g/L) and may be packaged as aseptic or non-aseptic frozen product. Pulp production begins with the extraction of pulpy juice that is then passed through a hydrocyclone defect removal system where centrifugal force brings about the separation of pulpy juice and defects such as seeds, peel particles, or miss colored pulp cells through density differences. Finally, the juice passes through a primary finisher where the pulp is brought to a concentration range of 500 g/L (Figure 1-4). The low concentration pulp can be pasteurized and packaged into drums and stored as aseptic chilled pulp. After the primary finisher and pasteurization, a secondary finisher is used to bring up the concentration to the high concentration range. Due to the finisher being considered a non-aseptic process the concentrated pulp is then filled in either in a box or drum and stored frozen (Braddock, 1999). A few high concentration pulp aseptic pasteurizers are manufactured but have not been optimized. Currently, small pipe diameters are used because of the heat transfer parameters of the viscous citrus pulp. The small pipe diameters used to fabricate the pasteurizers lead to high pressure drops which require a large and expensive pump.

Rheology of Citrus Products

The rheological properties of citrus products such as frozen concentrated orange juice (Tavares, Alcantara, Tadini & Telis-Romero, 2007; Vitali & Rao, 1984a, b), clarified

orange juice (Ibarz, Gonzalez & Esplugas, 1994), and molasses (Hendrickson & Kesterson, 1952; Togrul & Arslan, 2004) have been characterized while the rheological properties of high concentration citrus pulp are not well studied. Frozen concentrated orange juice (FCOJ) is produced in millions of metric tons every year. FCOJ is comprised of an average of 10% w/w pulp (Tavares, Alcantara, Tadini & Telis-Romero, 2007). Concentrated orange juice is a non-Newtonian, mild shear-thinning fluid with insignificant yield stress and has been described with the power law (Table 1-2) (Vitali & Rao, 1984a, b). The concentrated orange juice samples in these studies ranged from a soluble solids content of 46 to 65 ºBrix and were tested at temperatures from -19 to 30 ºC (Vitali & Rao, 1984a, b). From these studies it was found that the rheological properties of orange juice were a function of pulp concentration. As the pulp concentration increased at a fixed temperature, the apparent viscosity and consistency coefficient increased (Vitali & Rao, 1984a, b). Tavares and others (2007) reported that as the FCOJ soluble solids content increased the flow behavior index remained almost constant while the consistency coefficient increased. As temperature decreased the consistency coefficient of FCOJ increased (Tavares, Alcantara, Tadini & Telis-Romero, 2007). The Vitali and Rao studies determined the power law parameters for FJOC over a range of temperatures that included frozen to room temperatures.

Ibarz, Gonzalez and Esplugas (1994) found that orange juice without pulp or clarified orange juice is a Newtonian fluid across a wide range of temperatures (5 to 70 ºC) and SSC concentrations (30.7 to 63.5 ºBrix). The activation energy increased from 4.23 to 9.59 kcal/mol as SSC concentration increased from 30.7 to 63.5 °Brix. Viscosity

of clarified orange juice decreased with an increase in temperature for every concentration (Ibarz, Gonzalez & Esplugas, 1994).

Figure 1-5 shows the production of citrus molasses (Hendrickson & Kesterson, 1952, 1964). Hendrickson and Kesterson (1964) determined that citrus molasses viscosity increased with SSC from 60 to 84 °Brix; while showing a decrease in viscosity as the temperature increased from 5 to 65 °C. Toğrul and Arslan (1994) performed rheological studies on molasses not from citrus origin but harvested from a sugar factory. This study found that molasses had non-Newtonian pseudoplastic behavior that followed power law with a flow behavior index that ranged from 0.756 to 0.793 and a consistency coefficient that ranged from 19.51 to 9.23 ($Pa \cdot s^n$) as the temperature increased from 45 to 60 °C. The study also determined that molasses' apparent viscosity decreased with increasing temperature and shear rate (Table 1-3) (Togrul & Arslan, 2004).

In a preliminary study, Levati (2010) found that high concentration citrus pulp exhibits non-Newtonian, pseudoplastic behavior and its apparent viscosity is dependent on temperature. As temperature increased from 11 to 50 °C the consistency coefficient decreased from 97.31 to 50.84 ($Pa \cdot s^n$) while the flow behavior index increased from 0.08 to 0.15 (Levati 2010) (Table 1-4). In this study, slippage was not noted in the rheological characterization which could lead to incorrect reporting of power law parameters (Levati, 2010). Rheological characterization of most orange processing products and by-products has been done while the characterization of citrus pulp is lacking. Once the pulp has been characterized, optimized pasteurizers and transport systems can be built from the properties determined.

Rheology of Heterogeneous and Complex Foods

Determining the unique rheological properties of some foodstuffs is challenging. The lack of reliable and accurate rheological data of semi-solid foods is due to the limitations of wall slip and secondary flow. With these gaps, the design and selection of equipment is a trial and error process (Dervisoglu & Kokini, 1986). The most difficult foods on which to determine rheological properties include gels, emulsions, semi-liquids, soft foods, and spreadable foods (Sun & Gunasekaran, 2009b; Tabilo-Munizaga & Barbosa-Canovas, 2005).

Understanding the rheological properties of gels is complicated by their structural matrix of small solids surrounded by liquids. Gels have the ability to form a solid but also retain some characteristics of the principle liquid (Tabilo-Munizaga & Barbosa-Canovas, 2005). This dual behavior makes rheological characterization of gels a challenge. Emulsions like peanut butter, mayonnaise, margarine and chocolate are found throughout the food industry. Determining the rheological characteristics of emulsions is complicated because most emulsions experience damage when they are loaded into the test cup. Emulsions also display some degree of slippage. The type of emulsion (oil in water or water in oil) also affects the rheological properties. Water in oil emulsions tend to be higher in fat and have a self-lubricating effect (Campanella & Peleg, 1987; Sun & Gunasekaran, 2009a) The best way to overcome the rheological characterization difficulties with emulsions is to use the vane geometry or a modified squeeze-flow device (Sun & Gunasekaran, 2009a). Peanut butter is a pseudoplastic, time-independent emulsion that exhibits severe slip and has a yield stress that becomes negligible when fitted to the power law (Table 1-5) (Citerne, Carreau & Moan, 2001). Chocolate has rheological properties that are affected by particle size and level of

agitation. The International Office of Cocoa, Chocolate and Sugar Confectionary recommend the Casson Model to determine rheological properties. Both coarse ground (28 μm) and fine ground (14 μm) milk chocolate have been characterized (Table 1-5). For both types of milk chocolate, as the shear rate increased the apparent viscosity decreased (Karnjanolarn & McCarthy, 2006).

Semi-liquid like sauces, condiments, concentrates, and purees are difficult foods to characterize because these foods are complex (chemically/physically) which leads to the use of experimental models to predict their rheological properties (Krokida, Maroulis & Saravacos, 2001). Mexican sauces can be described as a multiphase dispersed systems with solid rigid particles, solid deformable particles and liquid deformable particles in a continue phase (usually water) A rheological study done on three homogeneous (fine particles less than 1 mm) and three heterogeneous (coarse particles greater than 1 mm) sauces with a vane geometry found that both types display slippage and were shear-thinning fluids that could be modeled by the power law. The power law parameters for the homogeneous (barbecue, chipotle, and valentine) and heterogeneous (verde, taquera, and ranchera) Mexican sauces are presented in Table 1-6 (Martinez-Padilla & Rivera-Vargas, 2006).

Tahin (tahini), a common sauce/condiment found in the Middle East, is made into a paste from ground de-hulled dry roasted sesame seeds. The rheological properties were determined for tahin at a temperature range of 30 to 75 °C (Table 1-5). It was found that as the temperature increased the consistency index decreased. The smaller the flow behavior index the greater the departure from Newtonian behavior. Tahin behaves as a pseudoplastic fluid with a viscosity that decreases as the temperature

increases and decreases as the shear rate increases from 0 to 70 rpm. When the tahin is heated molecular entanglement decreases and allows for a reduced molecular volume which in turn decreases the viscosity. The temperature sensitivity of tahin was determined with an Arrhenius-type equation and found that it has an activation energy of 30.329 kJ/mol (Alpaslan & Hayta, 2002). Tomato concentrate, another non-Newtonian pseudoplastic, power law semi-solid liquid, can be produced as cold (below 70 °C) or hot (85-90 °C) break depending on the thermal treatment during concentration. One study determined the rheological properties for both cold and hot tomato concentrate at soluble solids content ranging from 5 to 28 °Brix. Both power law characteristics can be found in Tables 1-7 and 1-8. For the cold break concentrate, the consistency coefficient increased as the soluble solids content increased from 5 to 25 °Brix; while K decreased as the temperature increased at each soluble solids content. The flow behavior index ranged from 0.45 to 0.33. Hot break tomato concentrate had a flow behavior index range of 0.22 to 0.4. The consistency coefficient showed a general trend of increasing as the soluble solids content increased; while K decrease as the temperature increased for each soluble solids content. The activation energy was also calculated for both cold (16.99 MJ $kgmol^{-1}$) and hot break concentrate (22.75 MJ $kgmol^{-1}$). The activation energy was lower for cold break because the particles are aligned in a pattern which allowed for easier flow (Fito, Clemente & Sanz, 1983).

Fruit and vegetable pulps are suspensions of high non-soluble solids. The power law parameters of many types of pulps and purees can be found in Table 1-9. For pulpy products the flow behavior index was close to 0.5 while it was close to 1.0 for clear juices but decreased with concentration. The concentration of soluble and insoluble

solids content has a profound non-linear effect on Newtonian viscosity along with the consistency coefficient and apparent viscosity of non-Newtonian foods (Krokida, Maroulis & Saravacos, 2001). The literature review presented on the fruit and vegetable purees is very extensive for materials that follow the power law parameters but only a few reported activation energy none mentioned slippage in any of the purees.

Dough also presents some rheological challenges. Dough is considered to be a soft-solid food that has viscoelastic properties, a defined yield stress, and displays slippage (Sofou, Muliawan, Hatzikiriakos & Mitsoulis, 2008). The most unique feature about dough is that it develops its strength in stages which complicates determining its rheological properties. The early stages of dough are marked with little resistance to deformation because of the lack of gluten chains, while the later stages have fully developed gluten chains that create more elasticity in the dough (Zheng, Morgenstern, Campanella & Larsen, 2000). Not only is the elasticity of the dough affected by the gluten development, the viscosity is also affected. The best method to test the rheological properties of dough would be to use extensional methods as opposed to the standard shearing (Gras, Carpenter & Anderssen, 2000).

In suspensions, slippage manifests as increased flow rate at the wall of the viscometer due to particle migration. Using the slip coefficient, corrected flow rate values can be calculated. Slip coefficient data of some common non-food materials and foods can be found in Tables 1-10, 1-11, and 1-12. Table 1-10 gives the slip coefficient for a rubber compound found in tire tread. Both the corrected slip coefficients and wall shear for foods rheologically similar to orange pulp can be found in Table 1-11. Table 1-12 is the slip coefficient equations and valid range of wall shear for a model suspension

of green peas and aqueous sodium carboxy-methylcellulose. Slippage has a huge impact and if it is not accounted for the accuracy of the rheological data is severely affected. Peanut butter, cement paste, wood pulp suspensions and mayonnaise are materials that show slippage but no slip coefficient has been determined.

Table 1-13 provides a summary of power law parameters, activation energies and slip coefficients for foods that are rheologically similar to citrus pulp.

Study Objectives

The long term goal of this research is to optimize flow systems for high concentration citrus pulp. The specific objective of this research was to characterize the rheological properties of citrus pulps. Two studies were proposed:

1. Rheological characterization using a rotational rheometer.
2. Determination of pressure drop by capillary viscometry.

It is expected that the results from this research will be used by processors, engineers and equipment manufactures to understand the relationship between pressure drop and rheological characteristics of high concentration citrus pulp which will allow the optimal design of flow systems for pulp.

Table 1-1. Rheological methods for yield stress determination (Chen, 2006).

	Method	Advantages	Disadvantages
Steady Stress Sweep	Stress or torque is logarithmically increased until material begins to flow and the yield point is determined	Mainly used for medium viscosity materials	Challenge for low and high viscosity suspension materials due to the slow incremental added stress Wall slip could lead to inaccurate measurement
Steady Rate Sweep	Shear rate is logarithmically decreased from high (100 s^{-1}) to low (10^{-5} s^{-1}) and yield point is reached when the stress of the sample becomes independent of the rate	Is ideal for low viscosity suspensions When sweeping from high to low all loading history is removed Good reproducibility	Challenge for medium and high viscosity materials
Dynamic Stress/Strain Sweep	Sinusoidal waves are used and the strain/strain is measured in the linear region with the additions of frequency variables G' and G"	Works with all types of materials but works best with high viscosity materials Can be performed on both stress/strain controlled rheometers Wall slippage is minimized with proper geometry Good reproducibility	

Table 1-2. Power law parameters for FJOC.

Material	Sample / Temperature	K	n
1.FJOC	65.1 °Brix (7.1% pulp) -19 to 30 °C	($N \cdot s^n/m^2$) 29.16-0.91	0.71-0.75
	65.1 °Brix (4.6% pulp) -19 to 30 °C	27.63-0.95	0.78-0.71
2.FJOC	65.04 °Brix -16 to 0 °C	($Pa \cdot s^n$) 105.58-34.04	0.55-0.52
	58.56 °Brix -14 to 0 °C	21.52-10.38	0.54
	46.56 °Brix -8 to 0 °C	3.02-2.04	0.57-0.58

1.(Vitali & Rao, 1984a, b) 2. (Tavares, Alcantara, Tadini & Telis-Romero, 2007)

Table 1-3. Power law parameters at different shear rate ranges for molasses (Togrul & Arslan, 2004).

Concentration (°Brix)	Temperature °C	N	K ($Pa \cdot s^n$)	$\gamma(s^{-1})$
81.46	45	0.756	19.51	1.33-11.7
	50	0.777	18.24	1.30-11.3
	55	0.776	15.81	1.30-16.2
	60	0.793	9.23	1.27-15.9

Table 1-4. Power law parameters and apparent viscosities at selected shear rates (s^{-1}) for 850 $g \cdot L^{-1}$citrus pulp (Levati, 2010)

Temperature °C	n	K ($Pa \cdot s^n$)	μ^1_{app}	μ^{10}_{app}	μ^{100}_{app}
11	0.082	97.31	97.31	11.767	1.423
25	0.114	67.286	67.286	8.744	1.136
38	0.137	53.226	53.226	7.296	1
50	0.152	50.836	50.836	7.211	1.023

Table 1-5. Power law and Casson model characteristics for rheologically difficult foods.

Material	Temperature °C	n	K ($Pa \cdot s^n$)	σ_{0CA} (Pa)	μ_{app} (Pa·s)	γ (s^{-1})
1.Peanut Butter	23	0.57	250.85	No Data	57.6	No Data
2.Coarse Ground Milk Chocolate	40	No Data	No Data	67.286	3.73	0-50
2.Fine Ground Milk Chocolate	40	No Data	No Data	34.8	11	0-50
3.Tahin	30	0.58	19.9	No Data	No Data	No Data
	40	0.58	19.4			
	50	0.58	16.3			
	60	0.48	14.7			
	65	0.51	10.2			
	75	0.58	6.79			
4.Ketchup	25	0.27		No Data	No Data	10-560
	45	0.29	18.7			
	65	0.29	16.0			
	95	0.25	11.3			
			7.45			
4.Minced Fish Paste	3-6	0.91	8.55	No Data	No Data	7-238
4.Mayonnaise	25	0.55	6.4	No Data	No Data	30-1300
		0.54	6.6			30-1300
		0.60	4.2			40-1100
		0.59	4.7			40-1100
4.Mustard	25	0.39	18.5	No Data	No Data	30-1300
		0.39	19.1			30-1300
		0.34	27.0			40-1100
		0.28	33.0			40-1100
4.Marshmallow Cream	25	0.379	563.10	No Data	No Data	No Data
4.Apple Butter	25	0.145	222.90	No Data	No Data	No Data
4.Stick Butter	25	0.085	199.28	No Data	No Data	No Data
5.Blueberry Pie Filling	20	0.43	6.08	No Data	No Data	No Data
5.Creamed Corn	23	0.35	23.8	No Data	No Data	No Data
	80	0.26	20.4			
5.Chunky Salsa	23	0.20	30.8	No Data	No Data	No Data
	80	0.28	10.9			

1.(Singh, Castell-Perez & Moreira, 2000) 2.(Karnjanolarn & McCarthy, 2006) 3.(Alpaslan & Hayta, 2002) 4.(Kokini, 1992) 5. (Steffe & Daubert, 2006)

Table 1-6. Flow behavior index and consistency coefficient for homogenous and hetrerogenous Mexican sauces with a 40 mm cup and shear rate range of 10-100 s^{-1}.

Mexican Sauce	n	K ($Pa \cdot s^n$)
Homogeneous		
Barbecue	0.33	16.52
Chipotle	0.21	5.83
Valentia	0.28	3.53
Heterogeneous		
Verde	0.47	3.78
Taquera	0.33	15.26
Ranchera	0.45	5.13

Table 1-7. Power law parameters for Cold Break tomato concentrate (Fito, Clemente & Sanz, 1983).

Temperature °C	Concentration (° Brix)	n	K ($N\ s^n\ m^{-2}$)
15	5 -25	0.43-0.34	0.45-29.32
20	5 -25	0.43-0.34	0.38-27.46
30	5 -25	0.38-0.34	0.56-25.94
40	5 -25	0.44-0.33	0.27-23.03
50	5 -25	0.41-0.35	0.40-19.41
60	5 -25	0.43-0.33	0.26-17.86
70	5 -25	0.45-0.34	0.12-15.08

Table 1-8. Power law parameters for Hot Break tomato concentrate (Fito, Clemente & Sanz, 1983).

Temperature °C	Concentration (° Brix)	n	K ($N\ s^n\ m^{-2}$)
15	10-28	0.28-0.40	6.98-76.90
20	10-28	0.29-0.37	7.00-81.25
30	10-28	0.25-0.36	7.24-76.69
40	10-28	0.27-0.37	6.03-86.82
50	10-28	0.26-0.38	4.84-67.74
60	10-28	0.22-0.37	4.75-87.60
70	10-28	0.24-0.35	4.49-43.55

Table 1-9. Power law parameters for various fruit and vegetables (Krokida, Maroulis & Saravacos, 2001).

Material	Temperature °C	Concentration (% solids)	Shear Rate (s^{-1})	n	K ($Pa \cdot s^n$)
Apple	25.0	18.2	100-2000	0.4	20.2
	29.2	63.2	5-50	1.0	0.2
	29.6	52.8	100-2000	0.9	40.1
	82.0	8.1	5-50	0.3	9.0
	27.0	8.1	100-2000	0.3	12.7
	30.0	8.09	5-50	0.3	11.6
Apricot	27.0	1.9	5-50	0.3	167.5
	30.0	5.3	5-50	0.3	6.8
	27.0	6.3	5-50	0.4	7.2
Currant black	32.5	49.9	ND	1	0.0
Guava	24.0	15.4	100-10000	0.8	5.3
	23.4	10.3	100-10000	0.5	3.9
Mango	25.0	16.0	20-250	0.3	12.3
	25.0	17.0	20-250	0.3	27.8
	50.0	18.7	20-250	0.4	4.3
	25.0	16.0	20-250	0.3	10.0
Navel	1.5	65.1	ND	0.7	9.2
orange	7.5	39.9	0-500	0.8	0.4
	36.4	28.8	100-600	0.8	0.4
	0.9	65.1	100-500	0.7	16.5
Peach	27.0	2.8	5-50	0.4	85.6
	26.9	54.9	50-700	1.0	0.1
	30.0	7.6	5-50	0.3	7.2
Pear	26.4	36.1	1-2000	0.4	81.4
	26.3	60.3	100-1000	1.0	0.2
	55.4	28.8	0.1-2600	0.5	10.4
	27.0	14.6	100-2000	0.4	5.3
Pineapple	7.5	41.1	0-500	0.8	0.8
	37.5	21.7	100-600	0.9	0.1
Raspberry	30.0	27.7	3-2000	0.9	0.5
Tamarind	24.0	21.8	3-1300	0.8	0.0
	46.9	35.7	10-400	0.7	1.2
Tomato	25.0	21.1	4-576	0.3	91.6
	40.7	18.7	ND	0.3	19.7
	55.6	15.5	500-800	0.4	3.9
	57.3	30.0	500-800	0.4	13.4
	20.0	8.1	0-10	0.4	5.7
	33.6	24.7	4-576	0.4	98.6
Valencia orange	7.5	42.5	0-500	0.7	1.0

Table 1-10. Approximate wall slip coefficient (mm/MPa·s) for tire tread compound found at different corrected wall shear stresses (Karrabi, Ghoreishy & Bakhshandeh, 2004).

Temperature °C	Corrected Wall Shear Stress for Different Rubbers (MPa)		
	0.6	0.9	1.1
80	225	290	340
100	235	295	330
120	190	260	300

Table 1-11. Corrected slip coefficients of four semi-solid foods (Kokini & Dervisoglu, 1990).

Food	Corrected Slip Coefficients $m^2 \cdot (Pa \cdot s)^{-1}$	Wall Shear Stress (Pa)
Apple Sauce		
	0.025	150
	0.022	136
	0.019	123
	0.016	109
	0.013	95
	0.010	81
	0.0076	68
	0.0051	54
	0.003	40
Ketchup	0.0420	200
	0.0350	181
	0.0290	163
	0.0230	144
	0.0180	125
	0.0130	107
	0.0093	88
	0.0060	69
	0.0034	50
Mustard	0.037	200
	0.032	181
	0.028	163
	0.024	144
	0.019	125
	0.015	107
	0.011	88
	0.0077	69
	0.0046	50
Tomato Paste	0.0065	750
	0.005	688
	0.0037	625
	0.0026	563
	0.0018	500
	0.00115	438
	0.0007	375
	0.00038	313
	0.00018	250

Table 1-12. Slip coefficients for a model coarse food suspension of green peas and aqueous sodium carboxy-methylcellulose at selected temperatures (Chakrabandhu & Singh, 2005).

Temperature °C	Slip Coefficient Equation $m\cdot(Pa\cdot s)^{-1}$	Wall Shear Stress (Pa)
85	$\beta = 1.176\times10^{-4}\sigma_w^{\,0.8023}$	80.84-124.73
110	$\beta = 4.193\times10^{-5}\sigma_w^{\,1.3410}$	22.51-57.52
135	$\beta = 8.698\times10^{-4}\sigma_w^{\,0.7398}$	19.41-29.10

Table 1-13. Summary of power law parameters, activation energies, and slip coefficients for materials similar to citrus pulp.

Material	n	K ($Pa\cdot s^n$)	E_a $kJ\cdot mol^{-1}$	β_C $m^2\cdot(Pa\cdot s)^{-1}$
Paste/Concentrate				
Peanut butter	0.57	250.85	ND	ND
Creamed corn	0.26-0.35	20.4-23.8	ND	ND
Tomato paste	0.22-0.45	0.12-87.60	16.99-22.75	0.00018-0.0065
Apple sauce	0.3-1.0	0.2-40.1	No Data	0.0051-0.010
Mango pulp[1]	0.16-0.19	27.41-31.85	8.9-11.8	ND
Aracá pulp[2]	0.17-0.25	13.52-32.66	11.03	ND
Citrus pulp with slip	0.082-0.152	50.836-97.31	ND	ND
Liquids				
Mexican sauces	0.21-0.47	3.53-16.52	ND	ND
Tahin	0.48-0.58	6.79-19.9	30.3	ND
FJOC[3]	0.52-0.58	2.04-105.58	6.6[3]	ND
Ketchup	0.25-0.29	7.45-18.7	ND	0.0034-0.042
Mustard	0.28-0.39	18.5-33.0	ND	0.0046-0.037

1.(Khandari, Gill & Sodhi, 2002) 2.(Haminiuk, Sierakowski, Vidal & Masson, 2006) 3.(Crandall, Chen & Carter, 1982).

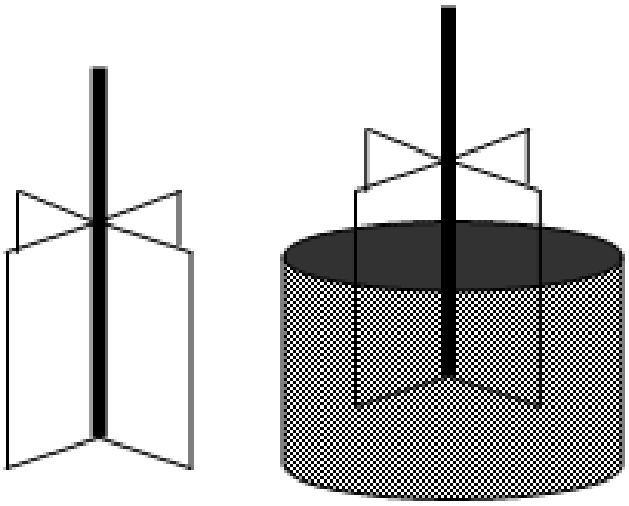

Figure 1-1. Vane-in-cup spindle.

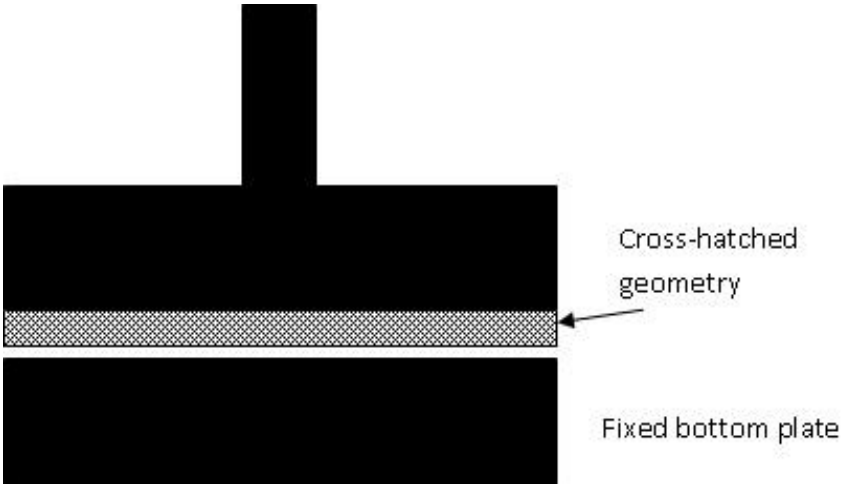

Figure 1-2. Roughened surface spindle.

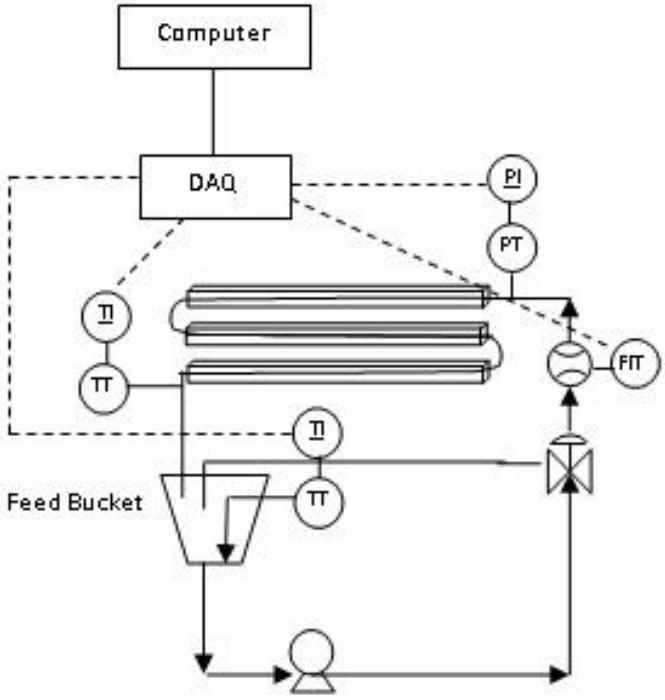

Figure 1-3. Schematic diagram of the tube viscometer used in this research.

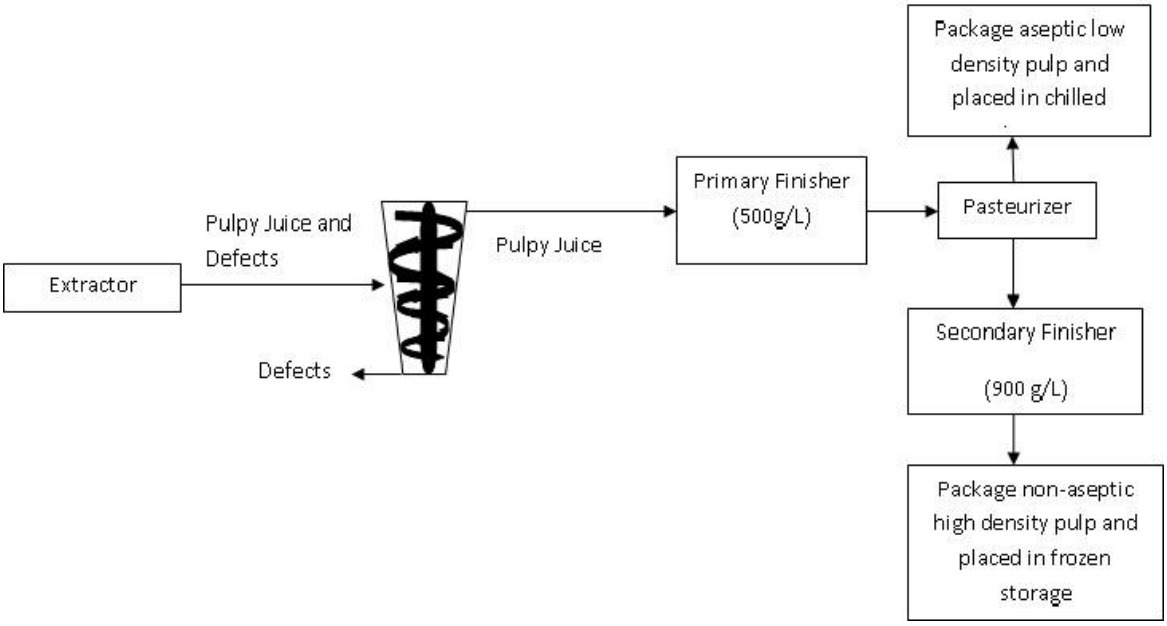

Figure 1-4. Schematic diagram of the production of low and high concentration pulp. Modified from Braddock (1999).

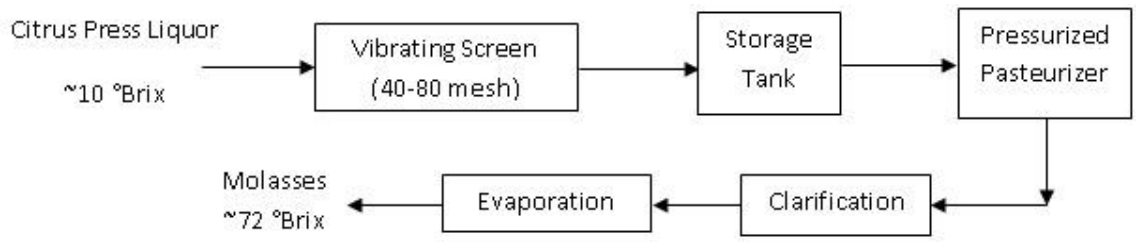

Figure 1-5. Schematic diagram of the production of citrus molasses.

CHAPTER 2
RHEOLOGICAL DETERMINATION OF ORANGE PULP

Introduction

During the 2004/05 growing season, Brazil and the United States were the leading orange producers (39%), while China (7%) and the European (17%) region accounted for a less significant portion. In the 2004/05 growing season over 36% of the oranges produced were processed and a total of 64% growth in world orange production was seen from the 80's (FAO, 2006). In the 2007/08 season, Florida's orange was processed into juice or juice products totaling 3,303.6 million dollars while the by-products: orange pulp, molasses, and essential oils were sold for 136 million dollars (Rahmani & Hodges, 2009).

In the last few years an interest of citrus flavored beverages with mouth feel supplied by pulp has increased, in particular in Asia. This trend has created a new market for intact pulp cells that retain their flavor and structure through processing and shipping. Post fruit extraction, defect removal and primary finishing, the concentration of pulp is approximately 500 $g \cdot L^{-1}$ which is deemed low concentration and can be pasteurized. To continue to remove juice from the pulp a second non-aseptic finisher is employed to bring the concentration of pulp to 800-900 $g \cdot L^{-1}$ which is deemed high concentration. This second concentration stage is necessary to reduce shipping and storage costs, but leaves a problem of sterility. High concentration pulp must be stored frozen in boxes or barrels. A few high concentration pulp aseptic pasteurizers are manufactured but have not been optimized. Currently, small pipe diameters are used to favor heat transfer to the pulp that flows under laminar regime because of its very large

apparent viscosity. The small pipe diameters used to fabricate the pasteurizers lead to high pressure drop which in turn, results in high capital and operating pumping costs. Knowledge of the rheological properties of high concentration pulp is needed for optimal design of processing equipment such as pasteurizers and flow systems. The rheological characterization of many types of paste-like foods including fruit pulps and purees have been performed. Apple pulp, mango puree, and banana puree were all described using the power law (Krokida, Maroulis & Saravacos, 2001). Tomato paste (Fito, Clemente & Sanz, 1983) and peanut butter (Singh, Castell-Perez & Moreira, 2000) have also been characterized. In a recent study, Levati (2010) found that high concentration orange pulp exhibited non-Newtonian, pseudoplastic behavior but shear stress *vs*. shear rate curves were noisy decreasing the reliability of the determinations of apparent consistency coefficient and flow index.

The objective of this study was to characterize the rheological properties of orange pulp at selected concentrations across a range of temperatures found under industrial processing conditions.

Materials and Methods

Materials

Early-mid orange citrus pulp (~500 $g \cdot L^{-1}$) samples donated by the Coca-Cola Company (Auburndale, FL), Early-mid orange citrus pulp (~1000 $g \cdot L^{-1}$) samples were donated by Citrosuco Company (Lake Wales, FL) and Valencia orange citrus pulp (~500 $g \cdot L^{-1}$) produced at the Citrus Research and Education Center (CREC) pilot plant (Lake Alfred, FL) were used for this study. Sodium benzoate was purchased from Fisher Scientific (Waltham, MA).

Equipment and Instrumentation

An industrial juice extractor, FMC 10-79 (Lakeland, FL) with pre-finisher #2 was used in conjunction with a FMC screw finisher (Model 35, FMC Corporation, Hoopeston, Illinois) at 50 psi with a J.U. 52 No. 20 mesh screen to produce high concentration pulp at the CREC pilot plant. A rheometer model AR 2000 interfaced to a PC and "AR Instrument Control" computer program from TA Instruments, (New Castle, DE) were used for the rheological characterization of the pulp.

Methods

Pulp preparation

Concentration determination. Initial pulp concentration was determined with a Quick Fiber apparatus (Philadelphia, PA) and the FMC, FoodTech Procedure for Citrus Products Analysis. Approximately 500 mL of pulp was weighed into a 20 mesh screen and placed on the Quick Fiber apparatus. After 2 min of mechanical shaking, the screen and pulp were weighed. Pulp concentration was calculated as using Equation- 2-1.

$$Concentration(g/l) = \left(\frac{weight\ of\ wet\ pulp(g)}{volume of\ \ juicy\ \ pulp(l)} \right) \quad (2\text{-}1)$$

Pulp concentration. Orange pulp with an initial concentration of ~500 $g.L^{-1}$ was concentrated using a Quick Fiber apparatus (Philadelphia, PA) and the FMC, FoodTech Procedure for Citrus Products Analysis. Approximately 500 mL of pulp was weighed into a 20 mesh screen and placed on the Quick Fiber apparatus. After 50 seconds of mechanical shaking, the screen and pulp were weighed. Pulp concentration was calculated with Equation 2-1. Approximately 4000 mL of ~ 800 $g.L^{-1}$ orange pulp was prepared. Concentration was adjusted by adding back pulp free single strength orange juice until the correct concentration was achieved. Concentration conformation was

performed by the same procedure used to determine initial pulp concentration. After determining that the Citrosuco sample was high concentration, dilutions were made with pulp free single strength orange juice to ~500, 600 and 650 $g.L^{-1}$. Just as before, the concentration was confirmed.

The average concentrations of the samples were 503 ± 8, 597 ± 11, 643 ± 6, and 795 ± 21 $g \cdot L^{-1}$. The large standard deviations in concentrations are due to the variability in pulp source and also the large quantity in which the samples were prepared. Sodium benzoate was added at 0.05% to act as a preservative and anti-mold agent.

Rheological characterization. Prior to any rheological characterization, samples were placed in a water bath model Isotemp 3016S from Fisher Scientific (Waltham, MA) to equilibrate the sample at the selected temperature of 4, 20, 37.5, 57.5, or 80 °C. These temperatures were selected because they fall within the range typically encountered during thermal processing or cold storage in the citrus industry. Preliminary experiments performed using concentric cylinder and hatched parallel plate geometries found a sudden decrease in apparent viscosity caused by slippage. Using a vane geometry, minimized slippage between the geometry surface and the sample because the orange pulp was able to yield between the blades of the vane (Figure 2-9).

After setting the normal force to zero and setting the gap to 4000 μm, approximately 35 mL of orange pulp was placed in the water jacketed cup and the 10.7 cm tall, 1.4 cm radius four-blade vane was placed at the assigned gap. The rheometer was set for continuous shear rate ramp control and to measure shear stress. Three shear rate ranges were selected: from 0 to 1 s^{-1} for 3 min with 60 points 0 to 10 s^{-1} for 6 min with 120 points or 0 to 80 s^{-1} for 6 min with 120 points. Each pulp batch was

analyzed separately. Rheological determinations were carried out in a block design with pulp batch and temperature blocks, and randomized by pulp concentration. Temperature was blocked to reduce experimental time associated with sample thermal equilibration. Pulp was also blocked based on availability from industrial donors. Analytical replicates were performed for each batch and the mean of shear stress and shear rate was reported. The effect of shear rate on shear stress was best fitted to power law after evaluating Herschel-Bulkley, Casson, and Modified Casson models as well. Linear regression was used for model fitting. Consistency coefficient and flow behavior index were determined. Standard errors were calculated from linear regression. The effect of temperature on the consistency coefficient was determined using an Arrhenius-like approach. The apparent activation energy was determined from the linear regression of ln K *vs.* 1/T plot. Linear regression parameters and standard errors were calculated using Microsoft Excel regression analysis tool.

Results and Discussion

The effect of shear rate on shear stress at the highest pulp concentration of this study, 776 $g \cdot L^{-1}$, between 4 and 80 °C for Valencia orange pulp can be seen in Figure 2-1. Shear stress increased up to 256.3 Pa as shear rate increased up to 3.3 s^{-1} at 4 °C. At 21 °C, shear stress increased to 212.5 Pa as shear rate increased to 2.6 s^{-1}. The same trend was seen at 37.5 °C. Shear stress increased to 167.7 Pa as shear rate increased to 2.2 s^{-1}. At 4, 21, and 37.5 °C a sharp increase in shear stress as shear rate increased was followed by immediate sharp decrease at shear rates above approximately 2 s^{-1} indicated slippage. At the higher temperatures of 57.5 and 80 °C, slippage was less pronounced but observed as the rapid leveling off of shear stress as shear rate increased. At 57.5 °C, shear stress increased to 141.3 Pa as shear rate

increased to 3.2 s^{-1}. At 80 °C, shear stress increased to 130.5 Pa as shear rate increased to 2.9 s^{-1}.

In contrast, Figure 2-2 shows the effect of shear rate on shear stress at the lowest pulp concentration of this study, 511 $g \cdot L^{-1}$, between 4 and 80 °C for Valencia orange pulp. For all temperatures below 57.5 °C a sharp peak in shear stress was seen at shear rates between 2.2 and 2.9 s^{-1} then followed by slippage. At 4 °C, shear stress increased to 90.5 Pa as shear rate increased to 2.2 s^{-1}. At 21 °C, shear stress increased to 79.8 Pa as shear rate increased to 2.9 s^{-1}. At 37.5 °C, shear stress increased to 70.1 Pa as shear rate increased to 2.9 s^{-1}. At 57.5 °C, shear stress increased to 65.5 Pa as shear rate increased to 2.6 s^{-1}. At 80 °C a distinct decrease in shear stress was not observed but slippage was indicated by the rapid leveling off of shear stress at a higher shear rate. At 80 °C, shear stress peaked at 41.2 Pa as shear rate increased to 3.2 s^{-1}. At all temperatures shear stress increased with pulp concentration as shown in Figures 2-1 and 2-2. It can be hypothesized that the higher the concentration the more particles present which in turn creates more particle interlocking and therefore a higher shear stress (Nindo, Tang, Powers & Takhar, 2007).

Slippage has been reported in multiphase systems and is a direct effect of the displacement of the dispersed phase away from the solid system boundaries leaving a low viscosity thin liquid layer that acts as a lubricant that cause the material to slip. Slippage comes from the combination of steric, hydrodynamic, viscoelastic, chemical and gravitational forces on the dispersed phase that is adjacent to the solid boundary. Slippage starts at different shear rates but for suspensions in which the dispersed phase consist mostly of large particles, slippage is greatest at low shear rates (Barnes,

1995). Slippage has been reported for food emulsions like peanut butter, mayonnaise and suspensions like tomato concentrate or other emulsions like cement. Slippage interference with true rheological characterization can be greatly reduced by using a vane geometry or roughened surfaces (Sun & Gunasekaran, 2009a, b). One study performed on cement paste using both a vane and concentric cylinder geometry showed that with the vane geometry the true maximum shear stress can be determined and was approximately 150 Pa higher when compared to the concentric cylinder maximum shear stress (Saak, Jennings & Shah, 2001).

Extrapolation of our experimental results indicate that the yield stress was practically zero supporting the use of the power law model to describe our experimental data. The reliability of yield stress measurements is dependent on the method of determination and the sensitivity of the instrument. Because the instrument used to determine the yield stress was very sensitive, accurate yield stress measurements were determined.

Figures 2-3 and 2-4 illustrate the effect of shear rate on shear stress of Valencia orange pulp at different concentrations. At 4 °C and 775 $g \cdot L^{-1}$, shear stress increased to 231.4 Pa as shear rate increased to 1.9 s^{-1}. At 4 °C and 649 $g \cdot L^{-1}$, shear stress increased to 166.9 Pa as shear rate increased to 1.9 s^{-1}. At 4 °C and 585$g \cdot L^{-1}$, shear stress increased to 159 Pa as shear rate increased to 2.9 s^{-1}. At 4 °C and 511 $g \cdot L^{-1}$, shear stress increased to 90.5 Pa as shear rate increased to 2.2 s^{-1}. Figure 2-4 describes the effect of shear rate on shear stress at different concentrations at 80 °C. At 511 $g \cdot L^{-1}$, shear stress increased to 40.4 Pa as shear rate increased to 2.5 s^{-1}. At 585 $g \cdot L^{-1}$, shear stress increased to 61.0 Pa as shear rate increased to 2.6 s^{-1}. At 649 $g \cdot L^{-1}$,

shear stress increased to 78.3 Pa as shear rate increased to 2.9 s^{-1}. Finally, at 775 $g \cdot L^{-1}$ shear stress increased to 130.5 Pa as shear rate increased to 2.9 s^{-1}. When comparing 775 $g \cdot L^{-1}$ at the extreme temperatures (4 and 80 °C), 4 °C had a more distinct peak with slippage taking place at a slower shear rate. Both figures show the same trend that the higher the concentration the higher the shear stress at any given shear rate. This trend is most likely due to the increased particle interlocking that caused more resistance to flow and therefore a higher shear stress. In agreement, as the soluble solid content of blueberry puree (without slippage) increased from 10 to 25 °Brix at 25 °C the shear stress increased from approximately 12 to 150 Pa (Nindo, Tang, Powers & Takhar, 2007).

The power law model was used to determine consistency coefficient (K) and flow behavior index (n) at selected concentrations and temperatures, at shear rates below the shear rate at which slippage occurs.

At an average concentration of 503 $g \cdot L^{-1}$, n-values ranged from 0.18 to 0.42 with the lowest n-value at the hottest temperature of 80 °C while the highest n was at 4 °C. At the next concentration, 597 $g \cdot L^{-1}$, the flow behavior index ranged from 0.22 to 0.41. Like 503 $g \cdot L^{-1}$ pulp, the lowest n was at the highest temperature while the highest n was at 37.5 °C. The flow behavior index ranged from 0.22 to 0.40 at an average concentration of 643 $g \cdot L^{-1}$. In the same fashion as the previous two concentrations the lowest n-value was at the hottest temperature. However, the highest n was at 20 °C. The highest concentration, 795 $g \cdot L^{-1}$, showed the same trends as the lowest two concentrations. The n-values for 795 $g \cdot L^{-1}$ ranged from 0.21 to 0.39. A flow behavior index of less than one defines the fluid as non-Newtonian pseudoplastic fluid (Steffe,

1996). Temperature and concentration did not have a large effect on the flow behavior index.

There are two general trends in the effects of temperature and concentration of the consistency coefficient data but with a few inconsistencies. First, as the concentration increased from 503 to 795 $g \cdot L^{-1}$ the consistency coefficient increased. Second, as the temperature increased from 4 to 80 °C the consistency coefficient decreased. For 503 $g \cdot L^{-1}$, the K ranged from 33.0 to 70.0 $Pa \cdot s^n$. At 597 $g \cdot L^{-1}$, K ranged from 59.9 to 123.5 $Pa \cdot s^n$, while at 643 $g \cdot L^{-1}$ it ranged from 74.9 to 137.2 $Pa \cdot s^n$. At the highest concentration 795 $g \cdot L^{-1}$, the consistency coefficient ranged from 112.3 to 233.6 $Pa \cdot s^n$. Both temperature and concentration had an effect on K. The decrease in K can be explained because as the temperature increased from 4 to 80 °C greater intermolecular distances (thermal expansion) existed which created a decrease resistance to flow and, therefore, a decrease in K or a decrease in apparent viscosity (Haminiuk, Sierakowski, Maciel, Vidal, Branco & Masson, 2006; Haminiuk, Sierakowski, Vidal & Masson, 2006). Similarly, the increase in K from the increase in concentration of solid particles in suspension can be attributed to the greater resistance to flow. Figure 2-8 shows the large variation among the orange pulp samples where two batches were from industry and one was produced in house. The variation among the samples can be explained by factors such as the type of finisher used to produce the pulp, different processing methods/conditions or the variety of orange. Orange pulp is a biological material in with inherent variation in size, shape, and length of the juice sac. A second place where the variation could account for the large difference between the power law parameters could be the type of extractor used. Either the Brown or the FMC extractor

would have been used. The Brown extractor reams the fruit at different pressures which could affect the quality of intact pulp sacs; the higher the pressure the more significant the pulp damage and the less accurate rheological characterization. In comparison, the FMC extractor works on the principle of squeezing the juice out of the fruit with a strainer tube attached to the extractor cup. The quality of pulp is dependent of the tube orifice size; the bigger the tube slots the less pulp damage. Finishing of the pulp could also account for the variation in the data. There are two types of finishers—paddle and screw finisher. Paddle finishers work at different speeds (rpm) and with adjustable paddle pitches. At a higher rpm, more pulp separation will take place. Also depending on screen size the dryness of the pulp will vary. The screw finisher works by turning a screw and forcing the pulpy juice against a pressurized discharge. The higher the pressure (tight/hard finish) the more dry pulp is produced. Just as the paddle finisher, different size screens can be used to adjust the quality of the pulp produced. Just like extraction, true rheological characterization should be done with high quality pulp. Depending on the type of finisher and extractor different qualities of intact pulp cells can be produced. At each different orange processing plant a different extractor and/or finisher was used to produce the samples which could have lead to some of the variation in the data. Sodium benzoate was added at such a small level (0.05%) that its effect on the results of the rotational rheometry analysis was negligible.

Mango pulp (20 °Brix) ranging in temperature from 30-70 °C had a flow behavior index range of 0.16 to 0.19 and a consistency coefficient range of 27.41 to 31.85 ($Pa \cdot s^n$) measured at a shear rate of 0 to 13 s^{-1} (Khandari, Gill & Sodhi, 2002). Apple pulp at 25 °C has a K value of 65.03 $Pa \cdot s^n$ and a flow behavior index of 0.084 (Kokini, 1992). All

three fruit pulps have flow behavior indexes below 1.0 with orange pulp being the highest and the apple pulp being the most pseudoplastic. When comparing the consistency coefficient for these three fruit pulps, the consistency coefficient was the same magnitude except for the orange pulp at the highest concentration. The variability in flow behavior index of orange pulp was greater than for other fruit purees and pastes because of the larger and more heterogeneous, variable size distribution of pulp particles. Power law parameters for other fruit pastes can be found in Table 2-2.

When comparing to an earlier report for high concentrated orange (Levati, 2010) pulp (Table 2-3), both studies had flow behavior indexes below 1.0. The Levati study flow behavior index ranged from 0.082 to 0.152 while the n-value ranged from 0.18 to 0.42 in this study. The consistency coefficient values were much lower in Levati (2010), 50.83 – 97.31 $Pa \cdot s^n$ while 47.93 – 233.6 $Pa \cdot s^n$ in this study. This difference in K can be attributed to the use of the shear rate range of 0-1300 s^{-1} by Levati (2010) that did not account for slippage occurring, as mentioned earlier at shear rate around 2 s^{-1}.

Other foods with complex rheology have been modeled by the power law. Tomato concentrates flow behavior index ranged from 0.24 to 0.44 while the K ranged from 0.12 to 86.82 ($Pa \cdot s^n$) for a temperature range of 15-70 °C (Fito, Clemente & Sanz, 1983). In the study performed by Fito, Clemente et al. (1983), no slippage was reported. Peanut butter is an emulsion that displayed slippage and has a flow behavior index of 0.57 and a consistency coefficient of 250.85 $Pa \cdot s^n$ at a shear rate of 38.3 s^{-1}(Citerne, Carreau & Moan, 2001; Singh, Castell-Perez & Moreira, 2000). Peanut butter, slippage occurred at a shear rate of 38.3 s^{-1}, higher than for orange pulp (~4 s^{-1}). This difference explains in

part the obvious difference between these two materials. According to Barnes (1995), concentrated suspensions with large dispersed phase have slippage at low shear rates.

The apparent activation energy (E_a) for the effect of temperature on K was calculated as:

$$\ln K = \ln A - (\frac{E_a}{RT}) \tag{2-2}$$

Where R is the gas constant, A is a constant and T is the absolute temperature.

Figure 2-5 shows the linearization of both shear stress and shear rate. The linear portion of the graph was determined and the slope and intercept were calculated. Linearization of power law:

$$\ln \sigma = \ln K + n \ln \gamma \tag{2-3}$$

Since two analytical replicates were done, both replicates were averaged to determine the power law parameters for that shear rate, concentration, and temperature combination. For all data, the linear portion always occurred at shear rates below 4 s^{-1}. Only the data for shear rates 0 to 10 s^{-1} were considered because the all data points before slippage fell within that range. Shear rates above 10 s^{-1} slippage occurred while shear rates in the range of 0-1 s^{-1} gave a pseudo-Newtonian fluid that does not accurately describe orange pulp. Table 2-1 shows the average power law parameters at different concentrations and temperatures. Figure 2-6 shows the activation energies calculated from Table 2-1 for all studied pulp concentrations.

For batch 1 generally E_a increased from 3.2 to 10.7 kJ·mol^{-1} except at 637 g·L^{-1} where the apparent activation energy was 7.8 kJ·mol^{-1}. The apparent activation energy for batch 2 first increased from 7.3 to 9.6 kJ·mol^{-1} then decreased to 6.2 kJ·mol^{-1} at 644 g·L^{-1} and increased to 8.0 kJ·mol^{-1} at 817 g·L^{-1}. Batch 3 had an approximately constant

apparent activation energy of 10.6 kJ·mol^{-1} then increased to 11.7 kJ·mol^{-1} at 775 g·L^{-1}(Figure 2-6). At an average concentration of 503 g·L^{-1}, the apparent activation energy ranged from 3.2 to 10.7 kJ·mol^{-1} while the standard error ranged from 71.7-5.4. The activation energy ranged from 8.9 to 10.5 kJ·mol^{-1} with a standard error range of 6.8-0.9 for an average concentration of 597 g·L^{-1}. At an average concentration of 643 g·L^{-1} the activation energy range was 6.2 to 10.6 kJ·mol^{-1} and a standard error range of 5.1 to 3.7. At an average concentration of 795 g·L^{-1} the activation energy range was 8.0 to 11.6 kJ·mol^{-1} with a standard error range of 8.7-6.8. As the average concentration increased from 503 g·L^{-1} to 795 g·L^{-1} the average activation energy increased from 7.1 to 10.2 kJ·mol^{-1} except at 643 g·L^{-1} where the apparent activation decreased. The higher the apparent E_a, the greater the effect of temperature on K which is especially seen at higher concentrations (Ozkanli, 2008; Steffe, 1996).

Comparing the apparent activation energies of the consistency coefficient to other fruit pulps, orange pulp is of similar magnitude. The consistency coefficient for mango pulp has an apparent activation energy range of 8.9 to 11. 8 kJ·mol^{-1} for a shear rate range of approximately 1-13 s^{-1} (Khandari, Gill & Sodhi, 2002). A study performed on whole araçá pulp found that at a constant shear rate of 50 s^{-1} the activation energy of the consistency coefficient was 11.03 kJ·mol^{-1} while the consistency coefficient of butia pulp had an activation energy range of 8.3 to 10.01 kJ·mol^{-1} for a shear rate range of 15.59 to 300 (s^{-1}) (Haminiuk, Sierakowski, Maciel, Vidal, Branco & Masson, 2006; Haminiuk, Sierakowski, Vidal & Masson, 2006). The consistency coefficient for orange juice concentrate had an activation energy of 6.6 kJ·mol^{-1} at approximate shear rates of

0-500 (s^{-1}).Comparing the activation energy for a food that displays slippage, tahin, had an E_a of 30.3 ($kJ \cdot mol^{-1}$) which was higher than orange pulp (Alpaslan & Hayta, 2002).

Industrial samples used to determine the rheological properties were probably pasteurized using a pulp pasteurizer while the non-industrial sample was pasteurized as pulpy juice before finishing. One sample was not pasteurized before finishing to assess the effect of pectin methylesterase. The unpasteurized sample was placed in refrigerated storage for 2 days before rheological analysis. Rheograms of shear stress versus shear stress showed a much higher shear stress for the unpasteurized sample while slippage was still present (Figure 2-7). Both the consistency coefficient and the apparent activation energy were higher for the unpasteurized sample. Pectin methylesterase (PME) desertifies pectin and results in gel formation with in the presence of divalent cations. Gel formation modifies the rheological properties of citrus juices and pulp. To minimize the removal of pectin methoxy groups, PME needs to be inactivated. Most PME is inactivated by heating at 88 °C for 10-15 seconds (Kimball, 1999). Gel formation in the pulp affects the quick fiber test by giving higher concentration values because less juice is mechanically removed as water molecules are entrapped in the gel and a more viscous liquid phase entangles the solid particles. The consistency coefficient ranged from 829.49 to 55.16 $Pa \cdot s^n$ while the E_a ranged from approximately 19 to 25 $kJ \cdot mol^{-1}$. Both of these increases are due to the gel formation in the pulp. The flow behavior index was not greatly affected and all values remained below 1.0 and ranged from 0.18 to 0.75. In order to have the true rheological characterization without the interference of gel formation, the pulpy juice should be pasteurized to inactivate pectin methylesterase.

Conclusion

Orange pulp 503 to 795 $g \cdot L^{-1}$ (standard deviation range of 6 to 21 $g \cdot L^{-1}$) behaved as a pseudoplatic fluid that was modeled with the power law at 4 to 80 °C, at shear rates below 2-4 s^{-1} .Orange pulp displayed slippage at shear rates above 2 and 4 s^{-1}. Slippage was more pronounced at low temperatures as well as at high concentrations. Both temperature and concentration had a small effect on the flow behavior index as it ranged from 0.18 to 0.42 and displayed no particular trend with temperature or concentration. Conversely, the consistency coefficient was greatly affected by temperature and concentration. As the temperature increased K decreased, while as the concentration increased the consistency coefficient increased. The average apparent activation energy for the consistency coefficient ranged from 7.1 to 10.2 $kJ \cdot mol^{-1}$ and was affected by concentration. Although similar in trend, the rheological behavior of orange pulp varied widely depending on the source and handling conditions. In this study the relationship between shear rate and shear stress was determined for orange pulp at different concentrations and temperatures. Because of the presence of slippage, with the determined parameters (K and n), only the friction factor without slippage, that is at very small shear rates can be calculated. Therefore, with these data alone, calculations cannot be performed to optimize and design processing equipment and determine proper pump selection because the relationship between shear rate and shear stress cannot be correlated directly to a friction coefficient. Hence, pressure drop in pipes and fittings cannot be calculated. Determination of slippage coefficients using capillary viscometry is needed to complete the characterization of orange pulp.

Table 2-1. Average (n = 3) power law parameters, activation energies, and relative standard deviation for different temperatures and concentrations of orange pulp.

Temperature (K)	503 g·L^{-1}		597 g·L^{-1}		643 g·L^{-1}		795 g·L^{-1}	
	n	K (Pa·s^n)	n	K (Pa·s^n)	n	K (Pa·s^n)	n	K (Pa·s^n)
	RSD (%)		RSD (%)		RSD (%)		RSD (%)	
277	0.42	70.0	0.41	123.5	0.36	137.2	0.39	233.6
	24.2	77.9	14.2	51.1	13.2	51.8	28.6	40.1
293	0.32	50.5	0.29	91.3	0.40	109.7	0.33	180.1
	3.74	60.0	5.3	49.4	22.8	43.5	14.5	51.7
311	0.37	50.9	0.34	83.6	0.30	88.9	0.30	146.7
	34.5	61.9	35.6	50.9	23.9	47.2	9.0	47.4
331	0.37	43.0	0.25	61.5	0.29	78.3	0.23	115.1
	34.2	47.9	16.5	48.5	17.9	45.1	4.5	47.6
353	0.18	33.0	0.22	59.9	0.22	74.9	0.21	112.6
	60.2	55.9	57.01	0.8	40.6	4.3	47.9	11.7
E_a (kJ·mol^{-1})	--	7.1	--	9.7	--	8.2	--	10.2
RSD (%)	--	53.0	--	8.1	--	27.4	--	18.5

Table 2-2. Power law parameters for various fruit and vegetables (Krokida, Maroulis & Saravacos, 2001).

Material	Temperature °C	Concentration (% solids)	Shear Rate (s^{-1})	n	K ($Pa \cdot s^n$)
Apple	25.0	18.2	100-2000	0.4	20.2
	29.2	63.2	5-50	1.0	0.2
	29.6	52.8	100-2000	0.9	40.1
	82.0	8.1	5-50	0.3	9.0
	27.0	8.1	100-2000	0.3	12.7
	30.0	8.09	5-50	0.3	11.6
Apricot	27.0	1.9	5-50	0.3	167.5
	30.0	5.3	5-50	0.3	6.8
	27.0	6.3	5-50	0.4	7.2
Currant black	32.5	49.9	ND	1	0.0
Guava	24.0	15.4	100-10000	0.8	5.3
	23.4	10.3	100-10000	0.5	3.9
Mango	25.0	16.0	20-250	0.3	12.3
	25.0	17.0	20-250	0.3	27.8
	50.0	18.7	20-250	0.4	4.3
	25.0	16.0	20-250	0.3	10.0
	24.2	9.3	20-250	0.3	2.1
	36.4	28.8	100-600	0.8	0.4
	0.9	65.1	100-500	0.7	16.5
Peach	27.0	2.8	5-50	0.4	85.6
	26.9	54.9	50-700	1.0	0.1
	30.0	7.6	5-50	0.3	7.2
Pear	26.4	36.1	1-2000	0.4	81.4
	26.3	60.3	100-1000	1.0	0.2
	55.4	28.8	0.1-2600	0.5	10.4
	27.0	14.6	100-2000	0.4	5.3
Pineapple	7.5	41.1	0-500	0.8	0.8
	37.5	21.7	100-600	0.9	0.1
Raspberry	30.0	27.7	3-2000	0.9	0.5
Tamarind	24.0	21.8	3-1300	0.8	0.0
	46.9	35.7	10-400	0.7	1.2
Tomato	25.0	21.1	4-576	0.3	91.6
	40.7	18.7	ND	0.3	19.7
	55.6	15.5	500-800	0.4	3.9
	57.3	30.0	500-800	0.4	13.4
	20.0	8.1	0-10	0.4	5.7
	33.6	24.7	4-576	0.4	98.6

Table 2-3. Power law parameters and apparent viscosities at selected shear rates (s^{-1}) for 850 $g \cdot L^{-1}$ orange pulp (Levati, 2010).

Temperature °C	n	K ($Pa \cdot s^n$)
11	0.082	97.31
25	0.114	67.286
38	0.137	53.226
50	0.152	50.836

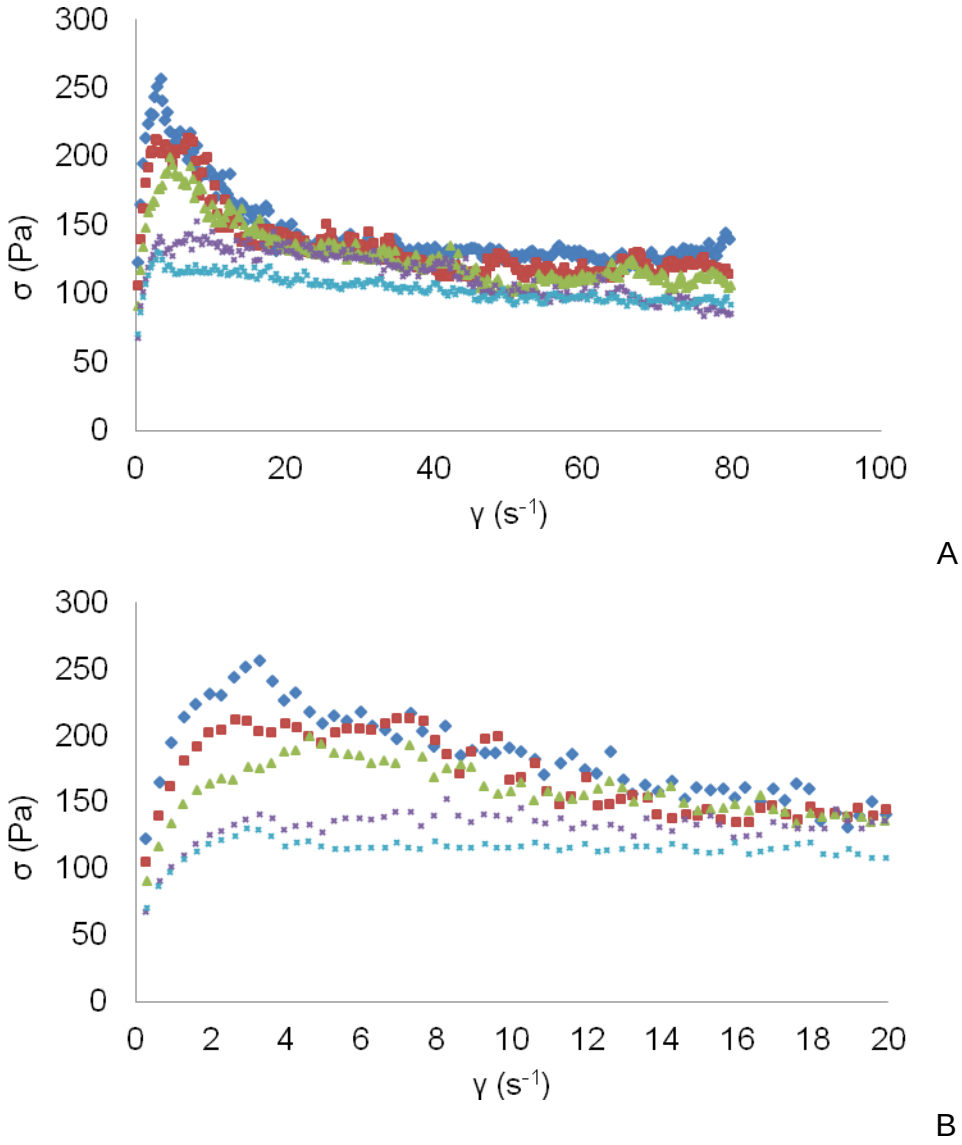

Figure 2-1. Effect of shear rate on shear stress at (♦) 4 °C, (■) 21 °C, (▲) 37.5 °C, (X) 57.5 °C and (*) 80 °C for 776 g·L^{-1} Valencia orange pulp. A) Shear rate 0-80 s^{-1}, B) Region prior and immediately after slippage occurs.

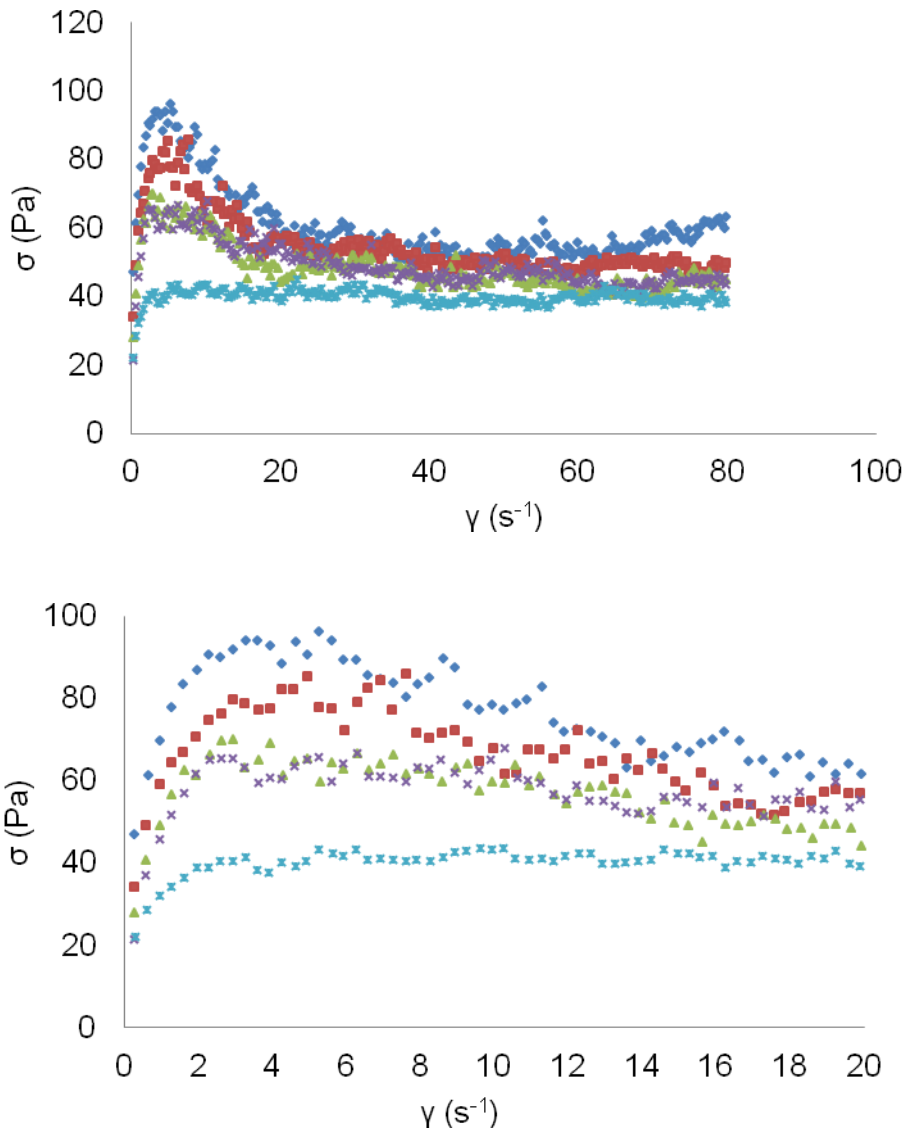

Figure 2-2. Effect of shear rate on shear stress at (♦) 4 °C, (■) 21 °C, (▲) 37.5 °C, (X) 57.5 °C and (*) 80 °C for 511 g·L^{-1} Valencia orange pulp. A) Shear rate 0-80 s^{-1}, B) Region prior and immediately after slippage occurs.

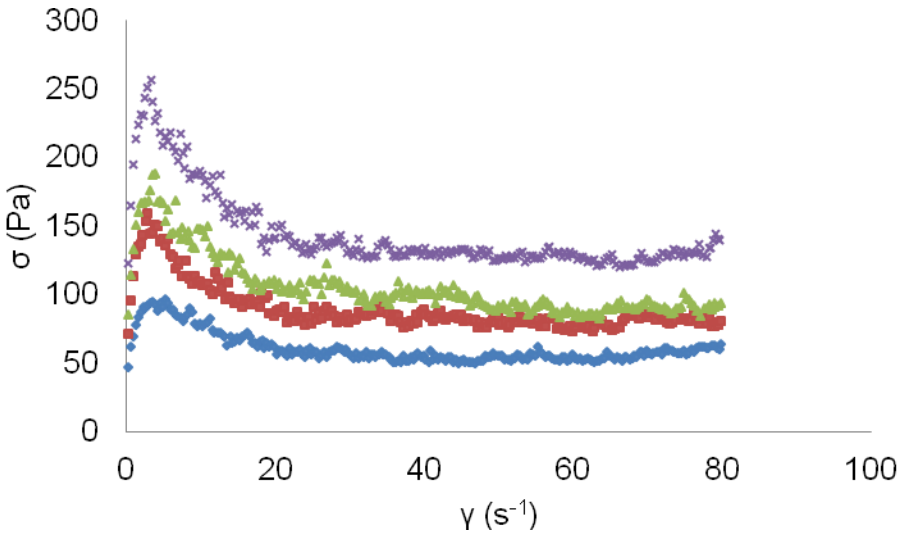

A

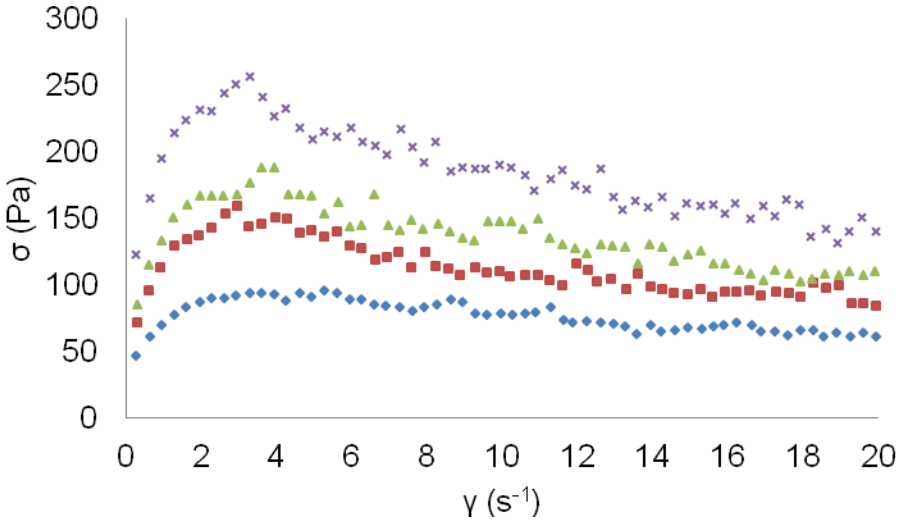

B

Figure 2-3. Effect of shear rate on shear stress at (♦) 511 g·L^{-1}, (■) 585·g·L^{-1}, (▲) 649 g·L^{-1} and (X) 775 g·L^{-1} for 4 °C for Valencia orange pulp. A) Shear rate 0-80 s^{-1}, B) Region prior and immediately after slippage occurs.

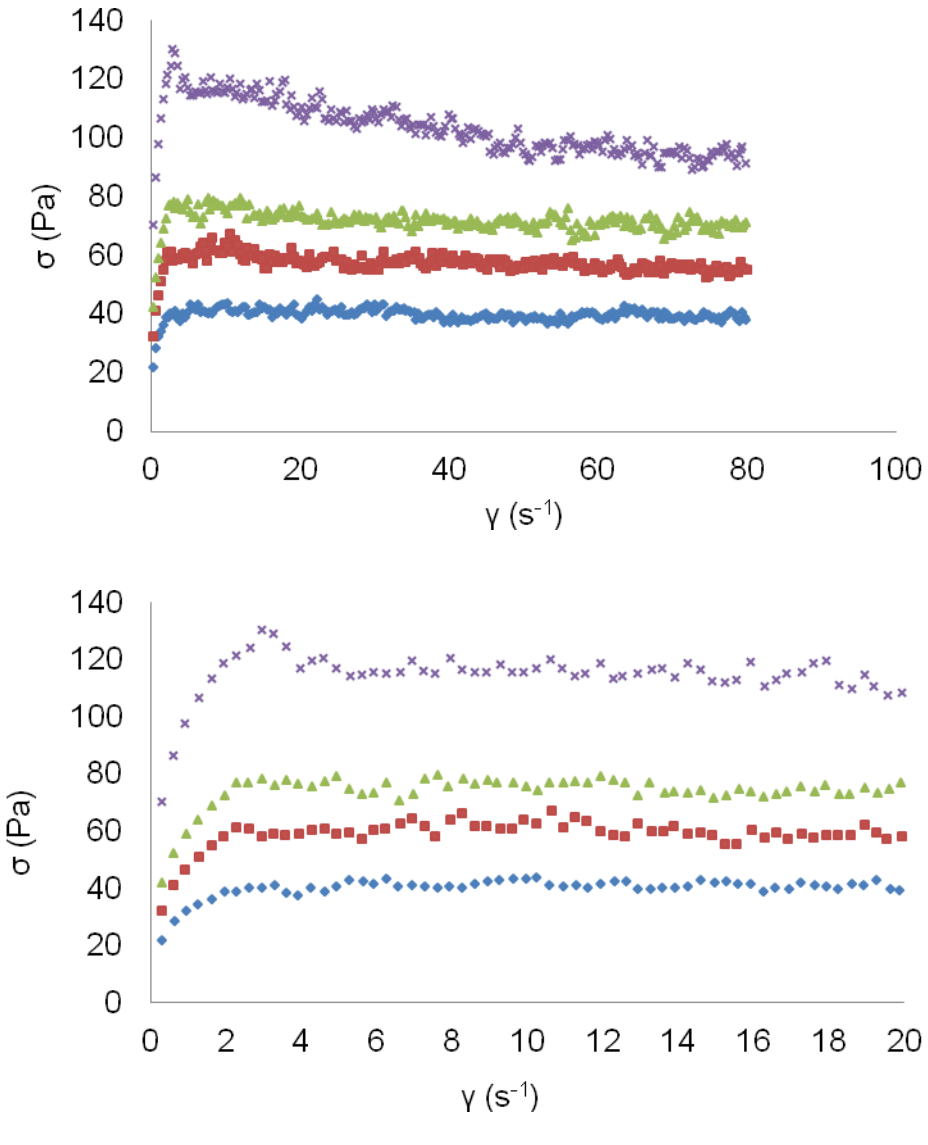

Figure 2-4. Effect of shear rate on shear stress at (♦) 511 g·L^{-1}, (■) 585·g·L^{-1}, (▲) 649 g·L^{-1} and (X) 775 g·L^{-1} for 80 °C for Valencia orange pulp. A) Shear rate 0-80 s^{-1}, B) Region prior and immediately after slippage occurs.

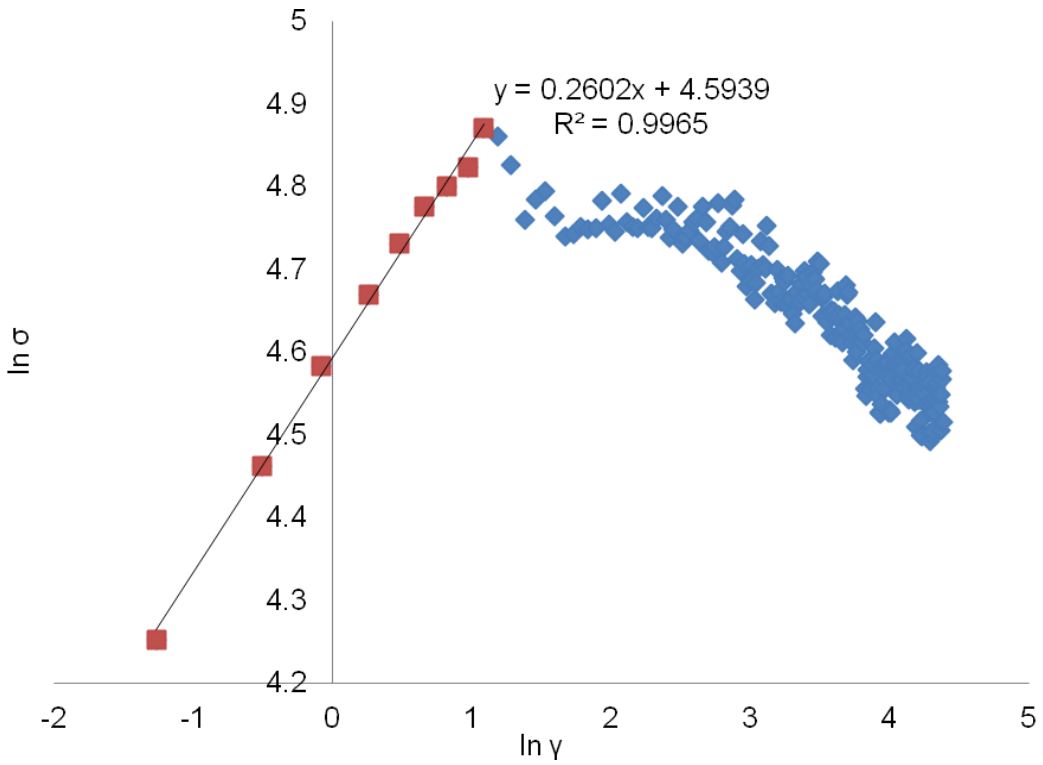

Figure 2-5. Plot of ln(σ) *vs*. ln(γ). The linear portion (■) indicates the region where power law applies.

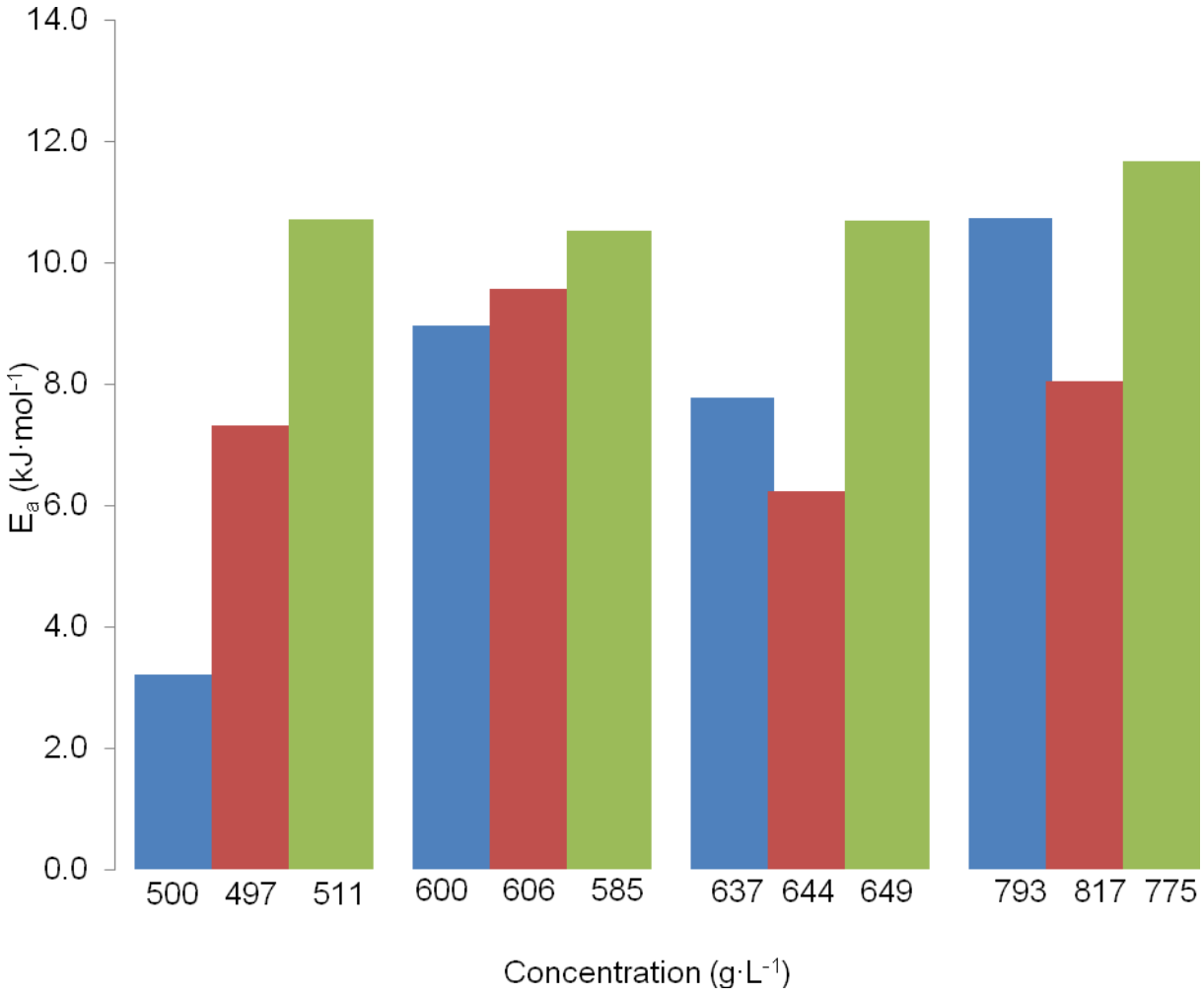

Figure 2-6. Apparent activation energy of consistency coefficient for each batch at low shear rates in the absence of slippage. (■) batch 1, (■) batch 2, (■) batch 3.

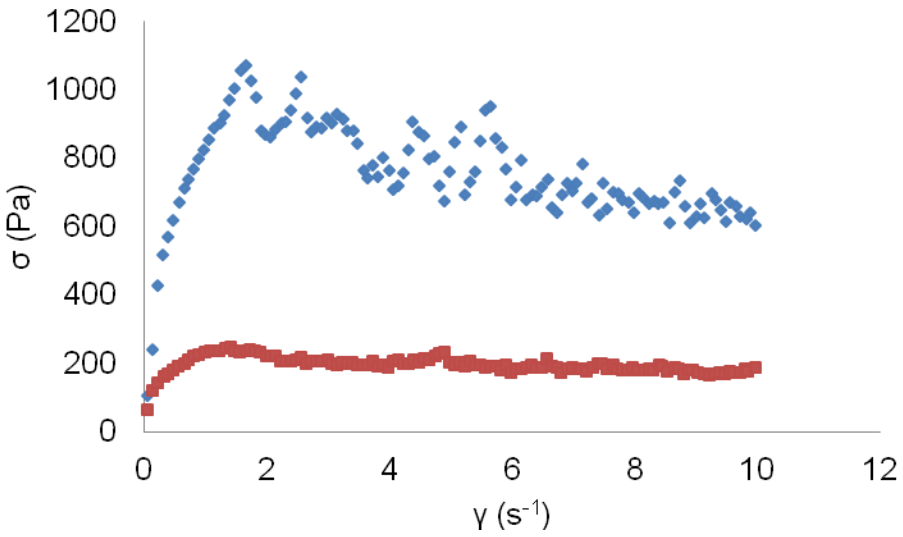

Figure 2-7. Effect of pasteurization on shear stress at selected shear rates at 4 °C for 795.1 g·L^{-1} orange pulp.(♦) Unpasteurized and (■) Pasteurized.

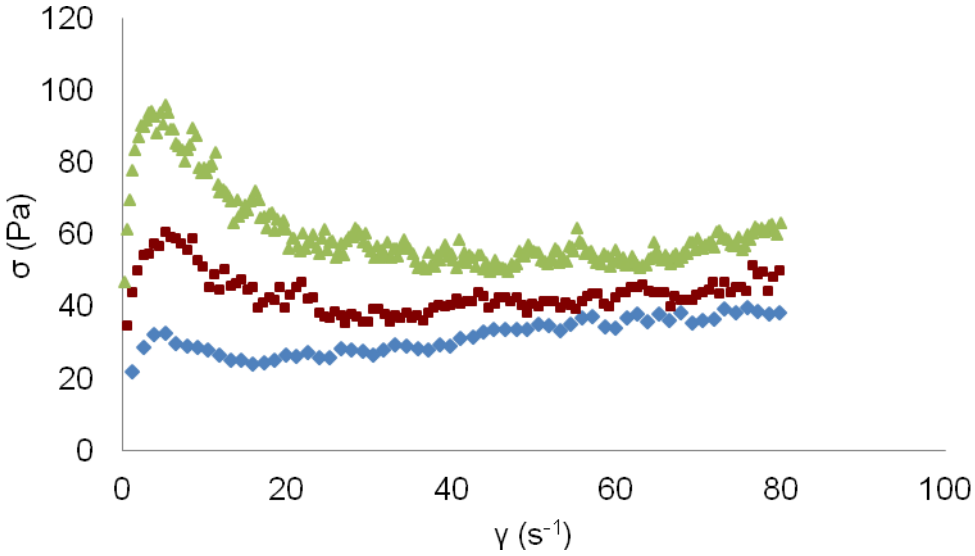

Figure 2-8. Variation among batches of industrial and non industrial orange pulp at 4 °C and 503 g·L^{-1}. (♦) Industrial Early-mid orange pulp source 1, (■) Industrial Early-mid orange pulp source 2 and(▲) Non industrial Valencia orange pulp

Figure 2-9. Vane geometry used with AR 2000 rheometer.

CHAPTER 3
DETERMINATION OF PRESSURE DROP FOR ORANGE PULP

Introduction

The complete fundamental rheological characteristics of orange pulp are not fully understood. Orange pulp can be described as a power law fluid that displays slippage at very low shear rates. Rheological characterization using rotational rheometers does not allow predicting friction factors, hence pressure drop in pipes and fittings because slippage occurs at shear rates lower than what is found in industrial conditions. Capillary viscometers are used to measure apparent viscosity of concentrated suspensions at shear rates produced in industrial processes such as extrusion, mixing, pumping, and conveying (Shukla & Rizvi, 1995; Wang, Lam, Joshi & Chen, 2010). The use of capillary viscometry to determine the slippage coefficient is recommended but complicated because it requires several independent determinations at several flow rates and with several pipe diameters. Other effects such as partial migration, and entrance effects need to be corrected for (Shukla & Rizvi, 1995).

Wall slippage can be detected through the methods of Mooney and Jastrzebski but are limited to Newtonian fluids and not suitable for non-Newtonian suspensions that have significant migration (Wang, Lam, Joshi & Chen, 2010). In capillary flow, the section that is perpendicular to the direction of flow has shear rates and shear forces that are different from the total flow which causes the particles in the suspension to migrate away from the wall and towards the center (Wang, Lam, Joshi & Chen, 2010). For pseudoplastic fluids with slippage, shear rates are higher at the wall (Shukla & Rizvi, 1995). Also when the particle density is different from the suspending liquid, particle migration is increased which increases flow instability. In less concentrated

fluids or fluids without suspended particles less friction is created and, therefore, have a decreased pressure (Wang, Lam, Joshi & Chen, 2010).

The objective of this study was to determine slippage coefficients and pressure drop of orange pulp by capillary viscometry. A modified correction approach was taken to correct for the effects of slippage and particle migration. Pressure drop and flow rate were measured and slip coefficients for orange pulp were calculated from capillary and rotational viscometry measurements.

Materials and Methods

Materials

Early-mid orange citrus pulp (~1000 $g \cdot L^{-1}$) samples were donated by Citrosuco Company (Lake Wales, FL) and Valencia orange citrus pulp (~850 $g \cdot L^{-1}$) produced at the Citrus Research and Education Center (CREC) pilot plant (Lake Alfred, FL) were used for this study. Sodium benzoate was purchased from Fisher Scientific (Waltham, MA).

Equipment and Instrumentation

An industrial juice extractor, FMC 10-79 (Lakeland, FL) with prefinisher #2 was used to produce pulpy juice that was pasteurized in a nominal 0.0254 m (1 in) diameter Feldmeier Double Tube Heat Exchanger (Syracuse, NY). The pulpy juice was heat treated to inactivate pectin methyl esterase at 91 °C for approximately 20 s and immediately cooled to 4 °C. Pasteurized pulpy juice was then finished with a FMC screw finisher (Model 35, FMC Corporation, Hoopeston, Illinois) at 50 psi with a J.U. 52 No. 20 mesh screen to produce high concentration pulp at the CREC pilot plant.

Pulp densities were determined with the FMC, FoodTech Procedure for Citrus Products Analysis. Approximately 500 g of pulp were weighed, poured in a 20 mesh

screen basket, placed on a Quick Fiber apparatus from FMC (currently John Bean Technology Corp.) Serial No. 67-94, (Philadelphia, PA) and mechanically shaken for 2 min. Pulp concentration was calculated as:

$$Concentration(g/l) = \left(\frac{weight\ of\ wet\ pulp(g)}{volume of\ juicy\ pulp(l)} \right) \quad (3\text{-}1)$$

Once high concentration was confirmed, sodium benzoate was added at 0.05% as a preservative to increase storage time.

Average concentrations of 854 $\pm$ 19, 749 $\pm$ 21, 649 $\pm$ 26, and 545 $\pm$ 20 g·L^{-1} were used. The large standard deviations in concentration are due to the variability in pulp source and to the difficulty in adjusting the concentration of the large quantities of juice by - adding single strength pulp free orange juice and confirming concentrations with the Quick fiber method explained above.

Figure 1-3 is a schematic of the experimental set-up. Prior to pressure readings, approximately 19 L of pulp were loaded in the feed tank and the a section of a 22.91 mm diameter (1 in nominal) pasteurizer was primed with a semihydraulic diaphragm pump model 9910-D1064 4 from Hypro High Pressure (New Brighton, MN). Pulp was re-circulated to the feed tank until a constant flow was achieved indicating the removal of any entrapped air and data pressure and flow rate data were collected.. The total system length (pipe and connection hoses) was 11.27 m. In addition, pulp temperature was adjusted (4, 10, 21.5, 33, or 50 °C $\pm$ 2.5) using the pasteurizer heating (steam) or cooling (chilled water) sections. Verification of steady state temperatures was done by ensuring that the temperature in the feed tank and the temperature at the discharge were within 2.5 °C. Temperature was measured with type-T thermocouples from Omega

(Stamford, CT). Pressure was determined with a PX44E0-500GI high-pressure flush diaphragm transmitter from Omega (Stamford, CT). The flow rate was controlled by adjusting the flow rate of a by-pass at the discharge of the pump that re-circulated a portion of the flow back to the feed bucket. Flow rate was measured with an electromagnetic flow meter model 8711 wafer sensor and transmitter model 8732 from Rosemount (Chanhassen, MN). The upper flow rate value limit was set to 8.37 $m^3 \cdot hr^{-1}$. Confirmation of flow meter calibration was done by weighting the total mass of pulp collected over selected periods of time at five flow rates with a concentration of approximately 543 $g \cdot L^{-1}$ at 21 °C. Pressure, temperature, and flow rate data was collected using a National Instruments data acquisition board model NI 9219 (Austin, TX) and a computer program written in LabVIEW10 (Austin, TX) (Figures 3-1 and 3-2).

Each pulp batch was analyzed separately. Capillary viscometry determinations were carried out in a block design with pulp batch and temperature blocks, and randomized pulp concentration. Temperature was blocked to reduce experimental time associated with sample thermal equilibration. Each pressure drop determination was run for 1 min. The mean and standard deviation of triplicates were reported.

Calculations

In this experiment, the inlet was the pressure from the pump while the outlet was atmospheric pressure therefore only one pressure sensor was needed. In this study, the pressure transducer was placed at approximately 2.6 m (114 diameter > 90 diameter required) from the discharge of the pump which results in fully developed flow. Therefore, entrance corrections were not necessary (Figure 1-3). The sensitivity of the pressure transducer was rather small in view of the low pressures (8.71-64.85 psi) that

were measured as a result of slippage. It would have been best to use a smaller range pressure transducer to achieve the most accurate pressure measurements.

Experimental pressure and flow rate data were collected knowing that slippage decreases pressure drop due to friction compared to flow without slippage (Appendix A). The corrected slip coefficient (β_c) was determined from the difference between the flow rates of the measured (Q_m) and calculated without slippage (Q_{ws}) at the same pressure. Data from chapter 2 of shear stress vs. shear rate at shear rates where slippage does not occur were used to calculate Q_{ws}. The procedure used for determining the flow rate without slippage for a given pressure drop for orange pulp is:

1. Estimate friction factor using the generalized Reynolds number for power law fluids (Equation 3-2).

$$\mathrm{Re}_n = 2^{3-n}\left(\frac{n}{3n+1}\right)^n\left(\frac{D^n \rho v^{2-n}}{K}\right) \tag{3-2}$$

Where D is the diameter (m), ρ density ($kg \cdot m^{-3}$), v is the velocity ($m \cdot s^{-1}$) and the power law parameters K and n at shear rates low enough to avoid slippage (Chapter 2). Approximations of both were determined from an Arrhenius-like approach because the temperatures used in the capillary viscosity experiments were different from the rotational rheology. Because in all cases Re was below the critical value for laminar flow, the friction factor was calculated as:

$$f = 16 \big/ \mathrm{Re}_n \tag{3-3}$$

2. Determine flow rate without slippage (Q_{ws}) at the same pressure drop recorded for pulp flow with slippage. Bernoulli's equation (Equation 3-4)

$$\Delta p = \frac{g(z_2 - z_1)}{g_c} + \frac{(v_2^{\,2} - v_1^{\,2})}{2g_c} + \frac{2f\bar{v}^2 L\rho}{g_c D} + K_{fe}\left(\frac{\bar{v}_a^{\,2}}{2g_c}\right) + K_{fc}\left(\frac{\bar{v}_b^{\,2}}{2g_c}\right) + K_{ff}\left(\frac{\bar{v}_a^{\,2}}{2g_c}\right) \tag{3-4}$$

Where p is pressure (Pa), g is gravity (m/s^2), z is elevation (m), g_c is Newton's law proportionality factor for gravitational force, L is length of pipe (m), K_{fe} is the coefficient for expansion, $\bar{v}_a$ is the velocity after expansion, K_{fc} is the coefficient for contraction, $\bar{v}_b$ is the velocity after contraction and K_{ff} is the coefficient for valves and fittings. The K_{ff} for a 180° U-Shaped bend was 0.2. Also the velocity is equal to the volumetric flow rate divided by cross sectional area. Due to the horizontal step up of the capillary system, the elevation term of Bernoulli's equation was null. The velocity term was also null because the pipe diameter was constant. There were no sudden contractions or expansions, therefore, those terms were neglected. Equation 3-4 can then be rewritten in terms of flow rate (without slippage) as:

$$Q_{ws} = (r^2\pi)\sqrt{\frac{(\Delta p_m)}{\frac{2fL\rho}{g_c D} + k_{ff}\left(\frac{1}{2g_c}\right)}} \tag{3-5}$$

Where r is the radius (m) and Δp_m is measured pressure drop (Pa).

3. Calculate the corrected slip coefficient (β_c) (Equation 3-6),

$$\beta_c = \left(\frac{Q_m - Q_{ws}}{\sigma_w r\pi}\right) \tag{3-6}$$

where shear stress at the wall (σ_w) is calculated from the measured pressure drop (Equation 3-7)

$$\sigma_w = \frac{\Delta p_m r}{2L} \tag{3-7}$$

Relative standard deviations of the measured flow rates were calculated.

Results and Discussion

Pressure Determination

Figures 3-3 to 3-7 show the relationship between measured flow rate and pressure drop at each concentration for selected temperatures. As the measured flow

rate increased the measured pressure drop increased. From these figures it can also be determined that as the concentration decreased the measured flow rate increased indicating that the performance of diaphragm pump used for this research was affected by pulp concentrations pulp. At 4 °C and a concentration of 870 $g \cdot L^{-1}$ the measured pressure drop increased from 250.9 to 376.9 kPa as the measured flow rate increased from 5.59 x 10^{-5} to 2.1 x 10^{-4} $m^3 \cdot s^{-1}$. At 4 °C and for a concentration of 870 $g \cdot L^{-1}$ the maximum flow rate was 2.1 x 10^{-4} $m^3 \cdot s^{-1}$ while at the same temperature the maximum flow rate for 570 $g \cdot L^{-1}$ was 7.66 x 10^{-4} $m^3 \cdot s^{-1}$. Figures 3-3 through 3-7 show the remaining relationships for the other concentrations at selected temperatures. The increase in flow rate caused more friction in the capillary tube therefore a higher pressure drop. As the concentration decreased there was less resistance to flow because fewer particles were present. At all temperatures, the higher the concentration, the higher the pressure drops. The highest pressure drop was at the fastest flow rate for the highest concentration and the lowest temperature.

Figures 3-8 to 3-11 show the relationship between measured flow rate and pressure drop at each temperature for selected concentrations. As the measured flow rate increased the measured pressure drop increased. At an average concentration of 854 $g \cdot L^{-1}$ and 4 °C the measured flow rate increased from 5.59 x 10^{-5} to 2.1 x 10^{-4} $m^3 \cdot s^{-1}$ as pressure drop increased from 250.9 to 376 kPa. At the same concentration but at 50 °C, the flow rate increase from 9.23 x 10^{-6} to 5.74 x 10^{-4} $m^3 \cdot s^{-1}$ as the pressure drop increased from 85.2 to 371.6 kPa. Figures 3-8 to 3-11 show the remaining relationships for the other temperatures at selected concentrations. Another relationship determined from these figures is that as the temperature increased the measured flow rate

increased because at higher temperatures more molecular movement (less particle entanglement) caused increased flow. Also the highest pressure drop was at the lowest temperature with the fast flow rate at all concentrations. All these observations are consistent with the results from rotational rheology determinations from Chapter 2

Some of the figures show pseudo linear trends for the relationship between flow rate and pressure drop because only four flow rates were tested. Using a greater range of flow rates would show the power relationship between flow rate and pressure drop.

Figures 3-12 and 3-13 illustrate the difference between experimental pressure drop and the calculated pressure drop assuming no slippage at the same flow rate. The calculated pressure drop was determined with Equation 3-4. The measured pressure drop was always smaller for every concentration at all temperatures because with slippage the pulp particles have migrated away from the wall leaving the slip layer of liquid which reduced the friction and therefore the pressure drop. The highest calculated pressure drops were at 4 °C and decreased as temperature increased. Tables 3-1 through 3-5 give the calculated pressures assuming no slippage for each temperature.

In summary, for all experimental conditions, as the measured flow rate increased the pressure drop increased. As the concentration decreased at a particular temperature the pressure drop decreased. As the concentration decreased the measured flow rate increased. Increasing the temperature at a particular concentration decreases the pressure drop. As the temperature increased at any concentration the measured flow rate increased.

Orange pulp was pumped through the capillary system using a diaphragm pump. Using this type of positive displacement pump had the issues of pulsing flow and not

being able to handle the same flow rates at all concentrations and temperatures. Due to orange pulp characteristics, a progressive cavity pump would have been most effective at providing non-pulsating flow rate, allowing more accurate determination of pressure drop and flow rate with higher signal to noise ratios (Appendix A). Relative standard deviations of the of the measured flow rate were calculated. The highest concentrations had the highest relative standard deviations (up to 69%) while the lowest concentration had the lowest relative standard deviations (up to 38%).

Other sources of variability in the data most likely came from the pulp its self. Two different sources of orange pulp were used along with two different types of oranges. Because orange pulp is a biological material it is subject to natural variability. One sample was extracted, pasteurized and finished on site while the other was from a commercial source. The commercial source had a more gel-like texture which could possibly affect its rheology and even the results of the quick fiber tests. Variations in the way the pulp was extracted, finished, and stored could have resulted in the different pulp quality which were used in the study. Fruit puree flow rates versus pressure curves have been determined for different diameter capillary viscometer systems and can be found in Table 3-6. All flow rates ranged from 2.77×10^{-5} to 1.6×10^{-3} $m^3 \cdot s^{-1}$ which fell in the flow rate range of the orange pulp tested. All fruits had significantly lower pressure readings at approximately the same diameter (0.025 m) capillary tubes. Apple puree had an approximate pressure range of 58-120 kPa while apricot puree ranged from 37 to 180 kPa. Nectarine puree had a smaller pressure range (10-50 kPa) in comparison to apple and apricot. With a pressure range of 10 to 42.5 kPa, strawberry puree had the smallest range. All four fruits tested in the Yeow et al. (2001) study had smaller

pressure drops when compared to orange pulp. A reason for this difference could be that a puree has smaller particles in suspension in comparison to the orange pulp tested which could lead to the lower pressures because of less friction. The Yeow et al. (2001) study did not state whether the purees displayed slippage which would have affected the flow rate and pressure drop.

A study performed by Levati (2010), calculated the pressure drop at different flow rates of high concentration orange pulp using calculated power law parameters (Table 3-7). One similar trend found in this study was that as the temperature increased from 11 to 50 °C the pressure drop decreased at all flow rates. At similar temperatures to this study, 10 and 50 °C, Levati, (2010) had higher measured flow rates which had higher pressure drops. First, the flow behavior index and consistency coefficient used in determining pressure were different. Levati used a shear rate range of approximately 0 to 1300 s^{-1} to determine n and K while only a shear rate range of up to 4 s^{-1} was used in this study because after 4 s^{-1} slippage began. Significantly smaller K and n values were used by Levati. A second major difference is that all values were not corrected for slippage. It is known that slippage has a big impact on flow rate, pressure drop and power law parameters.

The effect of slippage on calculated flow rate was determined by other studies and other materials. The first study was performed on a model suspension material composed of polymer Ethylene Vinyl Acetate 460 and soda-lime glass beads. For all particle concentrations of 35, 41, 45% and flow rates of 0 to 0.075 $cm^3 \cdot s^{-1}$, the experimental pressure data was lower when compared to the predicted without slippage (Lam, Wang, Chen & Joshi, 2007). The second study was performed on cultured

buttermilk at 5 °C. At both capillary diameters (1.86 and 3.34 mm) and flow rate ranges of 0.25 to 2 $m^3 \cdot s^{-1}$ the experimental was lower than the initial and equilibrium pressure drop (Butler & O'Donnell, 1999).

Flow Rate and Corrected Slip Coefficient Determination

Figure 3-14 shows the relationship between measured flow rate and the slippage coefficient. As the measured flow rate increased the slippage coefficient increased. At 50 °C, βc ranged from 4.7×10^{-6} to 1.7×10^{-3} $m^2 \cdot (Pa \cdot s)^{-1}$. At all temperatures this was seen except at 4 °C where at a concentration of 870 $g \cdot L^{-1}$ negative values were calculated. It has been proposed that negative values for βc indicate plug flow and sliding friction may be a significant factor (Steffe, 1996). All values of βc can be found in Tables 3-1 through 3-5. The higher the βc value the more slippage.

The slippage coefficient is used to determine the flow rate without slippage at the measured pressure drop. The movement of particles from the wall is a direct action of the heterogeneous shearing that is perpendicular to flow (Wang, Lam, Joshi & Chen, 2010). At higher flow rates more shearing takes place at the wall which causes more particle migration and a greater difference between the measured flow rates and the flow rates without slippage.

Figure 3-15 shows the corrected slippage coefficient at a constant flow rate of 2.10×10^{-4} $m^3 \cdot s^{-1}$. Only a clear relationship exists between concentration and corrected slippage coefficient at 4 and 30 °C. As the concentration decreased the βc increased. The lack of consistent trends on this graph could be due to the fact that these values are based on extrapolated data (Table 3-8).

Sources of error such as pulp source processing technique, machinery and pulp quality affected slippage coefficient determinations. A major difference between this study and other studies that determined slippage coefficients was that this study did not use multiple capillary tube radii because data without slippage at very low shear rates was available. Sodium benzoate was added at such a small level (0.05%) that no effect was seen on the results of the capillary viscometry data.

The corrected slip coefficient and wall shear for apple sauce, ketchup, mustard, and tomato paste was determined (Table 1-11) (Kokini & Dervisoglu, 1990). For apple sauce, the corrected slip coefficient ranged from 0.0030 to 0.025 $m^2 \cdot (Pa \cdot s)^{-1}$ while the wall shear stress ranged from 40 to 150 Pa. Ketchup has a corrected slip coefficient range of 0.0034 to 0.042 $m^2 \cdot (Pa \cdot s)^{-1}$ and a wall shear stress range of 50 to 200 Pa. Mustard corrected slip coefficient ranged from 0.0046 to 0.037 $m^2 \cdot (Pa \cdot s)^{-1}$ while the wall shear stress range was the same as for ketchup. Tomato paste which is the most similar to orange pulp had a corrected slip coefficient range of 0.00018 to 0.0065 $m^2 \cdot (Pa \cdot s)^{-1}$ and a wall shear stress range of 250-750 Pa. The study by Kokini and Dervisoglu (1990) also found that as wall shear stress increased the βc increased. When determining the slip parameters for the four semi-solid foods three different capillary radii were used with extremely small diameters (0.0043-0.0885 cm). The smaller capillary tubes produce smaller flow rates with less shearing. In food processing, small diameters like the ones used in this study to predict flow rate and slippage are not used. Another factor that needs to be considered when comparing the semi solid food data to orange pulp data is the size of the suspended solids. A suspension of orange pulp and single strength orange juice has much larger particles

than the particles suspended in ketchup or mustard. Because the conditions are not similar between the Kokini and Dervisoglu (1990) and this study a fair comparison cannot be made.

Using a model coarse food suspension of green peas and aqueous sodium carboxy-methylcellulose, an alternative method to wall slip correction was performed in a study by Chakrabandhu and Singh (2005). Instead of measuring at different radii, variable particle concentrations were used. Through the entire range of concentrations (0, 15, 20, 25, 30 %v/v), flow rates (1.26×10^{-4} to 3.15×10^{-4} $m^3 \cdot s^{-1}$) and temperatures (85, 110, 135 °C) the slip coefficient ranged from 3.09×10^{-3} to 1.01×10^{-2} $m \cdot (Pa \cdot s)^{-1}$ at wall shear stress range of 19.4 to 125 Pa. The slip coefficient was used instead of the corrected slip coefficient because it was not based on tube radius. That study also derived power equations to determine slip coefficient as a function of wall shear stress. Equations can be found in Table 1-12. Chakrabandhu and Singh (2005) also determined that as the wall shear stress increased the slip coefficient increased. Using model suspensions is a good way to confirm methods to determine the slip coefficient but using real materials allows determining variation in samples which need to be accounted for practical applications.

Conclusions

Orange pulp flow was characterized by capillary viscometry accounting for slippage at selected temperatures of (4, 10, 21, 30, and 50 °C) and a range of concentrations (854 g $\pm$ 19, 749 $\pm$ 21, 649$\pm$ 26, and 545 $\pm$ 20 $g \cdot L^{-1}$). As the measured flow rate increased the measured pressure drop increased monotonously confirming that at all flow rates in this experiment slippage was present. Generally as the measured

flow rate increased the slippage coefficient increased. The slippage coefficient ranged from 5.2×10^{-5} to 1.7×10^{-3} $m^2 \cdot (Pa \cdot s)^{-1}$ with a standard deviation range of 4.1×10^{-7} to 2.8×10^{-3}.

Overall Conclusions

Orange pulp is a very difficult fluid to characterize because it displays slippage over a range of temperatures (4 to 80 °C) and concentrations (~500 to ~850 $g \cdot L^{-1}$). Orange pulp is non-Newtonian pseudoplastic fluid that can be best modeled with the power law at very low shear rates 0 to 4 s^{-1}. Rheological data showed that slippage takes place at shear rates between 2 and 4 s^{-1} and is more pronounced at low temperatures and high concentrations. In general, as the concentration increased the average activation energy increased. To account for the increased flow rate at the slip layer an additional term, βc was added. The higher the βc value the more slippage. Having a complete characterization of orange pulp is the foundation for the design and optimization of processing equipment.

Future Work

Although we covered the most relevant factors affecting the rheological behavior of orange pulp (i.e. concentration and temperature) we became aware of other potential sources of variability that need to be addressed. First, biological variety would need to be addressed. Depending on the variety of orange fruit, different size and amount of juice vesicles could be present which could possibly affect the rheological behavior. A second factor that could possible affect rheological behavior is the equipment and processing conditions used to produce citrus pulp. For example we hypothesize that the pressure used in the extraction and finishing, affects the rheological behavior of citrus pulp. The last source of variability that needs to be addressed is the different pulp

storage conditions and time. Depending of the storage conditions/time structural changes such as ice crystal formation in the pulp could affect the rheological characterization. Additional research could also be done with the capillary viscometer study. Determining pressure drop at more flow rates would lead to a better understanding of the power relationship between flow rate and pressure drop. Also the pump used in the study was only temperature rated to 60 °C, using a pump that functioned at higher temperatures could provide pressure drop data at higher temperatures. Knowing the true flow rates and pressure drops at higher temperatures would be important in the designing and optimization pulp processing equipment.

Table 3-1. Average values of experimental and calculated pressure, measured and corrected flow rate for slippage, wall shear stress and corrected slip coefficient for orange pulp at 4 °C and capillary diameter of 0.02291 m.

Concentration ($g \cdot L^{-1}$)	Experimental pressure (kPa)	Calculated pressure at Q_m assuming no slip (kPa)	Q_m ($m^3 \cdot s^{-1}$)	Q_{ws} ($m^3 \cdot s^{-1}$)	Wall shear stress (Pa)	Bc $m^2 \cdot (Pa \cdot s)^{-1}$
870	376.9	5558.4	2.10E-04	8.27E-05	191.5	1.68E-05
	321.8	4623.9	1.20E-04	4.92E-05	163.5	-1.02E-04
	281.9	3964.1	8.37E-05	3.24E-05	143.2	-8.30E-05
	250.9	3257.7	5.59E-05	1.93E-05	127.4	-5.04E-05
761	414.6	4982.7	4.89E-04	9.38E-05	210.7	5.21E-05
	384.3	4492.6	3.77E-04	7.13E-05	195.3	4.34E-05
	343.7	4113.6	2.59E-04	5.54E-05	174.6	3.23E-05
	315.4	3786.4	1.96E-04	4.46E-05	160.3	2.63E-05
675	372.4	5072.1	6.13E-04	1.35E-04	189.28	7.03E-05
	346.0	4619.5	4.97E-04	1.07E-04	175.86	6.15E-05
	333.9	4366.6	4.16E-04	9.33E-05	169.69	5.28E-05
	311.9	3974.8	3.28E-04	7.37E-05	158.50	4.45E-05
570	318.4	4278.4	7.66E-04	1.49E-04	161.7	1.06E-04
	298.4	3975.0	6.36E-04	1.24E-04	151.6	9.38E-05
	292.7	3883.3	5.83E-04	1.17E-04	148.7	8.70E-05
	278.8	3672.5	5.01E-04	1.02E-04	141.6	7.84E-05

Table 3-2. Average values of experimental and calculated pressure, measured and corrected flow rate for slippage, wall shear stress and corrected slip coefficient for orange pulp at 10 °C and capillary diameter of 0.02291 m.

Concentration ($g \cdot L^{-1}$)	Experimental pressure (kPa)	Calculated pressure at Q_m assuming no slip (kPa)	Q_m ($m^3 \cdot s^{-1}$)	Q_{ws} ($m^3 \cdot s^{-1}$)	Wall shear stress (Pa)	Bc $m^2 \cdot (Pa \cdot s)^{-1}$
843	397.9	2661.5	2.83E-04	9.25E-05	202.2	4.2E-04
	334.8	2281.7	1.82E-04	6.09E-05	170.1	3.2E-04
	292.9	1986.4	1.37E-04	4.45E-05	148.8	1.6E-04
	262.8	1774.2	9.37E-05	3.05E-05	133.6	1.6E-04
767	391.6	2835.2	5.53E-04	1.39E-04	199.0	5.8E-05
	367.4	2658.1	4.61E-04	1.14E-04	186.7	5.2E-05
	339.1	2456.7	3.61E-04	9.66E-05	172.3	4.3E-05
	310.9	2241.6	2.65E-04	7.28E-05	158.0	3.4E-05
663	361.1	3166.6	7.23E-04	1.58E-04	183.5	8.6E-05
	353.5	3040.7	6.37E-04	1.43E-04	179.7	7.7E-05
	334.4	2892.2	5.35E-04	1.25E-04	170.0	6.7E-05
	310.7	2685.6	4.15E-04	1.03E-04	157.9	5.5E-05
557	306.5	2508.6	8.86E-04	2.32E-04	155.7	1.2E-04
	300.8	2432.2	8.26E-04	2.17E-04	152.9	1.1E-04
	288.5	2302.6	7.16E-04	1.90E-04	146.6	1.0E-04
	272.3	2193.7	6.32E-04	1.72E-04	138.4	9.3E-05

Table 3-3. Average values of experimental and calculated pressure, measured and corrected flow rate for slippage, wall shear stress and corrected slip coefficient for orange pulp at 21 °C and capillary diameter of 0.02291 m.

Concentration ($g \cdot L^{-1}$)	Experimental pressure (kPa)	Calculated pressure at Q_m assuming no slip (kPa)	Q_m ($m^3 \cdot s^{-1}$)	Q_{ws} ($m^3 \cdot s^{-1}$)	Wall shear stress (Pa)	Bc $m^2 \cdot (Pa \cdot s)^{-1}$
827	390.8	2129.7	3.74E-04	1.34E-04	198.61	8.7E-04
	350.1	1948.8	2.86E-04	1.02E-04	177.93	7.0E-04
	316.0	1723.4	1.95E-04	6.94E-05	160.61	4.1E-04
	284.0	1595.5	1.51E-04	5.28E-05	144.32	3.8E-04
763	383.2	2530.5	5.75E-04	1.85E-04	194.8	5.6E-05
	344.6	2411.3	5.51E-04	1.56E-04	175.1	6.2E-05
	332.8	2170.6	4.91E-04	1.22E-04	169.1	6.0E-05
	310.2	2046.5	3.84E-04	1.00E-04	157.6	5.0E-05
658	341.8	2552.9	8.24E-04	2.37E-04	173.7	9.4E-05
	323.8	2412.4	7.05E-04	2.01E-04	164.6	8.5E-05
	310.1	2271.9	6.18E-04	1.70E-04	157.6	7.9E-05
	302.4	2192.4	5.57E-04	1.53E-04	153.7	7.3E-05
549	286.5	1882.3	1.04E-03	3.08E-04	145.6	1.4E-04
	276.9	1849.1	9.33E-04	2.83E-04	140.7	1.3E-04
	273.4	1799.8	8.92E-04	2.64E-04	138.9	1.3E-04
	260.9	1269.8	8.01E-04	2.38E-04	132.6	1.2E-04

Table 3-4. Average values of experimental and calculated pressure, measured and corrected flow rate for slippage, wall shear stress and corrected slip coefficient for orange pulp at 30 °C and capillary diameter of 0.02291 m.

Concentration ($g \cdot L^{-1}$)	Experimental pressure (kPa)	Calculated pressure at Q_m assuming no slip (kPa)	Q_m ($m^3 \cdot s^{-1}$)	Q_{ws} ($m^3 \cdot s^{-1}$)	Wall shear stress (Pa)	Bc $m^2 \cdot (Pa \cdot s)^{-1}$
868	384.6	2200.3	4.70E-04	1.60E-04	195.4	1.3E-03
	328.7	1955.9	2.91E-04	9.71E-05	167.0	1.1E-03
	275.1	1720.1	1.65E-04	5.39E-05	139.8	7.4E-04
	168.7	896.0	1.28E-05	3.95E-06	85.7	1.4E-04
724	309.3	2123.2	6.83E-04	2.14E-04	157.2	8.3E-05
	291.2	1402.3	5.73E-04	1.78E-04	148.0	7.4E-05
	225.3	1649.1	2.53E-04	7.64E-05	114.5	4.3E-05
	78.4	695.3	1.02E-05	2.84E-06	39.9	5.2E-06
608	265.6	1596.3	7.86E-04	2.60E-04	135.0	1.1E-04
	227.8	1373.4	5.18E-04	1.69E-04	115.8	8.5E-05
	188.1	1041.5	2.79E-04	8.96E-05	95.6	5.6E-05
	71.1	365.2	6.20E-06	3.14E-06	36.1	2.3E-06
522	231.5	1143.1	8.79E-04	3.29E-04	117.7	1.3E-04
	200.0	1037.7	6.24E-04	2.25E-04	101.6	1.1E-04
	168.0	914.7	4.00E-04	1.39E-04	85.4	8.5E-05
	107.3	304.5	2.54E-04	4.39E-06	54.5	7.4E-05

Table 3-5. Average values of experimental and calculated pressure, measured and corrected flow rate for slippage, wall shear stress and corrected slip coefficient for orange pulp at 50 °C and capillary diameter of 0.02291 m.

Concentration ($g \cdot L^{-1}$)	Experimental pressure (kPa)	Calculated pressure at Q_m assuming no slip (kPa)	Q_m ($m^3 \cdot s^{-1}$)	Q_{ws} ($m^3 \cdot s^{-1}$)	Wall shear stress (Pa)	Bc $m^2 \cdot (Pa \cdot s)^{-1}$
864	371.6	1879.3	5.74E-04	2.10E-04	188.8	1.7E-03
	306.0	1764.4	4.38E-04	1.49E-04	155.5	1.5E-03
	236.0	1421.4	1.99E-04	6.66E-05	119.9	8.6E-04
	85.2	638.5	9.23E-06	2.75E-06	43.2	1.4E-04
729	291.1	1878.2	7.73E-04	2.50E-04	147.9	9.8E-05
	258.4	1700.5	5.34E-04	1.70E-04	131.3	7.7E-05
	205.4	1352.1	2.38E-04	7.62E-05	104.3	4.3E-05
	79.2	550.7	9.25E-06	2.88E-06	40.2	4.4E-06
644	249.2	1376.1	8.58E-04	2.98E-04	126.7	1.2E-04
	220.9	1240.8	6.03E-04	2.08E-04	112.2	9.8E-05
	178.2	1011.2	3.06E-04	1.05E-04	90.6	6.2E-05
	68.4	328.4	9.46E-06	3.52E-06	34.8	4.8E-06
529	211.5	957.2	9.59E-04	3.67E-04	107.5	1.5E-04
	188.8	848.8	6.34E-04	2.43E-04	95.9	1.1E-04
	147.8	710.5	3.46E-04	1.29E-04	75.1	8.0E-05
	63.6	249.3	9.26E-06	3.81E-06	32.3	4.7E-06

Table 3-6. Approximate flow rate and pressure drop for various fruit purees (Yeow, Perona & Leong, 2001).

Fruit Puree	Diameter X Length (cm x m)	Temperature °C	Approximate Q ($m^3 \cdot s^{-1}$)	Approximate Pressure (kPa)
Apple	2.5 x 7	30	$2.77 \times 10^{-5} – 1.6 \times 10^{-3}$	58-120
Apricot	2.5 x 7	30	$2.77 \times 10^{-5} – 1.6 \times 10^{-3}$	37-180
	3.65 x 6	30	$2.77 \times 10^{-5} – 1.6 \times 10^{-3}$	18-40
Nectarine	2.5 x 7	30	$2.77 \times 10^{-5} – 1.6 \times 10^{-3}$	10-50
	3.65 x 6	30	$2.77 \times 10^{-5} – 1.6 \times 10^{-3}$	5-15
Strawberry	2.5 x 7	25	$2.77 \times 10^{-5} – 1.6 \times 10^{-3}$	10-42.5

Table 3-7. Pressure drop of orange pulp for a capillary system of 49 mm inner diameter at different temperatures and flow rates (Levati, 2010).

Temperature °C	Approximate Q ($m^3 \cdot s^{-1}$)	Approximate Pressure (kPa)
11	1.38×10^{-4} -1.8×10^{-3}	1420-1800
25	1.38×10^{-4} -1.8×10^{-3}	610-900
38	1.38×10^{-4} -1.8×10^{-3}	400-590
50	1.38×10^{-4} -1.8×10^{-3}	375-500

Table 3-8. Extrapolated pressure drop, flow rate without slippage, wall shear stress and corrected slipped coefficient at a measured flow rate of 2.1×10^{-4} $m3 \cdot s^{-1}$.

Temperature °C	Concentration ($g \cdot L^{-1}$)	Extrapolated pressure drop (kPa)	Q without slippage ($m^3 \cdot s^{-1}$)	Wall shear stress (Pa)	βc $m^2 \cdot (Pa \cdot s)^{-1}$
4	870	382.1	7.24E-05	194.2	1.97E-05
	761	324.1	3.80E-05	164.7	2.90E-05
	675	291.6	3.76E-05	148.2	3.23E-05
	570	236.3	3.44E-05	120.1	4.06E-05
10	843	348.1	6.91E-05	176.9	2.21E-05
	767	296.1	6.71E-05	150.5	2.64E-05
	663	278.3	7.84E-05	141.4	2.58E-05
	557	218.7	1.00E-04	111.1	2.74E-05
21	827	316.2	5.87E-05	160.7	2.62E-05
	763	249.6	5.56E-05	126.9	3.38E-05
	658	250.0	1.38E-04	127.1	1.58E-05
	549	199.3	1.53E-04	101.3	1.55E-05
30	868	321.3	5.57E-05	163.3	2.63E-05
	724	221.8	1.95E-07	112.7	5.17E-05
	607.6	167.8	2.71E-07	85.3	6.83E-05
	521.6	106.0	9.80E-10	53.9	1.08E-04
50	863.7	245.9	6.63E-05	125.0	3.19E-05
	728.6	196.1	7.27E-05	99.7	3.83E-05
	644.3	152.4	1.12E-04	77.5	3.53E-05
	528.9	123.1	5.30E-06	62.5	9.10E-05

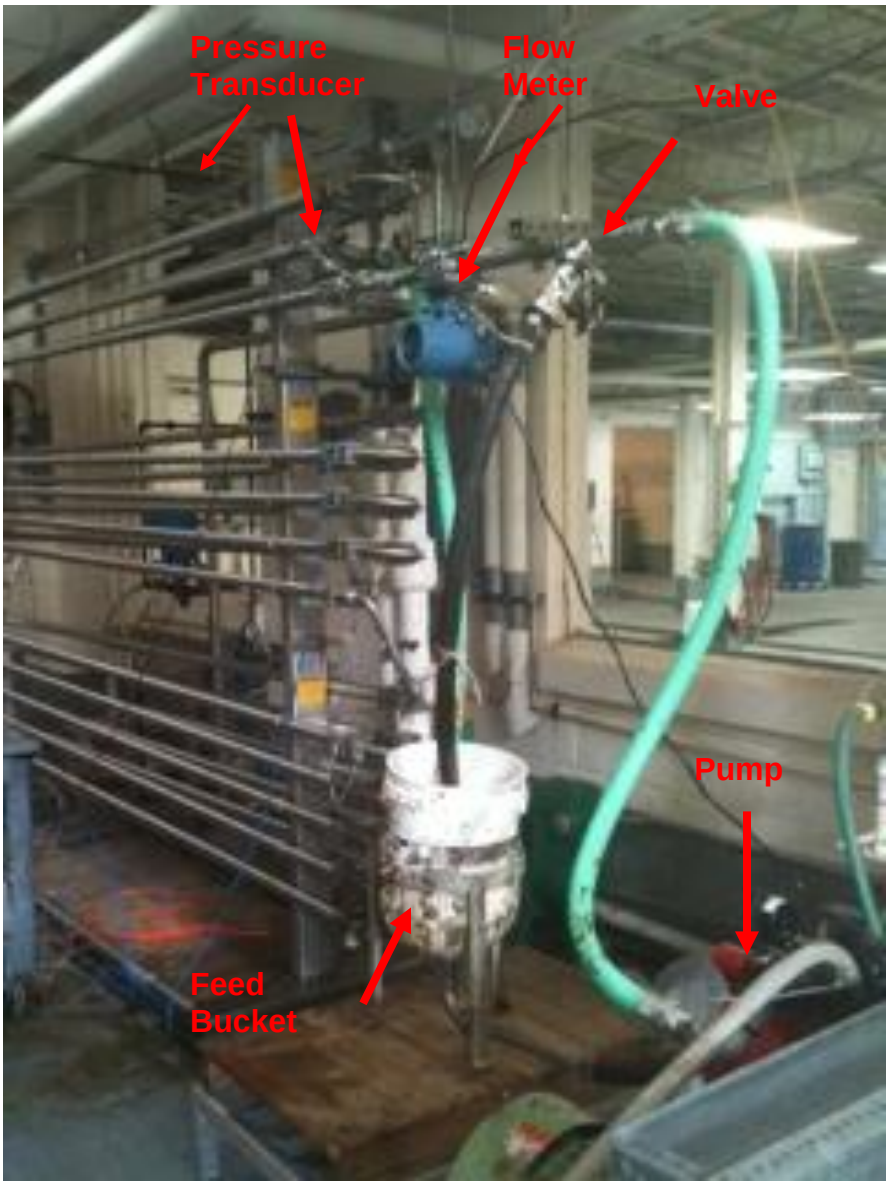

Figure 3-1. Complete 1 inch capillary system setup to measure the pressure drop and flow rate of orange pulp.

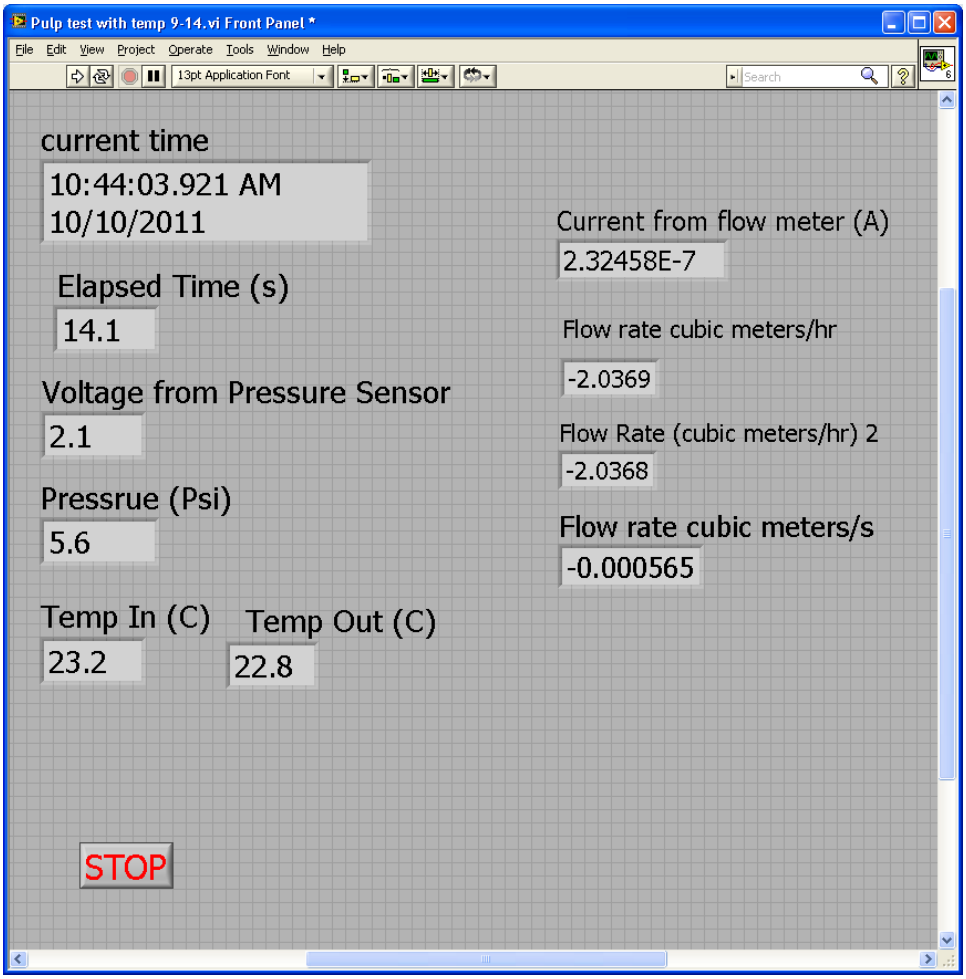

Figure 3-2. Screen shot of LabVIEW X front panel.

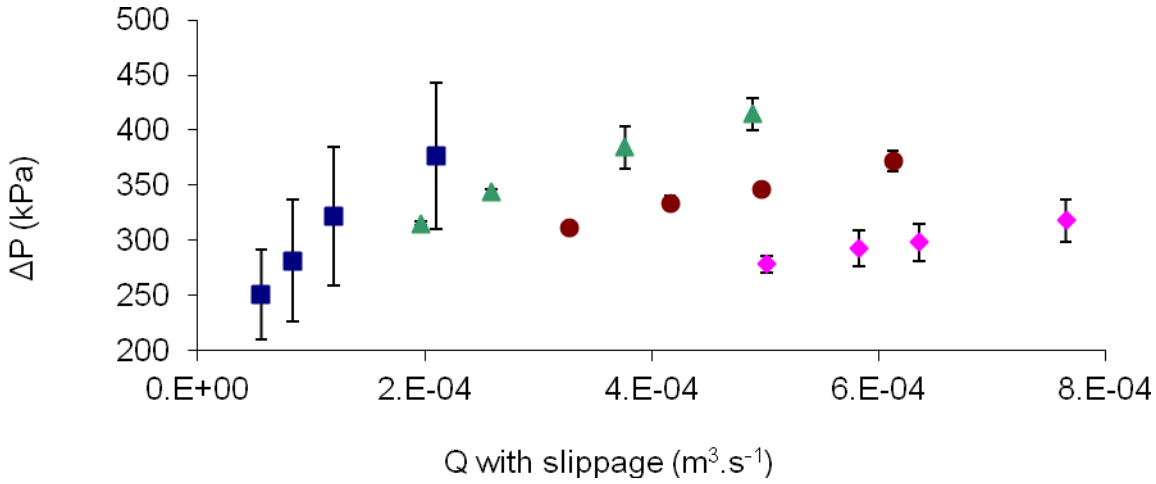

Figure 3-3. Measured pressure drops and standard deviations produced at flow rates with slippage at 4 °C and selected concentrations: 870 ± 7 g·L^{-1} (■), 760 ± 24 g·L^{-1} (▲), 675 ± 13 g·L^{-1} (●)and 569 ± 11 g·L^{-1} (♦).

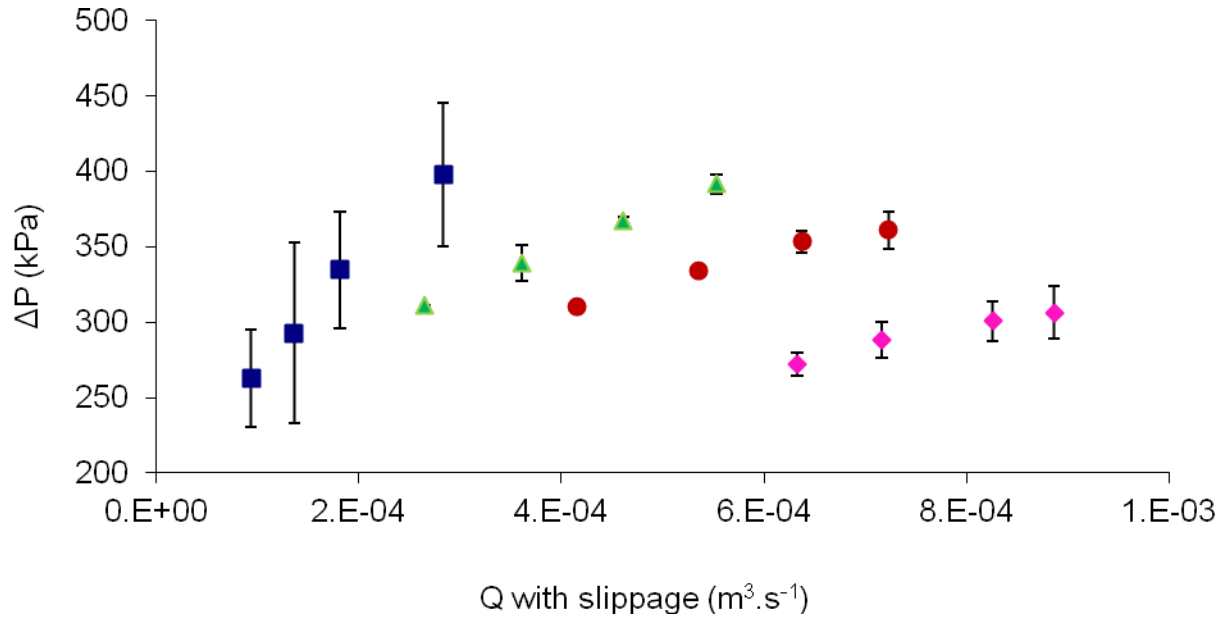

Figure 3-4. Measured pressure drops and standard deviations produced at flow rates with slippage at 10 °C and selected concentrations: 843 ± 16 g·L^{-1} (■), 767 ± 8 g·L^{-1} (▲), 663 ± 27 g·L^{-1}(●) and 557 ± 6 g·L^{-1} (♦).

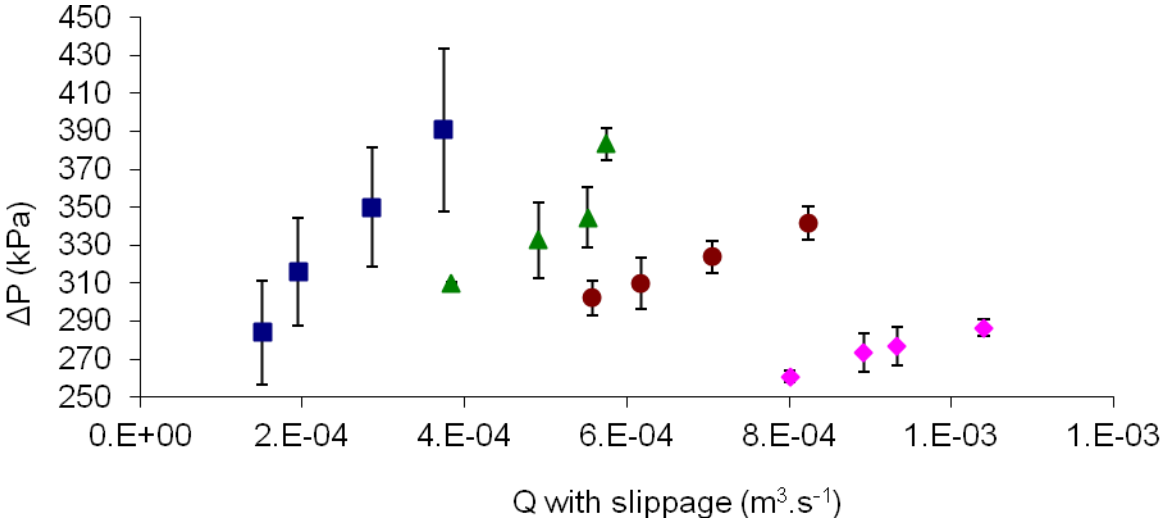

Figure 3-5. Measured pressure drops and standard deviations produced at flow rates with slippage at 21 °C and selected concentrations: 827 ± 32 g·L^{-1} (■), 763 ± 21 g·L^{-1} (▲), 658 ± 23 g·L^{-1}(●) and 549 ± 19 g·L^{-1} (♦).

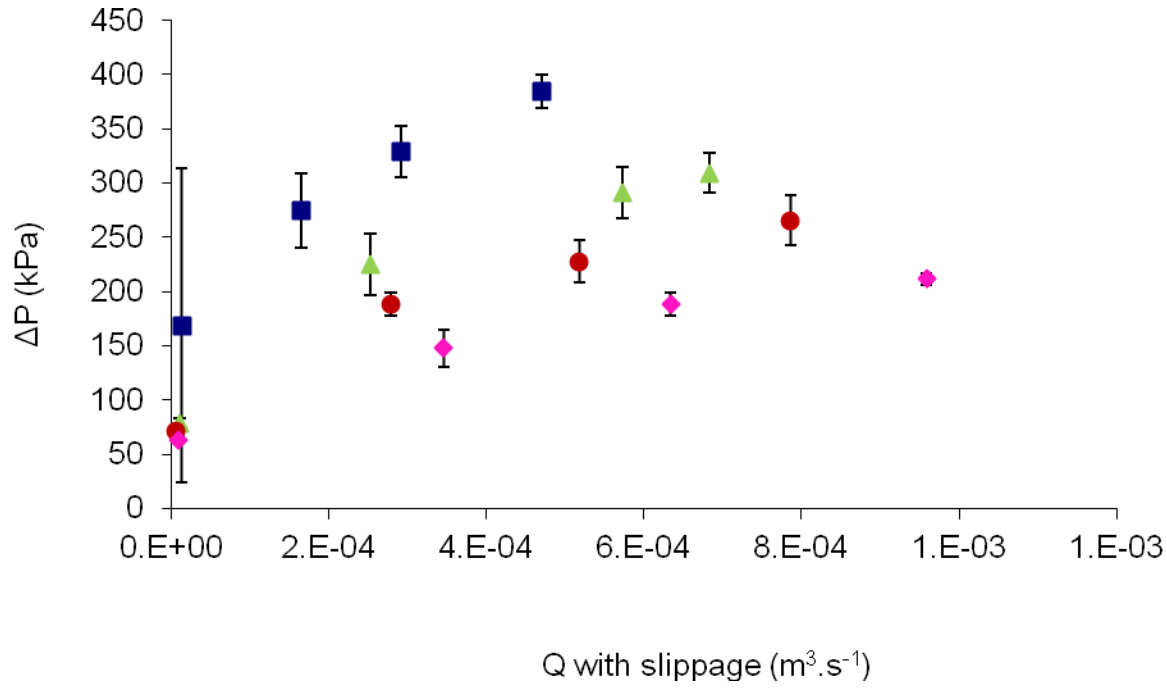

Figure 3-6. Measured pressure drops and standard deviations produced at flow rates with slippage at 30 °C and selected concentrations: 868 ± 34 g·L^{-1} (■), 724 ± 21 g·L^{-1} (▲), 607 ± 49 g·L^{-1}(●) and 522 ± 46 g·L^{-1} (♦).

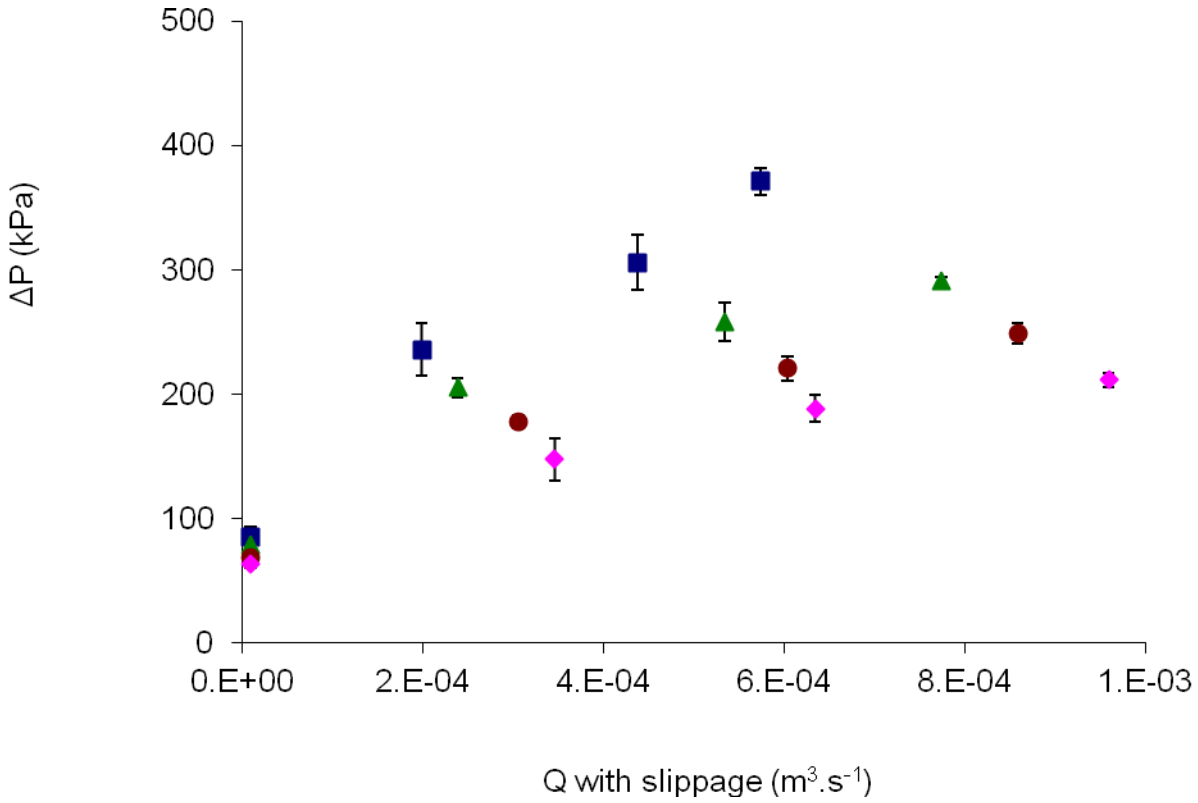

Figure 3-7. Measured pressure drops and standard deviations produced at flow rates with slippage at 50 °C and selected concentrations: 864 ± 39 g·L^{-1} (■), 729 ± 44 g·L^{-1} (▲), 644 ± 35 g·L^{-1}(●) and 529 ± 3 g·L^{-1} (♦).

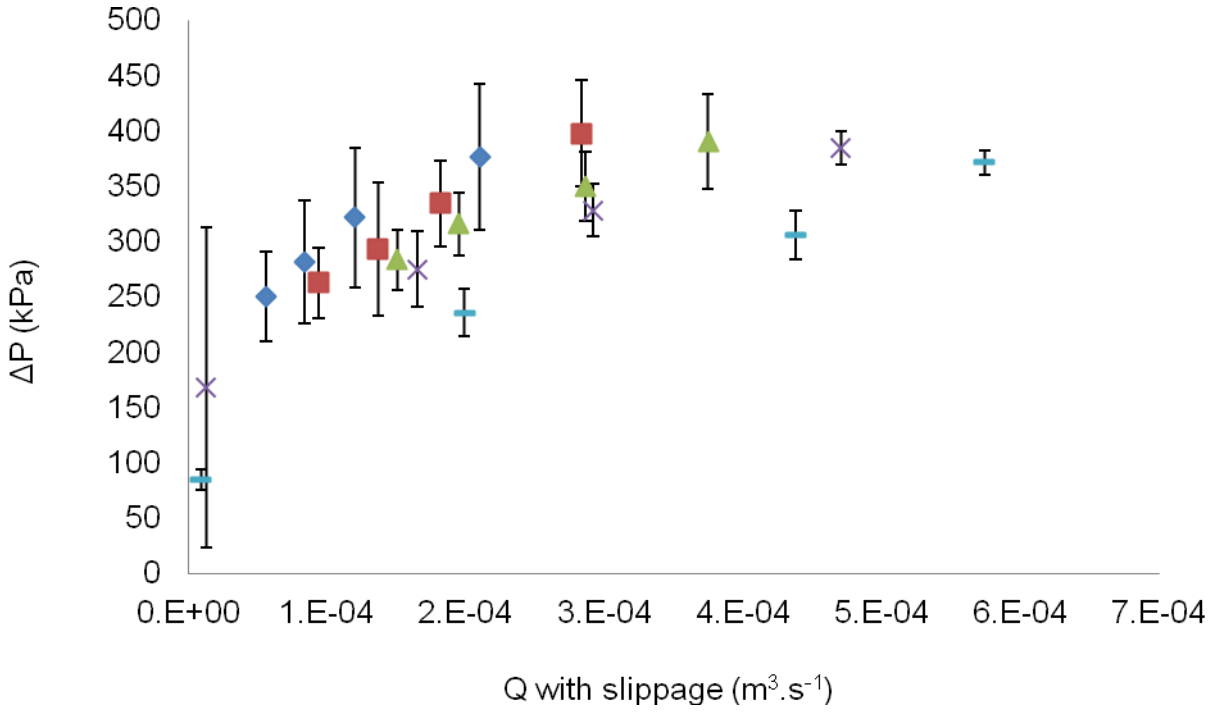

Figure 3-8. Measured pressure drops and standard deviations produced at flow rates with slippage at an average concentration of 854 g·L^{-1} and selected temperature: 4 °C (♦),10 °C, (■) 21 °C, (▲), 30 °C (x) and 50 °C (-) .

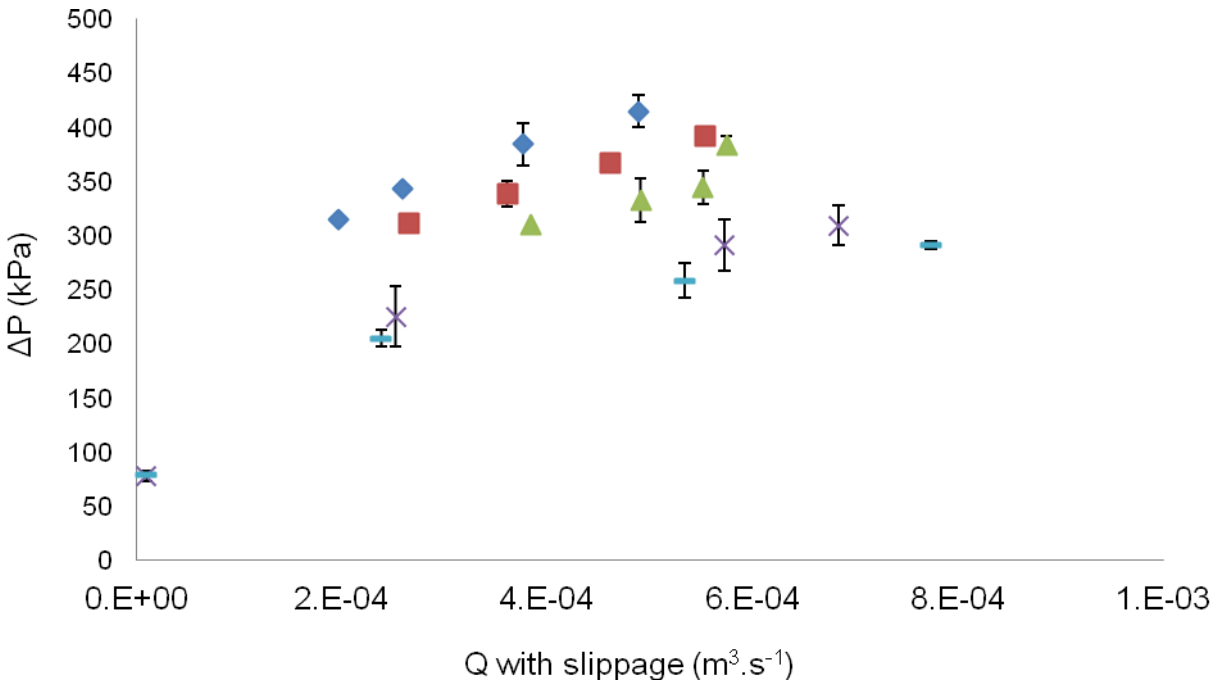

Figure 3-9. Measured pressure drops and standard deviations produced at flow rates with slippage at an average concentration of 749 g·L^{-1} and selected temperature: 4 °C (♦),10 °C, (■) 21 °C, (▲), 30 °C (x) and 50 °C (-) .

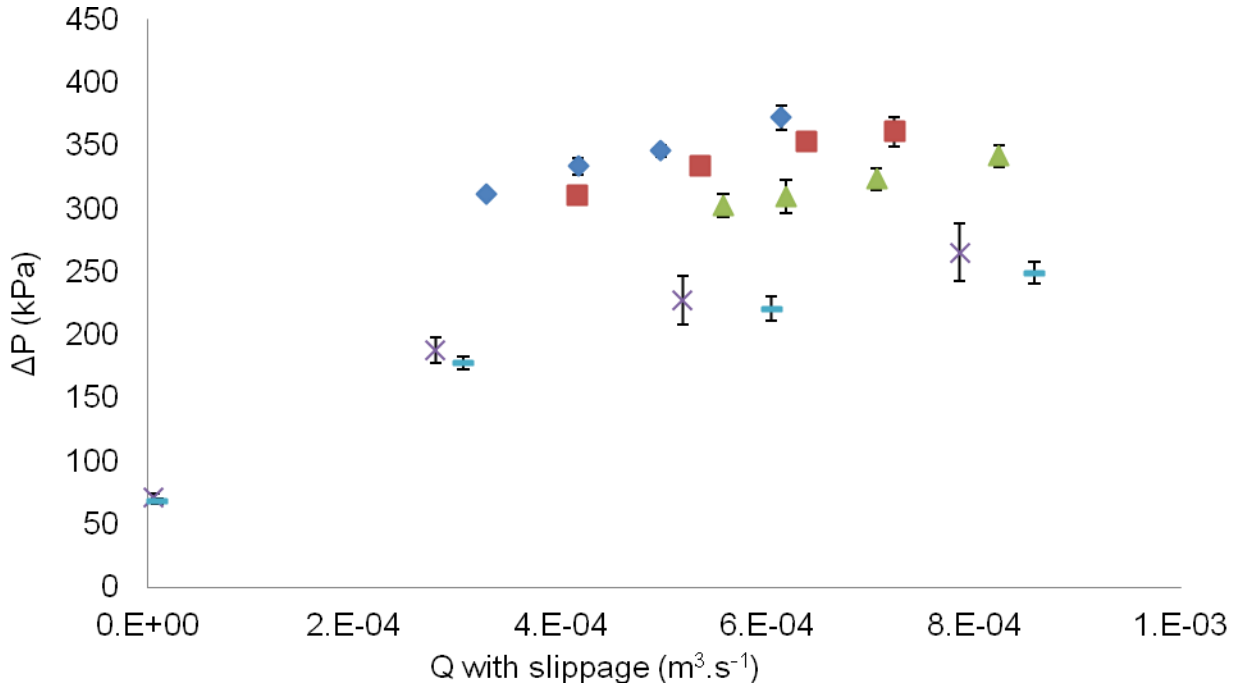

Figure 3-10. Measured pressure drops and standard deviations produced at flow rates with slippage at an average concentration of 649 g·L^{-1} and selected temperature: 4 °C (♦),10 °C, (■) 21 °C, (▲), 30 °C (x) and 50 °C (-) .

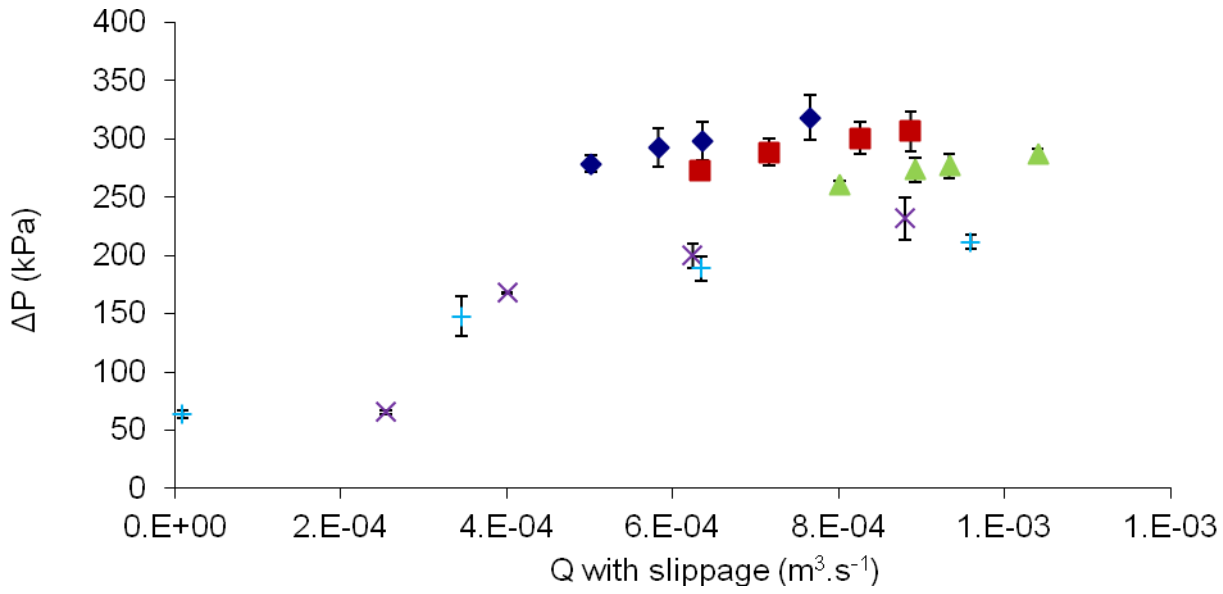

Figure 3-11. Measured pressure drops and standard deviations produced at flow rates with slippage at an average concentration of 543 g·L^{-1} and selected temperature: 4 °C (♦),10 °C (■), 21 °C (▲), 30 °C (x) and 50 °C (-) .

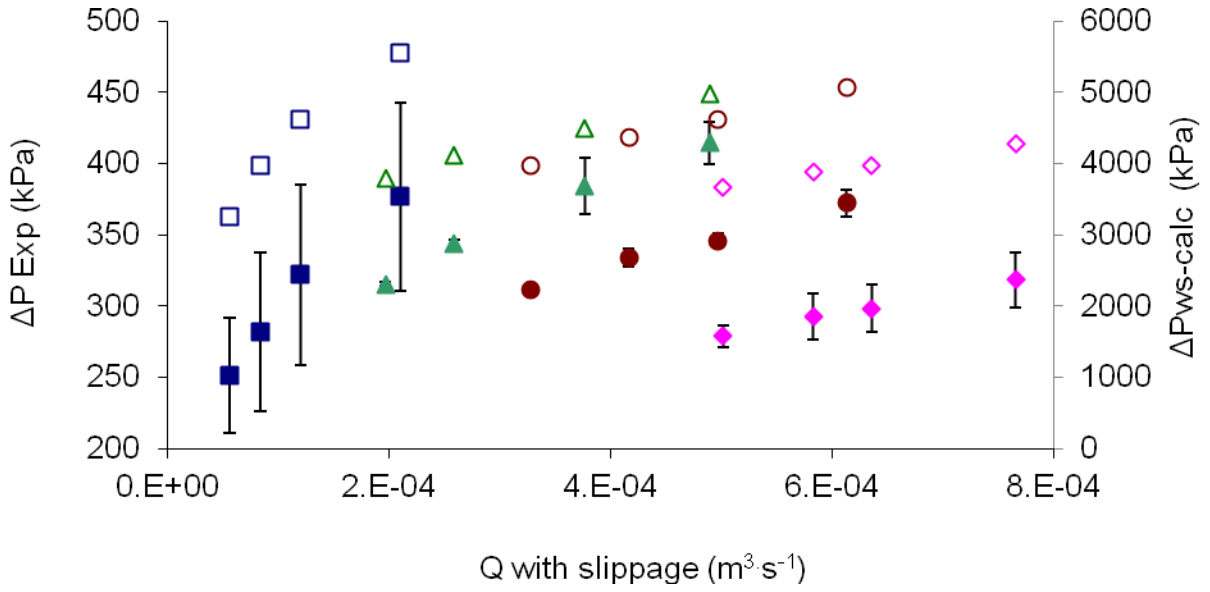

Figure 3-12. Experimental and calculated pressure drop of orange pulp at different flow rates for 4 °C and average concentrations. 871 g·L^{-1} (□) calculated (■) experimental, 761 g·L^{-1} (Δ) calculated (▲) experimental, 675 g·L^{-1} (○) calculated (●) experimental and 569 g·L^{-1} (◊) calculated (♦) experimental.

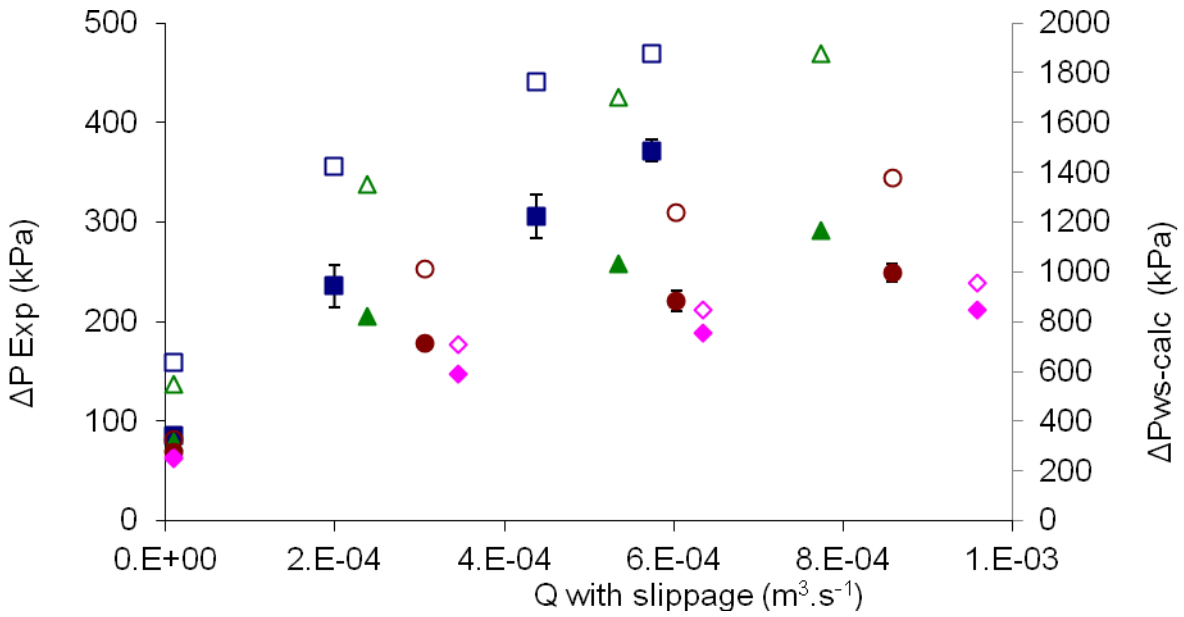

Figure 3-13. Experimental and calculated pressure drop of orange pulp at different flow rates for 50 °C and average concentrations. 864 g·L^{-1} (□) calculated (■) experimental, 729 g·L^{-1} (Δ) calculated (▲) experimental, 644 g·L^{-1} (○) calculated (●) experimental and 529 g·L^{-1} (◊) calculated (♦) experimental.

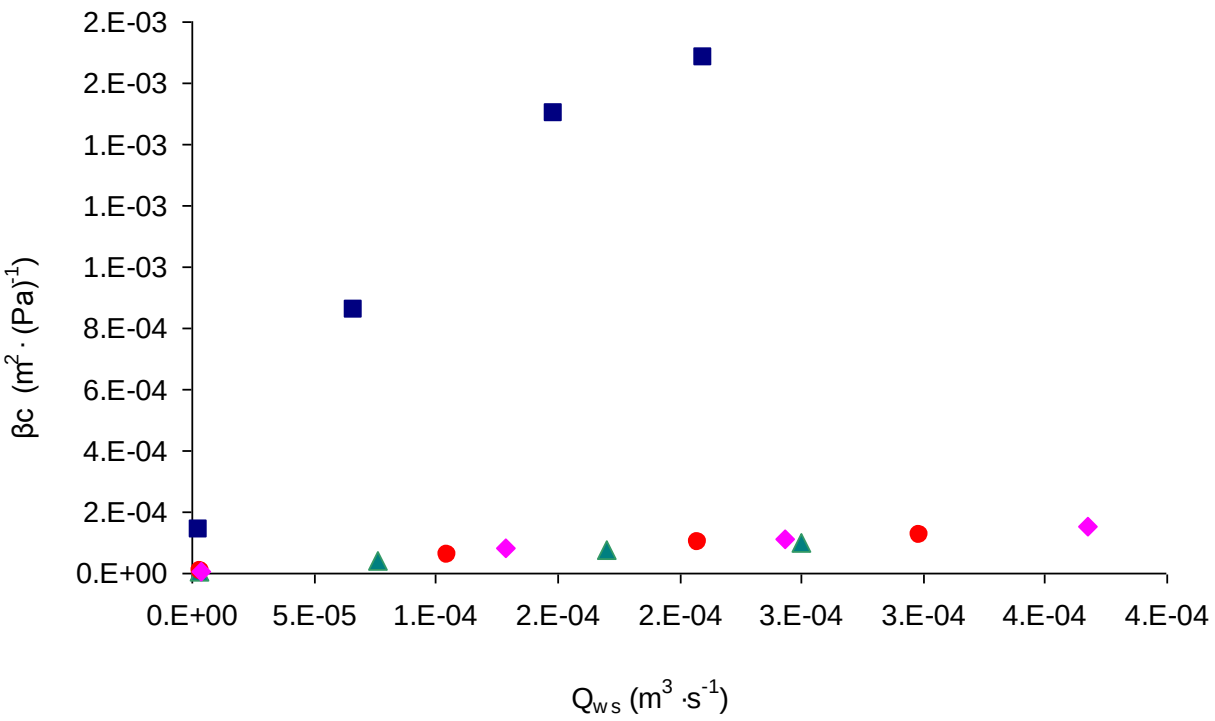

Figure 3-14. Measured flow rate vs. slip coefficient for 50 °C at selected concentrations: 864 g·L^{-1} (■), 729 g·L^{-1} (▲), 644 g·L^{-1}(●) and 529 g·L^{-1} (♦).

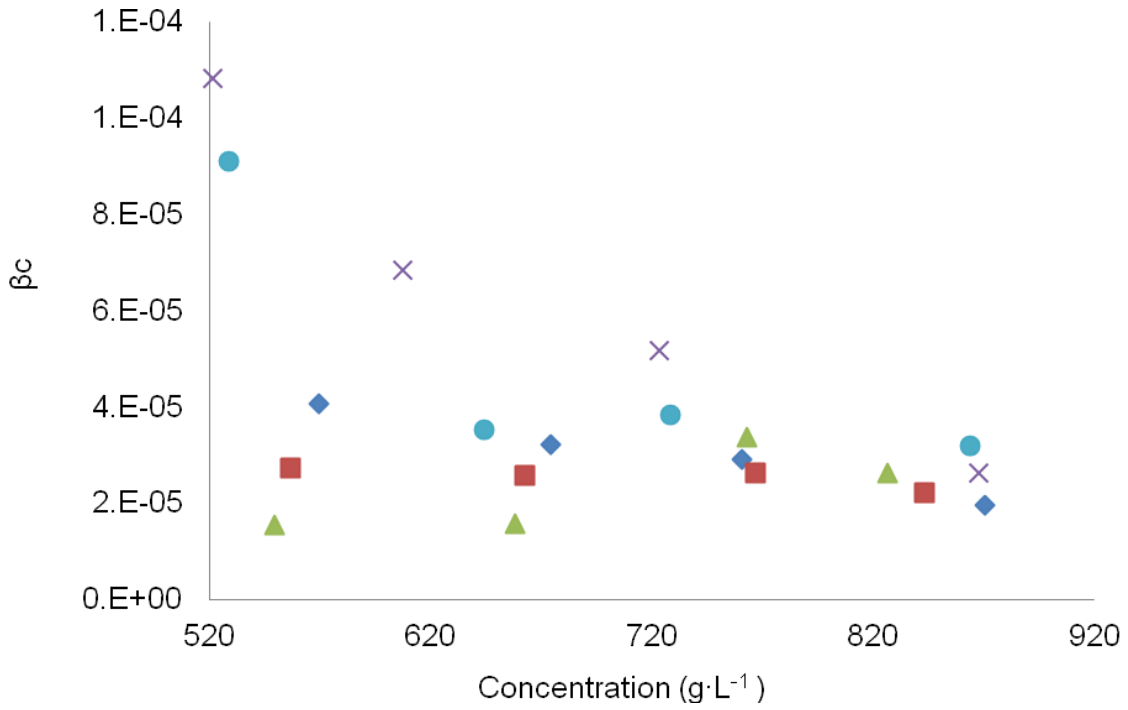

Figure 3-15. Corrected Slippage coeffecient at a constant flow rate of 2.1×10^{-4} $m^3 \cdot s^{-1}$ at selected temperatueres: 4 °C (♦), 10 °C (■), 21 °C (▲), 30 °C (x), and 50 °C (●).

APPENDIX
CAPILLARY VISCOMETRY

In the LabVIEW X program, pressure (pounds per square inch), temperature at the inlet of the pump and exit of the capillary system (°C) and measured flow rate ($m^3 \cdot hr^{-1}$) were measured.

With the data collected in LabVIEW the pressure in pounds per square inch was converted to Pascal and average for each concentration and temperature combination. The measured flow rate was converted to $m^3 \cdot s^{-1}$ and then averaged for each concentration and temperature combination. The velocity was calculated from the measured flow rate in $m^3 \cdot s^{-1}$ and the cross sectional area. With these variables determined the procedure for determining flow rate without slippage and slip coefficient for a given pressure drop for orange pulp was determined (Equations 3-5 through 3-10).

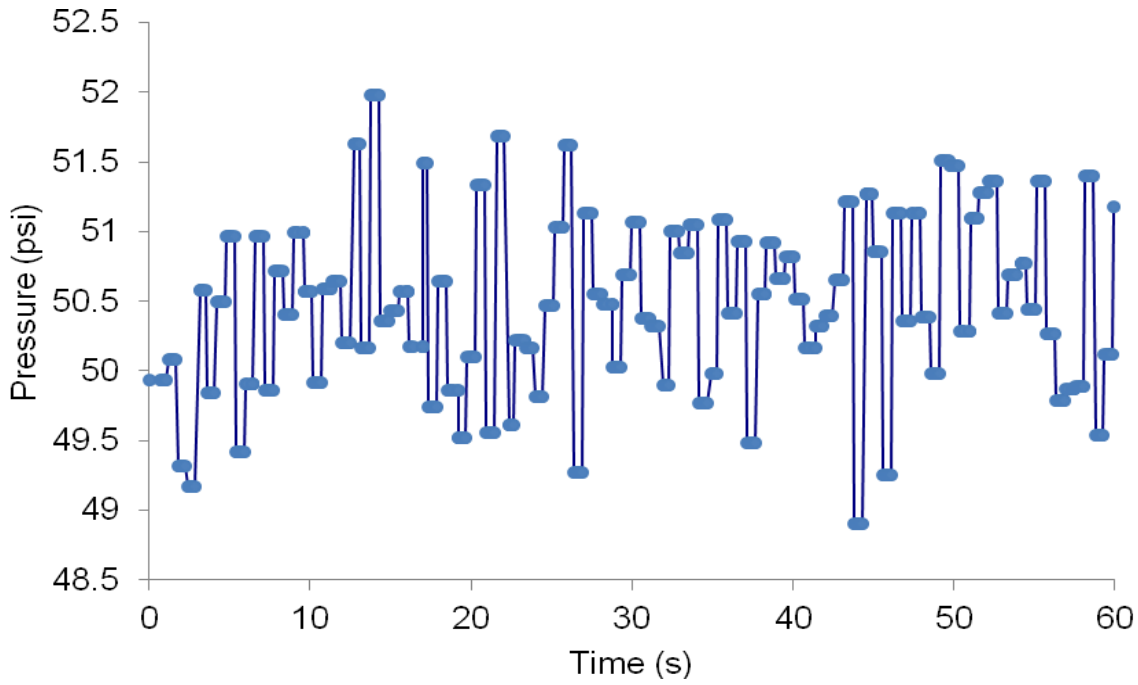

Figure A-1.Pressure drop (psi) over time (s) for replicate 3 at 30 °C and 840 $g \cdot L^{-1}$

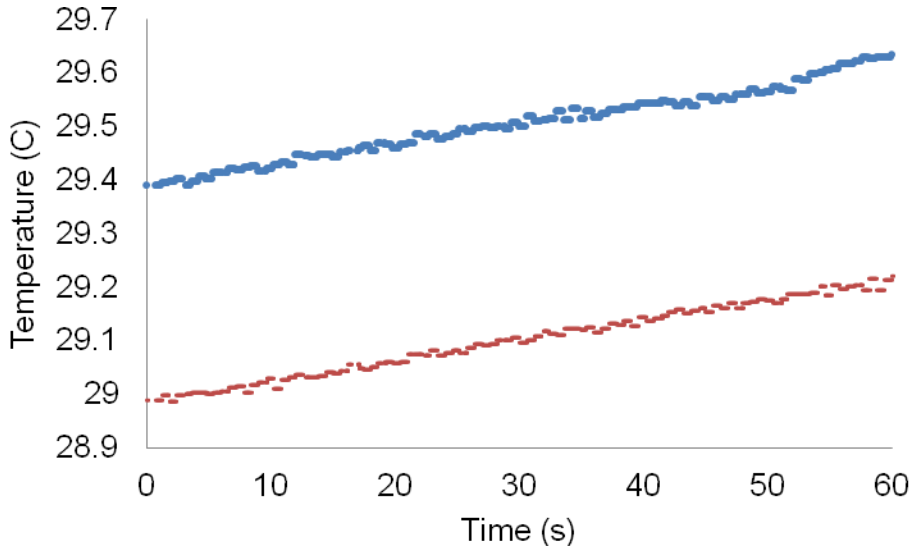

Figure A-2 Inlet (•) and outlet (-) temperatures of 30 °C and 840 g·L^{-1}collected in LabVIEW for replicate 3.

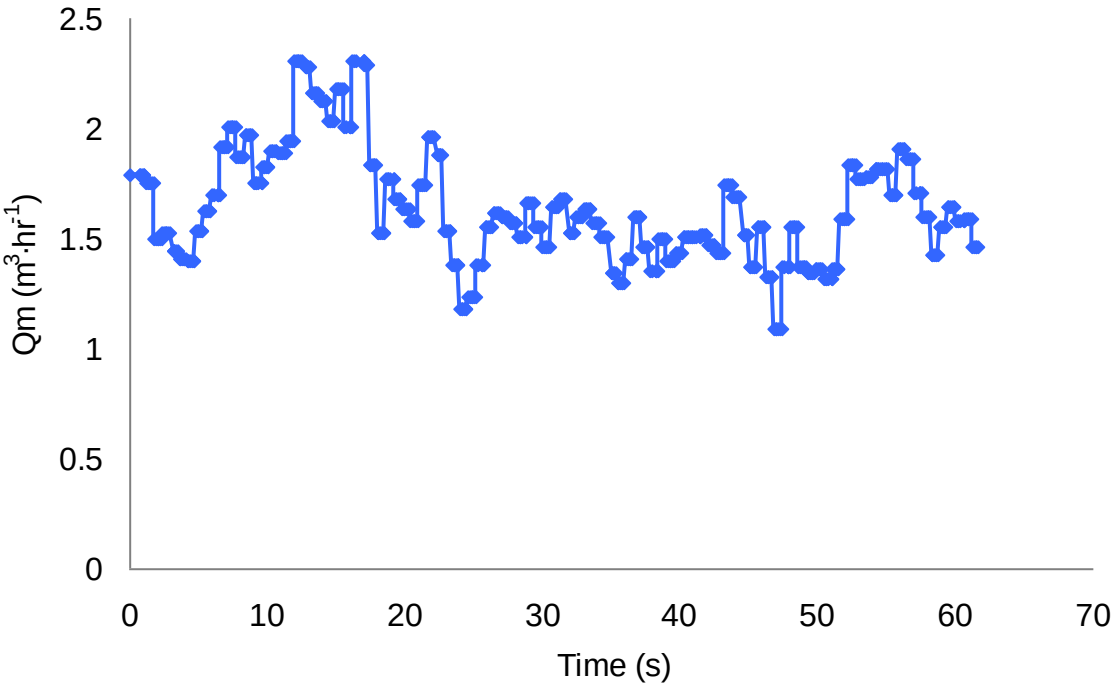

Figure A-3. Flow rate (m^3·s^{-1}) over time (s) for 30 °C and 840 g·L^{-1} for replicate 3.

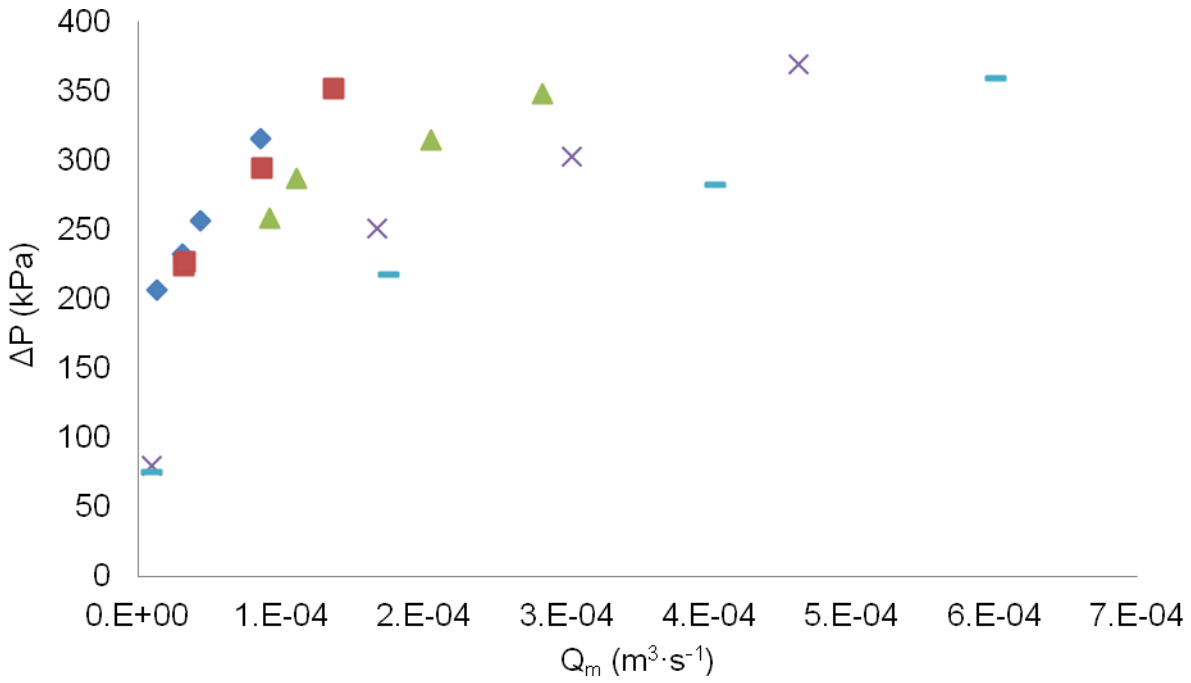

Figure A-4. Measured pressure drops produced at flow rates with slippage at an average concentration of 843 g·L^{-1} and selected temperature for replicate 3: 4 °C (♦),10 °C (■), 21 °C (▲), 30 °C (x) and 50 °C (-)

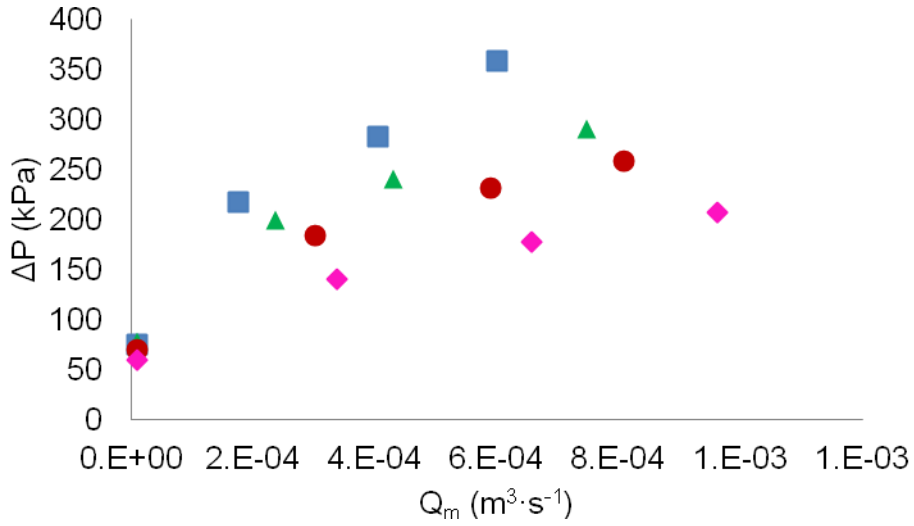

Figure A-5. Measured pressure drops produced at flow rates with slippage at 50 °C and selected concentrations for replicate 3: 820 g·L^{-1} (■), 692 g·L^{-1} (▲), 672 g·L^{-1}(●) and 526 g·L^{-1} (♦).

LIST OF REFERENCES

Ahmed, J., Ayad, A., Ramaswamy, H. S., Am, I., & Shao, Y. (2007). Dynamic viscoelastic behavior of high pressure treated soybean protein isolate dispersions. *International Journal of Food Properties*, 10, 397-411.

Alpaslan, M., & Hayta, M. (2002). Rheological and sensory properties of pekmez (grape molasses)/tahin (sesame paste) blends. *Journal of Food Engineering*, 54, 89-93.

Barbosa-Canovas, G. V. (2005). *Newtonian and non-Newtonian flow*. Food Engineering: UNESCO.

Barnes, H. A. (1995). A review of the slip (wall depletion) of polymer-solutions, emulsions and particle suspensions in viscometers - its cause, character, and cure. *Journal of Non-Newtonian Fluid Mechanics*, 56, 221-251.

Belibagli, K. B., & Dalgic, A. C. (2007). Rheological properties of sour-cherry juice and concentrate. *International Journal of Food Science and Technology*, 42, 773-776.

Bourne, M. (2002). *Food texture and viscosity: concept and measurement*. New York: Academic Press.

Braddock, R. (1999). *Handbook of citrus by-product and processing technology*. Lake Alfred: John Wiley & Sons, Inc.

Butler, F., & O'Donnell, H. J. (1999). Modeling the flow of a time-dependent viscous product (cultured buttermilk) in a tube viscometer at 5 degrees c. *Journal of Food Engineering*, 42(4), 199-206.

Campanella, O. H., & Peleg, M. (1987). *Squeezing flow viscosimetry of peanut butter*. *Journal of Food Science*, 52, 180-184.

Carrington, S. (2005). *Viscometer or rheometer? Making the decision*. 2010.

Chakrabandhu, K., & Singh, R. K. (2005). Wall slip determination for coarse food suspensions in tube flow at high temperatures. *Journal of Food Engineering*, 70, 73-81.

Chen, T. (2006). *Rheological techniques for yield stress analysis*. New Castle, Delaware: TA Instruments.

Citerne, G. P., Carreau, P. J., & Moan, M. (2001). Rheological properties of peanut butter. *Rheologica Acta*, 40, 86-96.

Crandall, P. G., Chen, C. S., & Carter, R. D. (1982). Models for predicting viscosity of orange juice concentrate. *Food Technology*, 36, 245-252.

Dervisoglu, M., & Kokini, J. L. (1986). Steady shear rheology and fluid-mechanics of 4 semisolid foods. *Journal of Food Science*, 51, 541-546.

FAO. (2001). *Economic and financial comparison of organic and conventional citrus-growing systems in spain*.

FAO. (2006). *Citrus fruit: fresh and processed - annual statistics 2006.*

Fito, P. J., Clemente, G., & Sanz, F. J. (1983). Rheological behaviour of tomato concentrate (hot break and cold break). *Journal of Food Engineering*, 2, 51-62.

Fung, D., & Matthews, R. (1991). *Instrumental methods for quality assurance in foods*. Milwaukee: Marcel Dekker, Inc.

Geraghty, R., & Butler, F. (1999). Viscosity characterization of a commercial yogurt at 5c using a cup in bob and a vane geometry over a wide shear rate range (10(-5) s-1-10(3) s(-1)). *Journal of Food Process Engineering*, 22, 1-10.

Gras, P. W., Carpenter, H. C., & Anderssen, R. S. (2000). Modelling the developmental rheology of wheat-flour dough using extension tests. *Journal of Cereal Science*, 31, 1-13.

Gunasekaran, S., & Ak, M. M. (2000). Dynamic oscillatory shear testing of foods - selected applications. *Trends in Food Science & Technology*, 11, 115-127.

Haminiuk, C. W. I., Sierakowski, M. R., Maciel, G. M., Vidal, J., Branco, I. G., & Masson, M. L. (2006). Rheological properties of butia pulp. *International Journal of Food Engineering*, 2, 12.

Haminiuk, C. W. I., Sierakowski, M. R., Vidal, J., & Masson, M. L. (2006). Influence of temperature on the rheological behavior of whole araca pulp (psidium cattleianum sabine). *Food Science and Technology*, 39, 427-431.

Hendrickson, R., & Kesterson, J. W. (1952). Viscosity of citrus molasses. Florida State Horticultural Society. Lake Alfred, FL.

Hendrickson, R., & Kesterson, J. W. (1964). Citrus molasses. Florida Agricultural Experiment Stations Technical Bulletin, 677.

Ibarz, A., Gonzalez, C., & Esplugas, S. (1994). Rheology of clarified fruit juices .3. Orange juices. *Journal of Food Engineering*, 21, 485-494.

Jastrzebski, Z. (1967). Entrance effects and wall effects in an extrusion rheometer during flow of concentrated suspensions. *Industrial & Engineering Chemistry Fundamentals*, 6, 445-454.

Karnjanolarn, R., & Mccarthy, K. L. (2006). Rheology of different formulations of milk chocolate and the effect on coating thickness. *Journal of Texture Studies*, 37, 668-680.

Karrabi, M., Ghoreishy, M. H. R., & Bakhshandeh, G. (2004). Rheological study of tyre tread compound - (part i): determination of wall slip coefficient and elastic swell using capillary rheometer. *Iranian Polymer Journal*, 13, 317-325.

Khandari, P., Gill, B. S., & Sodhi, N. S. (2002). Effects of concentration and temperature on the rheology of mango pulp. *Journal of Food Science and Technology*, 39, 152-154.

Kimball, D. (1999). *Citrus processing a complete guide*. Gaithersburg: Aspend Publishers, Inc.

Kokini, J. L. (1992). *Rheological properties of foods. Handbook of food engineering* (pp. 1-38). New York: Marcel Dekker, Inc.

Kokini, J. L., & Dervisoglu, M. (1990). Wall effects in the laminar pipe flow of four semi-solid foods. *Journal of Food Engineering*, 11, 29-42.

Kress-Rogers, E., & Brimelow, C. (2001). *Instrumentation and sensors for the food industry*. Norwich, NY.

Krokida, M. K., Maroulis, Z. B., & Saravacos, G. D. (2001). Rheological properties of fluid fruit and vegetable puree products: compilation of literature data. *International Journal of Food Properties*, 4, 179-200.

Kyereme, M., Hale, S. A., & Farkas, B. E. (1999). Modeling the temperature effect on the flow behavior of sweet potato puree. *Journal of Food Process Engineering*, 22, 235-247.

Lam, Y. C., Wang, Z. C., Chen, X., & Joshi, S. C. (2007). Wall slip of concentrated suspension melts in capillary flows. *Powder Technology*, 177(3), 162-169.

Leongpoi, L., & Allen, D. G. (1992). Direct measurement of the yield stress of filamentous fermentation broths with the rotating vane technique. *Biotechnology and Bioengineering*, 40, 403-412.

Levati, M. (2010). *Rheological behavior of citrus pulp and its application to aseptic processing*. American Society of Mechanical Engineers 56th Florida Section Citrus Engineering Conference (P. 32). Lake Alfred, FL.

Martinez-Padilla, L. P., & Rivera-Vargas, C. (2006). Flow behavior of mexican sauces using a vane-in-a-large cup rheometer. *Journal of Food Engineering*, 72, 189-196.

Mccabe, W., Smith, J., & Harriott, P. (1985). *Unit operations of chemical engineering*. New York: Mcgraw-Hill Book Company.

Missaire, F., Qiu, C. G., & Rao, M. A. (1990). Yield stress of structured and unstructured food suspensions. *Journal of Texture Studies*, 21, 479-490.

NASS. (2010). *Citrus fruits 2010 summary*.

Nindo, C. I., Tang, J., Powers, J. R., & Takhar, P. S. (2007). Rheological properties of blueberry puree for processing applications. *Food Science and Technology*, 40, 292-299.

Ozkanli, O. T., A. (2008). Rheological behaviors of sumac concentrate. *International Journal of Food Properties*, 11(1), 213-222.

Rahmani, M., & Hodges, A. (2009). *Economic impacts of the florida citrus industry in 2007-08.*

Rao, M. A., & Steffe, J. F. (1997). Measuring yield stress of fluid foods. *Food Technology*, 51, 50-52.

Saak, A. W., Jennings, H. M., & Shah, S. P. (2001). The influence of wall slip on yield stress and viscoelastic measurements of cement paste. *Cement and Concrete Research*, 31, 205-212.

Shukla, A., & Rizvi, S. S. H. (1995). Measurement of flowability of butter by capillary rheometry. *Journal of Texture Studies*, 26, 299-311.

Singh, R., & Heldman, D. (2001). *Introduction to food engineering*. Oxford, UK: Academic Press.

Singh, S. K., Castell-Perez, M. E., & Moreira, R. G. (2000). Viscosity and textural attributes of reduced-fat peanut pastes. *Journal of Food Science*, 65, 849-853.

Smith, P. (2003). *Introduction to food process engineering*. New York: Springer.

Sofou, S., Muliawan, E. B., Hatzikiriakos, S. G., & Mitsoulis, E. (2008). Rheological characterization and constitutive modeling of bread dough. *Rheologica Acta*, 47, 369-381.

Spreen, T. (2001). *Projections of world production and consumption of citrus to 2010*. 2009.

Steffe, J. (1996). *Rheological methods in food process engineering*. East Lansing, Mi: Freeman Press.

Steffe, J., & Daubert, C. (2006). *Bioprocessing pipelines: rheology and analysis*. East Lansing, Mi: Freeman Press.

Sun, A., & Gunasekaran, S. (2009a). Measuring rheological characteristics and spreadability of soft foods using a modified squeeze-flow apparatus. *Journal of Texture Studies*, 40, 275-287.

Sun, A., & Gunasekaran, S. (2009b). Yield stress in foods: measurements and applications. *International Journal of Food Properties*, 12, 70-101.

Tabilo-Munizaga, G., & Barbosa-Canovas, G. V. (2005). Rheology for the food industry. *Journal of Food Engineering*, 67, 147-156.

Tavares, D. T., Alcantara, M. R., Tadini, C. C., & Telis-Romero, J. (2007). Rheological properties of frozen concentrated orange juice (fcoj) as a function of concentration and subzero temperatures. *International Journal of Food Properties*, 10, 829-839.

Togrul, H., & Arslan, N. (2004). Mathematical model for prediction of apparent viscosity of molasses. *Journal of Food Engineering*, 62, 281-289.

Van Wazer, J. R., Lyons, J. W., Kim, K. Y., & Colewell, R. E. (1963). *Viscosity and flow measurement*. New York: Interscience Publishers.

Velez-Ruiz, J. F., & Barbosa-Canovas, G. V. (1998). Rheological properties of concentrated milk as a function of concentration, temperature and storage time. *Journal of Food Engineering*, 35, 177-190.

Vitali, A. A., & Rao, M. A. (1984a). Flow properties of low-pulp concentrated orange juice - effect of temperature and concentration. *Journal of Food Science*, 49, 882-888.

Vitali, A. A., & Rao, M. A. (1984b). Flow properties of low-pulp concentrated orange juice - serum viscosity and effect of pulp content. *Journal of Food Science*, 49, 876-881.

Walls, H. J., Caines, S. B., Sanchez, A. M., & Khan, S. A. (2003). Yield stress and wall slip phenomena in colloidal silica gels. *Journal of Rheology*, 47, 847-868.

Wang, Z. Y., Lam, Y. C., Joshi, S. C., & Chen, X. (2010). Determination of pressure drop for concentrated suspension in a capillary flow. *Polymer Composites*, 31(5), 792-798.

Wilhelm, L., Suter, D., & Brusewitz, G. (2004). *Food and process engineering technology*. Portland, OR: American Society of Agricultural Engineers.

Yeow, Y. L., Perona, P., & Leong, Y. K. (2001). A reliable method of extracting the rheological properties of fruit purees from flow loop data. *Journal of Food Science*, 67(4), 1407-1411.

Zheng, H., Morgenstern, M. P., Campanella, O. H., & Larsen, N. G. (2000). Rheological properties of dough during mechanical dough development. *Journal of Cereal Science*, 32, 293-306.

BIOGRAPHICAL SKETCH

Elyse Meredith Payne was born in Spartanburg, South Carolina but raised in Orlando, Florida. She attended the University of Florida from 2004 to 2009 where she completed a Bachelor of Food Science and Human Nutrition. Continuing her education at the University of Florida, she joined Dr. Reyes De Corcuera's lab team to pursue a master's degree.

Upon completion of the requirements for a master in food science at the University of Florida, Elyse intends to seek a position within the citrus industry where she can apply her current and developing skill set.